PROSPECTS OF DARK MATTER IN STANDARD MODEL EXTENSIONS

To be submitted in the partial fulfilment for the degree of **DOCTOR OF PHILOSOPHY IN PHYSICS**

BY

SINGIRALA SHIVA RAMA KRISHNA 13PHPH12



Under the supervision of **Prof. RUKMANI MOHANTA**

School of Physics
University of Hyderabad
Hyderabad 500 046, INDIA

December 2018

DECLARATION

I hereby declare that, this thesis titled Prospects of Dark Matter in Standard

Model Extensions submitted by me, under the guidance and supervision of Prof.

Rukmani Mohanta, is a bonafide research work and is free from plagiarism. I also

declare that it has not been submitted previously, in part or in full to this University

or any other University or Institution, for the award of any degree or diploma. I hereby

agree that my thesis can be deposited in Shodhganga/INFLIBNET.

A report on plagiarism statistics from the University Librarian is enclosed.

Hyderabad

(Singirala Shiva rama krishna)

Date:

Reg. No.: 13PHPH12

iii



CERTIFICATE

This is to certify that the thesis entitled **Prospects of Dark Matter in Standard Model Extensions** submitted by Singirala Shiva rama krishna bearing registration number 13PHPH12 in partial fulfilment of the requirements for award of Doctor of Philosophy in the School of Physics is a bonafide work carried out by him under my supervision and guidance.

This thesis is free from plagiarism and has not been submitted previously in part or in full to this or any other University or Institution for award of any degree or diploma.

Further, the student has the following publications before the submission of the thesis for adjudication.

- 1) S. Singirala, R. Mohanta and S. Patra, The European Physical Journal Plus 133, 477 (2018), (ISSN No: 2190-5444 (online)), Chapter 2.
- S. Singirala, R. Mohanta, S. Patra and S. Rao, Journal of Cosmology and Astroparticle Physics 1811, 026 (2018), (ISSN No: 1475-7516 (online)), Chapter 3.
- 3) S. Singirala, Chinese Physics C **41**, 043102 (2017), (ISSN No: 1674-1137 (online)), Chapter 4.
- 4) S. Singirala, S. Sahoo and R. Mohanta, [arXiv:1809.03213], Chapter 5.

Further, the student has passed the following courses towards fulfilment of coursework requirement for Ph.D:

Course Code	Name	Credits	Pass/Fail
PY801	Advanced Quantum Mechanics	4	Pass
PY803	Advanced Statistical Mechanics	4	Pass
PY804	Advanced Electromagnetic Theory	4	Pass
PY821	Research Methodology	4	Pass

Prof. Rukmani Mohanta

Thesis Supervisor School of Physics University of Hyderabad Prof. Bindu A. Bambah

Dean School of Physics University of Hyderabad

Date:

Acknowledgements

At this moment, it gives me great pleasure to thank people who helped me during my long academic career.

First and foremost, I would like to express my heartfelt gratitude and respect to my advisor Prof. Rukmani Mohanta. Her endless dedication towards work and calmness is an inspiration. The intellectual and moral support that she has given me during the difficult stages of research career is invaluable.

I am grateful to my collaborators Dr. Sudhanwa Patra and Dr. Soumya Rao. The discussions with them improved me a lot in research perspective and also taught me the way of writing a research article. Thanks to Dr. Subhadip Mitra for the help in CalcHEP code. I convey my regards to Prof. Subhendu Rakshit, IIT Indore for inviting me to visit and learn the work. I also thank Prof. Anjan Giri for the motivational words and suggestions.

I am thankful to my doctoral committee members Prof. E. Harikumar and Dr. Soma Sanyal for their fruitful suggestions during the meetings. My gratitude to the Dean, Prof. Bindu A. Bambah for inspiring me through her lectures and led me to choose high energy physics field as my research career. I would like to thank the former Deans of SoP, Prof. C. Bansal, Prof. S.P. Tiwari and Prof. S. Chaturvedi and Prof. Rajender Singh. I convey my regards to the HEP faculty members Prof. M. Sivakumar, Prof. P. K. Suresh and Dr. Barilang Mawlong.

I convey regards to my M.Sc teachers, especially Prof. Ashok Kapoor. A perfect teacher who gives full justification to the course dealt and the confidence that he have given me in the subject of Quantum Mechanics is immense. I am grateful to Prof. KPN Murthy, Prof. Nirmal, Prof. V. Seshubai, Prof. Srinath, Prof. Anantha Lakshmi. I also thank Dr. Ashoka VS, Prof. Ashok Chatterjee, Prof. S. Dhara and Prof. S. N. Kaul, Mr. Srinivas, Mr. Mukunda Reddy and all the other faculty members of SoP.

I also thank the non-teaching staff Mr. Abraham, Mrs. Deepika, Mr. Sudarshan, Mr. Sekhar, Mrs. Shailaja and Mr. Prasad.

I am grateful to the financial assistance of DST-Inspire division for the fellowship during my Ph.D and SHE scholarship during my B.Sc and M.Sc. I thank DST-ITS division for giving the financial support to attend the conference in the most beautiful place, Zurich Switzerland. My regards to Mr. Asgar, Mrs. Madhavi, Mr. Jaffer and Mr. Kashyap in the finance section.

I would like to thank my teachers, who built my career. Starting with B.Sc, Sri. Ramesh Reddy garu, Sri Malla Reddy garu, Sri Ramgopal garu, Mr. Rajkumar, Mr. Venkatesham, Mr. B. Srinivas, Mr. Varaprasad, Mr. Raghupathi and Mr. Srinivas. My +2 teachers, Sri. V. Narender Reddy garu, Sri. Rajesham garu, Sri. D. Nagender garu, Mr. P. Srinivas and Mrs. Sunita. From my schooling, Sri. J Venkateshwar Rao garu, Sri. Laxman Rao garu, Mr. Niaz, Mr. Moinuddin, Mr. Srinivasan, Mr and Mrs. Prabhakaran, Mrs. Seshumani and Mr. Chary. My primary school teachers, Mrs. Jhansi, Mrs. Radharani and Mr. David.

I thank my colleagues Nabil, Jitu, Alkathy, Ravi, Umesh, Suadat, Samlan, Mudasir, Dr. Fakhereh, Shihab and specially to Dr. Suchismita, Robertson, Chakradhar, Pundareekam. I thank my juniors Akshay, Atasi, Rudra, Mitesh, Aishwarya, Pooja, Subhasmita, Manas, Abhishek, Tluanga. I also thank my seniors Dr. Deepthi, Dr. Srinu, Dr. Soumya, Dr. Sruthi, Dr. Anjana, Dr. Zuhair, Dr. Siva Kaseti, Dr. Naveen, Dr. Sanjeev, Dr. Aalu, Dr. Narsimharaju, Dr. Ravi, Dr. Ramesh, Dr. Raju, Dr. IV Shankar and Dr. Pd Shankar. My hostel buddies, Nagaraju and Pankaj.

I would like to thank all my friends starting with M.Sc buddies, especially Ramesh, S. Mahesh, Seshu, B. Krishna, V. Mahesh, Vijay, Tariq, Govind, Aswathy, Anukarana and late Saba Ahmed. My B.Sc friends Niranjan, Ashraf, Ramesh, Vinod, Sandeep duo, Rajender, Bharath, Mahender, Tirupati, Prasanna, Ramya, Soumya, Madhavi. My best dudes of +2, Saikiran, Venu, Sai Srinivas, Yashash. My childhood friends Satish, Bharath and Jayaram. My school friends Saicharan, G. Rakesh, James, Anirudh, Rohith, Manmohan.

I convey my gratitude and respect to my well wishers Sri. C. Prabhakar Reddy garu, Sri. G. Ramulu garu, Sri. P. Krishnamurthy garu, Sri. K. Sagar Rao garu and late Sri. M. Ramaswamy garu.

The most important, I thank my beloved family for their endless love and care. My parents, Sri. Vittal garu (my inspiration) and Smt. Rajamani garu who have worked so hard to bring us up. My sisters and brother-in-laws Annapurna-Sathyanarayana, Krishnaveni-Nomraj and Vanaja-Bharath. Special thanks to my younger sister Vanaja, who gave me all the inspiration to take up physics. Lots of love to my little champs Chaitra, Apple, Nikhil and Aadya. You all are my strength and I missed you a lot during my Ph.D. Finally, the struggles and failures in life made me a better person and the best quotation that keeps me on "Success does not teach you much but a failure does".

Abstract

The most consistent theory that has unfolded the basic building blocks of visible matter content and its dynamics to the level of experimental accuracy is questionable when it comes to the ingredients and dynamics of dark matter in the Universe. The demand for extended frameworks of the standard model that can flash light on this mysterious matter component from the probes of available experimentally feasible observables are piling up. In this concern, we scrutinize few simple beyond standard model frameworks in connection to neutrino and flavor sectors possessing well measured observables.

We start by presenting a comprehensive study of singlet scalar and Majorana dark matter in a $U(1)_{B-L}$ gauge extension of the standard model, where three exotic fermions with B-L charges as -4, -4, +5 are added to make the model free from the triangle gauge anomalies. The enriched scalar sector and the new heavy gauge boson Z', associated with the $U(1)_{B-L}$ symmetry make the model advantageous to be explored in dual portal scenarios for the search of dark matter signal. Without the need of any ad-hoc discrete symmetry, the B-L charge plays a crucial role in stabilizing the dark matter particle. Analyzing the effect of two mediators separately, the scalar portal channels give a viable parameter space consistent with relic density from Planck data and the direct detection limits from various experiments such as LUX, XENON1T and PandaX. While the Z' mediated channels get additional constraints from the LHC searches for Z' in the dilepton channel. A massless physical Goldstone boson plays a key role in the scalar portal relic density. We shed light on the semi-annihilation in the case of scalar dark matter. We show the mechanism of generating the light neutrino mass at one-loop level where the dark matter particle runs in the loop.

We then investigate neutrino phenomenology and dark matter in the context of the scotogenic model. We examine the the radiative neutrino mass matrix by considering the neutrino mixing matrix to be of tri-bimaximal form with additional perturbations to accommodate the recently observed non-zero value of reactor mixing angle θ_{13} . We obtain the relation between various neutrino oscillation parameters and the model parameters. Working in degenerate heavy neutrino mass spectrum, we obtain light neutrino masses obeying normal hierarchy and also study the relic abundance of fermionic dark matter candidate including coannihilation effects. We display a viable parameter space consistent with neutrino oscillation data, relic abundance and various lepton flavor violating decays such as $\ell_{\alpha} \to \ell_{\beta} \gamma$ and $\ell_{\alpha} \to 3 \, \ell_{\beta}$.

Moving on to dark matter and flavor connection, we explore Majorana dark matter in a new variant of $U(1)_{L_{\mu}-L_{\tau}}$ gauge extension of Standard Model, where the scalar sector is enriched with an inert doublet and a $(\bar{3}, 1, 1/3)$ scalar leptoquark. We compute

the WIMP-nucleon cross section in leptoquark portal and the relic density mediated by inert doublet components, leptoquark and the new Z' boson. We constrain the parameter space consistent with Planck limit on relic density, PICO-60 and LUX bounds on spin-dependent direct detection cross section. Furthermore, we constrain the new couplings from the present experimental data on $\text{Br}(\tau \to \mu \nu_{\tau} \bar{\nu}_{\mu})$, $\text{Br}(B \to X_s \gamma)$, $\text{Br}(B \to K\tau\tau)$, R_K and $B_s - \bar{B}_s$ mixing, which occur at one-loop level in the presence of Z' and leptoquark. Using the allowed parameter space, we estimate the form factor independent $P'_{4,5}$ observables and the lepton non-universality parameters R_{K^*} and R_{ϕ} . We also briefly discuss about the neutrino mass generation at one-loop level.

Contents

D	eclar	ation			iii
C	ertific	cate			v
A	cknov	wledge	ments		ix
${f A}$ l	bstra	ct			xi
Li	st of	Figure	es	2	xvii
Li	st of	Tables	S		xxi
1	${f Intr}$	oducti	ion		1
	1.1	Revisi	ting the S	Standard Model	1
		1.1.1	Symmet	ries and gauge invariance	2
			1.1.1.1	U(1) local gauge invariance	2
			1.1.1.2	SU(N) local gauge invariance	4
		1.1.2	Electrow	veak theory	5
			1.1.2.1	Higgs mechanism	6
		1.1.3	Shortcon	mings of Standard Model	8
	1.2	Introd	uction to	$\operatorname{dark} \operatorname{matter} \ldots \ldots \ldots \ldots \ldots \ldots \ldots$	8
		1.2.1	Brief his	story	8
			1.2.1.1	Rotation curves	8
			1.2.1.2	Primordial nucleosynthesis and CMBR	10
			1.2.1.3	Numerical simulations	11
			1.2.1.4	Bullet cluster	11
		1.2.2		nature of dark matter	11
		1.2.3	-	niverse dynamics	12
			1.2.3.1	Equilibrium thermodynamics	13
			1.2.3.2	Non-equilibrium thermodynamics - Relic density	14
			1.2.3.3	Direct detection	
	19	Aim a	nd orrowri	over of thosis	20

Contents

2		glet scalar dark matter, massless Goldstone and neutrino mass in a
	new	A B - L model 21
	2.1	Introduction to $B-L$ frameworks
	2.2	The model framework
		2.2.1 Anomaly cancellation with additional fermions having exotic $B-L$
		charges
		2.2.2 Vacuum stability criteria and unitarity constraints 26
	2.3	Spontaneous symmetry breaking, masses and mixing
		2.3.1 Mixing in scalar sector
		2.3.2 Stability of singlet scalar dark matter
	2.4	Z' portal phenomenology
		2.4.1 Relic abundance
		2.4.2 Direct searches
		2.4.3 Collider bounds
	2.5	Scalar portal phenomenology
		2.5.1 Relic density
		2.5.2 Direct searches
	2.6	Light neutrino mass
	2.7	Semi-annihilations of scalar dark matter
	2.8	Conclusion
3	Ma	jorana dark matter in a $U(1)_{B-L}$ extension of the standard model 43
	3.1	Recap of proposed model and outlook
	3.2	Revisiting the exotic fermion mass matrix
	3.3	Dark matter phenomenology
		3.3.1 Relic density for Majorana dark matter
		3.3.1.1 Scalar mediated
		3.3.1.2 Vector mediated
		3.3.2 Direct searches
	3.4	Collider studies
	3.5	Light neutrino mass
	3.6	Conclusion
4	Fer	mionic dark matter and neutrino oscillation in the scotogenic model $$ 55
	4.1	Brief note on neutrino oscillation
	4.2	Scotogenic model
	4.3	Neutrino phenemenology
	4.4	Relic abundance
	4.5	Lepton flavour violating decays 61
	4.6	Conclusion
_	_	
5	_	ploring Majorana dark matter in connection to flavor anomalies in
	,	$-L_{ au}$ Model 67
	5.1	Brief note on flavor anomalies
	5.2	New $L_{\mu} - L_{\tau}$ model with a scalar leptoquark
	5.3	Mixing in the fermion and scalar sector
	5.4	Dark matter phenomenology
		5.4.1 Relic abundance

Contents

	Neu A.1 Flav	trino oscillations and fermionic dark matter Loop functions	85 87 91 91
	A.1 Flav B.1	Loop functions	91 93 93
D;	1. 1•	graphy	95

List of Figures

1.1	Rotation curves of high-luminosity galaxies as a function of radial distance [20]	9
1.2	CMBR power spectrum [22] with the blue curve representing Λ CDM	
1.3	based fit to Planck data. Error bars denote $\pm 1\sigma$ diagonal uncertainties. Images of Bullet cluster [25] with green contours representing the weak lensing reconstruction. Left panel shows the X-ray picture obtained by 500 ks exposure to Chandra. Right panel shows Magellan pictures of merging cluster 1E0657-558	10 12
1.4	Current experimental upper limits on WIMP-nucleon cross-section [42]. Left panel shows the bound on SI contribution and right-panel depicts the same in case of SD cross-section	20
2.1	The one-loop triangle gauge anomalies for the present $B-L$ model	23
2.2	Feynman diagrams leading to decay of scalar singlet dark matter ϕ_{DM} . The choice of $B-L$ charge to forbid these decay and stability of scalar singlet dark matter ϕ_{DM} is discussed in the text	30
2.3	Feynman diagrams for dark matter annihilation (left and middle) and scattering of DM from nucleon/quark (right panel) through Z' exchange. First two diagrams contribute to the relic density observable and the third one is appropriate in direct detection studies	31
2.4	Variation of relic abundance Ωh^2 with the mass of DM shown with two representative values of $g_{\rm BL}$ (left panel) and $M_{Z'}$ (right panel) for $n_{\rm DM} = 4$. Here the horizontal dashed lines denote the 3σ range in current relic density [88]	32
2.5	Left panel denotes the parameters space in the plane of $(M_{Z'}, g_{\rm BL})$ that satisfy the current relic density [88] in 3σ range and XENON1T [37]. The right panel depicts the WIMP-nucleon SI cross section with the mass of the scalar DM for the parameter space shown in the left panel. Here, the horizontal dashed lines denote the current bounds on spin-independent WIMP-nucleon cross section from the direct detection experiments LUX [36] and XENON1T [37]	33
2.6	Dilepton constraints from ATLAS on the current model are shown here. The black dashed line in the left panel represents the exclusion limit from ATLAS [96], with the colored lines being the dilepton signal cross sections for various values of $g_{\rm BL}$ as a function of $M_{Z'}$. The right panel shows exclusion limits from LEP-II and ATLAS exclusion limits in the plane of $M_{Z'} - g_{\rm BL}$. The red points are consistent with the 3σ range of the relic	
2.7	density limit of Planck and the direct detection limits from XENON1T Feynman diagrams contributing to relic density in the scalar portal case	34
	except the figure of t-channel process is relevant in direct detection studies	35

List of Figures xviii

2.8	Variation of relic abundance Ωh^2 with the mass of DM for various values of μ_{D8} parameter	36
2.9	Region of $M_{\rm DM}-M_{H_3}$ that meets the 3σ range on current relic density limit of Planck in left panel. Right panel denotes the parameter space taken from left panel that satisfies the XENON1T limit as well. Dashed lines denote the upper limit on WIMP-nucleon cross section by LUX [36] and XENON1T [37]	37
2 10	Radiative generation of neutrino mass	39
2.11	Feynman diagram for the semi-annihilation vertex	39
	with the choice of $n_{\rm DM}=1/3$	39
3.1	All the s-channel Feynman diagrams contribute to relic density while the t-channel process is relevant for the direct searches	46
3.2	Scalar-portal relic abundance as a function of DM mass M_{D1} for two specific mass values of the physical scalar H_3 . The horizontal dashed lines represent the 3σ value of the current relic density [88]	48
3.3	Feynman diagrams contributing to relic density in the vector-mediated case	49
3.4	Variation of relic abundance Ωh^2 with the mass of DM with $(M_{H_2}, M_{H_3}) = (1, 1.5)$ TeV. Left panel depicts the variation for fixed Z' mass and varying $B - L$ gauge coupling $g_{\rm BL}$. The right panel displays the behavior for constant coupling $g_{\rm BL}$ and varying mediator mass	49
3.5	Left panel shows the parameter space satisfying the 3σ range in current relic density and the most stringent PandaX limit. Right panel depicts WIMP-nucleon cross section for the parameters space depicted in the left panel. The dashed lines denote the upper bound on SI cross section from	
3.6	LUX [36], XENON1T [37] and PandaX [38]	50
	of $M_{Z'}-g_{\rm BL}$	
3.7	Radiative generation of neutrino mass	52
4.1	Radiative generation of neutrino mass	57
4.2	Parameter space of h_1 and r_1 consistent with 3σ relic abundance	
4.3	Variation of relic abundance with DM mass for various values of h_1 at $r_1 = 0.5$ (left panel) and $r_1 = 0.6$ (right panel) where the horizontal line (magenta) represents the central value of the relic density [136] and the black lines denote their corresponding 3σ range	62
4.4	Diagrams contributing to $l_{\alpha} \to l_{\beta} \gamma$	63
4.5	Parameter space of h_3 and r_3 (left panel) and variation of h_1 with M_1 (right panel) consistent with neutrino oscillation data, relic density and	
4.0	$\operatorname{Br}(\mu \to e\gamma)$	63
4.6	Correlation plot between $Br(\tau \to e\gamma)$ and $Br(\tau \to \mu\gamma)$	64
4.7	Penguin diagram contributions to $\ell_{\alpha} \to 3 \ell_{\beta}$. The mediator (wavy line) denotes either a photon or a Z-boson	65

List of Figures xix

4.8	Box diagram contributions to $\ell_{\alpha} \to 3 \ell_{\beta}$	65
4.9	Correlation plots between $Br(\mu \to eee)$ and $Br(\mu \to e\gamma)$ (left panel) and between $Br(\tau \to \mu\mu\mu)$ and $Br(\tau \to eee)$ (right panel)	66
	between $BI(r \to \mu\mu\mu)$ and $BI(r \to eee)$ (right paner)	00
5.1	Feynman diagrams contributing to relic density	72
5.2	Behavior of relic density plotted against DM mass with $M_{H_2} = 2.2$ TeV, shown with varying $M_{Z'}$ and $g_{\mu\tau}$ (left panel) and y_{qR} (right panel). Black	70
5.3	horizontal dotted lines denote the 3σ range of Planck limit [22] Left panel depicts the $M (y_{qR})^2$ parameter space consistent upto 3σ level of Planck limit [22] on relic density. Right panel gives the SD WIMP-proton cross section as a function of DM mass. Dashed lines represent the recent bounds obtained from PICO-60 [39] and LUX [40]. Green (red) data points in both the panels represent Planck allowed and PICO	72
	excluded (Planck and PICO allowed)	74
5.4	Box diagrams of $B_s - \bar{B}_s$ mixing with leptoquark in the loop	76
5.5	Penguin diagram of $b \to sll$ processes, where $l = \mu, \tau$ with leptoquark in	
	the loop	77
5.6	Feynman diagram of $b \to s \gamma$ processes in the presence of scalar leptoquark.	79
5.7	One loop box diagram of $\tau \to \mu \nu_{\tau} \bar{\nu}_{\mu}$ processes	79
5.8	Left panel projects the constraint on $g_{\mu\tau}$ and $M_{Z'}$ obtained from R_K , $\operatorname{Br}(B \to K\tau\tau)$ and $\operatorname{Br}(\tau \to \mu\nu_{\tau}\bar{\nu}_{\mu})$ observables. In the right panel, blue data points denote the allowed parameter space obtained from R_K , $B_s - \bar{B}_s$ mixing, $\operatorname{Br}(B \to K\tau\tau)$, $\operatorname{Br}(B \to X_s\gamma)$ experimental data, which are also consistent with Planck [22] and PICO-60 limit [39]. Here, green (red) data points denote PICO-60 and flavor excluded (PICO-60 allowed and flavor excluded) region.	80
5.9	The q^2 variation of R_{K^*} (left panel) and R_{ϕ} (right panel) LNU parameters	00
	in the $L_{\mu}-L_{\tau}$ model. Here the blue dashed lines represent the SM prediction, the cyan (magenta) bands stand for the NP contribution from the dark matter studies i.e., DM-I (DM-II). Orange bands are due to the	
	contribution from both the flavor and DM sectors (DM+Flavor). The	
	experimental data points (with 2σ error bars) [138] are shown in black lines	83
5.10	lines	09
	shown in black [141]. Note that P_4' LHCb = $-P_4'$	83

List of Tables

1.1	model	2
1.2	Spin fractions for quark content in proton and neutron	19
2.1	Particle spectrum and their charges of the proposed $U(1)_{B-L}$ model	25
2.2	Fixed parameters for Z' -mediated DM observables	32
2.3	Dark matter couplings to scalars	36
2.4	Parameters and their ranges for scalar portal analysis	37
2.5	Sample benchmark for radiative ν -mass	38
3.1	Parameters and their ranges for scalar portal analysis	50
3.2	Inert doublet and its charge assignment	51
4.1	Best-fit values with their 3σ ranges of the neutrino oscillation parameters	
	from [113] where NO indicates normal ordering.	
4.2	Scotogenic model parameters with their range	64
5.1	Fields and their charges of the proposed $U(1)_{L_{\mu}-L_{\tau}}$ model	69
5.2	Predicted allowed range of parameters M_{-} and $(y_{qR})^2$. Here DM-I and DM-II represent two regions in Fig. 5.3 consistent with only DM observables, DM+Flavor denotes the region favored by both the dark matter	
	and flavor studies	80
5.3	Predicted numerical values of LNU parameters (R_V) and $P'_{4,5}$ observables of $B \to V ll$, $V = K^*, \phi$ processes in the high and low recoil limits. The upper part represents the results for $\bar{B} \to \bar{K}^* \mu^+ \mu^-$ and the lower part is	
	for $B_s \to \phi \mu^+ \mu^-$. Here q^2 is in GeV ²	84

Dedicated to my family

Chapter 1

Introduction

To the present knowledge, four different kinds of interactions, namely strong, weak, electromagnetic and gravitational exist. Understanding gravitational interactions requires coordinate invariance as described in Einstein's general theory of relativity. The rest can be explained by the field theories based on Lorentz invariance. The manifestation of interactions at fundamental level in theoretical view point is based on symmetries which are the subsets of Lorentz transformations. Standard Model (SM) of particle physics is one such low energy gauge theory, over the years has produced tremendous success in giving theoretical demonstration for the fundamental physics in particle accelerators with an optimal accuracy.

1.1 Revisiting the Standard Model

Standard model is a gauge theory, invariant under $SU(3)_C \times SU(2)_L \times U(1)_Y$ symmetry group. The particle content with their corresponding charges are listed in Table. 1.1. The fermion content includes six quarks and six leptons and their anti-particles. Left-handed particles transform as doublets, while right-handed particles transform as singlets under $SU(2)_L$, where L denotes the handedness. $SU(3)_C$ does not distinguish the handedness, both left and right-handed quarks transform as colored triplets and all the leptons are represented as singlets. Only quarks participate in strong interactions, governed by $SU(3)_C$ gauge symmetry. All the left-handed fermions undergo weak interactions dictated by $SU(2)_L$ gauge group. Both the left and right-handed particles participate in electromagnetic interaction, described by the U(1) gauge group. The electromagnetic and weak interactions can be studied in a unified framework of electroweak interactions governed by $SU(2)_L \times U(1)_Y$ gauge symmetry, where Y denotes the hypercharge. All the interactions are mediated by the gauge bosons which are generators of

	Fields	$SU(3)_C$	$SU(2)_L$	$U(1)_Y$	T_3'	$Q = T_3' + Y$
Quarks	$Q_L \equiv \begin{pmatrix} u \\ d \end{pmatrix}_L$	3	2	1/6	$\begin{pmatrix} 1/2 \\ -1/2 \end{pmatrix}$	$\begin{pmatrix} 2/3 \\ -1/3 \end{pmatrix}$
	u_R	3	1	2/3	0	2/3
	d_R	3	1	-1/3	0	-1/3
Leptons	$\ell_L \equiv \begin{pmatrix} u \\ e \end{pmatrix}_L$	1	2	-1/2	$\begin{pmatrix} 1/2 \\ -1/2 \end{pmatrix}$	$\begin{pmatrix} 0 \\ -1 \end{pmatrix}$
	e_R	1	1	-1	0	-1
Scalar	Н	1	2	1/2	$\begin{pmatrix} 1/2 \\ -1/2 \end{pmatrix}$	$\begin{pmatrix} 1 \\ 0 \end{pmatrix}$

Table 1.1: Fermions and scalars with their corresponding charges in the standard model.

the associated group that governs the interaction. Eight massless gluons mediate the short range strong interactions, three massive weak bosons transfer the short range weak force and one massless photon mediates the long range electromagnetic interactions. Finally, the SU(2) scalar doublet H is introduced in the manifestation for the origin of mass in standard model.

1.1.1 Symmetries and gauge invariance

One of the fantastic perception in theoretical physics is that the interactions are governed by the principles of symmetries. These symmetries indeed point to the conserved quantities in accordance to Noether's theorem [1]. For instance, the invariance under global transformation leads to a conserved quantity. However, from a physicist's perspective, it implies some unmeasurable quantity i.e.,

$$\psi(x) = e^{i\beta}\psi(x)$$
, where β is unphysical. (1.1)

Furthermore, taking space time dependent transformation leads to the interesting requirement of interacting field called 'gauge field', which mediates the interactions and the invariance is termed as local gauge invariance. Concerning to SM, all interactions obey local gauge invariance under $SU(3)_C \times SU(2)_L \times U(1)_Y$ symmetry group.

1.1.1.1 U(1) local gauge invariance

We start with the free Dirac Lagrangian

$$\mathcal{L} = \overline{\psi}(i\gamma^{\mu}\partial_{\mu} - m)\psi. \tag{1.2}$$

We want this Lagrangian to be invariant under a more general transformation of the fermion field ψ as

$$\psi'(x) = e^{i\beta(x)} \ \psi(x). \tag{1.3}$$

Under this transformation, the Dirac Lagrangian becomes

$$\mathcal{L}' = \overline{\psi} \left(i \gamma^{\mu} \partial_{\mu} \psi - \gamma^{\mu} \psi \partial_{\mu} \beta - m \psi \right). \tag{1.4}$$

Clearly, the Lagrangian is not invariant $(\mathcal{L} \neq \mathcal{L}')$ due to the presence of derivative term. Defining a covariant derivative D_{μ} with a gauge field A_{μ} as

$$D_{\mu} = \partial_{\mu} - ieA_{\mu},\tag{1.5}$$

where A_{μ} obeys the transformation rule

$$A_{\mu} \to A_{\mu} + \frac{1}{e} \partial_{\mu} \beta.$$
 (1.6)

Now, one can obtain a U(1) local gauge invariant Lagrangian,

$$\mathcal{L}_{U(1)} = \overline{\psi} (i\gamma^{\mu} D_{\mu} - m) \psi$$

$$= \overline{\psi} (i\gamma^{\mu} \partial_{\mu} - m) \psi + e \overline{\psi} \gamma^{\mu} \psi A_{\mu}. \tag{1.7}$$

The introduced gauge field A_{μ} is paving the way for local gauge invariant dynamics. The mass term for the gauge field is prohibited as it violates the gauge invariance. The long range dynamics of electromagnetic interactions can be embedded in a U(1) local gauge invariant Lagrangian, named Quantum Electrodynamics (QED) and the associated gauge field in this regard represents the massless photon. The full Lagrangian thus becomes

$$\mathcal{L}_{\text{QED}} = \overline{\psi} \left(i \gamma^{\mu} \partial_{\mu} - m \right) \psi + e \overline{\psi} \gamma^{\mu} A_{\mu} \psi - \frac{1}{4} F^{\mu\nu} F_{\mu\nu}, \tag{1.8}$$

where -e denotes the electric charge of the Dirac fermion ψ , $-\frac{1}{4}F^{\mu\nu}F_{\mu\nu}$ denotes the kinetic term for the photon field A_{μ} with $F_{\mu\nu} = \partial_{\mu}A_{\nu} - \partial_{\nu}A_{\mu}$.

1.1.1.2 SU(N) local gauge invariance

Moving to the non-abelian case of SU(N), the fermion multiplet Ψ is represented by

$$\Psi = \begin{pmatrix} \psi_1 \\ \psi_2 \\ . \\ . \\ \psi_i \end{pmatrix}. \tag{1.9}$$

Accordingly, the Dirac Lagrangian takes the form

$$\mathcal{L} = \overline{\Psi} \left(i \gamma^{\mu} \partial_{\mu} - m \right) \Psi = \sum_{i} \overline{\psi_{i}} \left(i \gamma^{\mu} \partial_{\mu} - m \right) \psi_{i}. \tag{1.10}$$

We perform the local SU(N) transformation to the fermion multiplet as

$$\Psi(x) \to e^{i\alpha_a(x)T_a}\Psi(x) , \qquad (1.11)$$

where, the generators T_a satisfy $[T_a, T_b] = i f_{abc} T_c$ with f_{abc} being real constants. In analogy to the abelian case, we define

$$D_{\mu} = \partial_{\mu} + igT_a A^a_{\mu} , \qquad (1.12)$$

provided with A^a_μ transformation rule

$$A^a_\mu \to A^a_\mu - \frac{1}{g} \partial_\mu \alpha_a - f_{abc} \alpha_b A^c_\mu \ . \tag{1.13}$$

Thus one can write the SU(N) local gauge invariant Lagrangian as

$$\mathcal{L}_{SU(N)} = \overline{\Psi} \left(i \gamma^{\mu} \partial_{\mu} - m \right) \Psi - g \left(\overline{\Psi} \gamma^{\mu} T_{a} \Psi \right) A_{\mu}^{a} . \tag{1.14}$$

Following the above expression, the $SU(3)_C$ local gauge invariant QCD (Quantum Chromodynamics) Lagrangian that explains the strong interactions is given by

$$\mathcal{L}_{\text{QCD}} = \overline{\Psi}_q \left(i \gamma^{\mu} \partial_{\mu} - m \right) \Psi_q - g_s \left(\overline{\Psi}_q \gamma^{\mu} T_a \Psi_q \right) G_{\mu}^a - \frac{1}{4} G_{\mu\nu}^a G_a^{\mu\nu}, \tag{1.15}$$

where Ψ_q stands for quark triplet, g_s defines the coupling strength associated with SU(3) group and $G^a_{\mu\nu} = \partial_\mu G^a_\nu - \partial_\nu G^a_\mu - g_s f_{abc} G^b_\mu G^c_\nu$ corresponds to the gluon field tensor with G^a_μ (a=1,2,..8) denoting the eight massless gluon fields.

1.1.2 Electroweak theory

Weak and electromagnetic interactions can be demonstrated in a unified framework of $SU(2)_L \times U(1)_Y$ gauge invariant theory [2–4]. To illustrate, first we perform the local gauge transformation to the chiral fermion multiplet

$$\varphi_L \rightarrow e^{i[\alpha'_a(x) \cdot T'_a + \beta'(x)Y]} \varphi_L,$$

$$\varphi_R \rightarrow e^{i\beta'(x)Y} \varphi_R, \qquad (1.16)$$

where $\varphi_{L,R} = \frac{1}{2}(1 \mp \gamma_5)\varphi$ and $T'_a = \tau_a/2$ with τ_a (a = 1, 2, 3) being the Pauli matrices,

$$\tau_1 = \begin{pmatrix} 0 & 1 \\ 1 & 0 \end{pmatrix}, \quad \tau_2 = \begin{pmatrix} 0 & -i \\ i & 0 \end{pmatrix}, \quad \tau_3 = \begin{pmatrix} 1 & 0 \\ 0 & -1 \end{pmatrix}. \tag{1.17}$$

In the above transformation, Y and T'_a correspond to the generators of $U(1)_Y$ and $SU(2)_L$ gauge groups respectively. They are normalized as

$$Q = T_3' + Y, (1.18)$$

where Q denotes the electric charge and T_3' stands for the neutral generator of SU(2) group. The local gauge invariance requires the introduction of covariant derivative replacing the derivative in the interaction Lagrangian and is given as

$$\mathcal{L} = \overline{\varphi_L} \gamma^{\mu} \left(i \partial_{\mu} - \frac{g}{2} \tau^a \cdot W_{\mu}^a - g' Y B_{\mu} \right) \varphi_L + \overline{\varphi_R} \gamma^{\mu} \left(i \partial_{\mu} - g' Y B_{\mu} \right) \varphi_R
- \frac{1}{4} B_{\mu\nu} B^{\mu\nu} - \frac{1}{4} W_{\mu\nu} W^{\mu\nu},$$
(1.19)

where, the field tensors are given by $W_{\mu\nu} = \partial_{\mu}W_{\nu} - \partial_{\nu}W_{\mu} - gW_{\mu} \times W_{\nu}$ and $B_{\mu\nu} = \partial_{\mu}B_{\nu} - \partial_{\nu}B_{\mu}$. In the above Lagrangian of unified framework, the coupling constants g and g' correspond to SU(2) and U(1) groups respectively. As mentioned earlier in section. 1.1.1, the mass terms of the gauge fields violate the gauge invariance. However, short-range behavior of weak force requires the gauge bosons to be massive. The puzzle of mass generation for the gauge fields can be achieved by the mechanism of spontaneous symmetry breaking, will be discussed in the following subsection.

1.1.2.1 Higgs mechanism

In electroweak theory, mass can be generated for all the weak bosons using an $SU(2)_L$ complex doublet H with hypercharge Y = 1/2,

$$H = \frac{1}{\sqrt{2}} \begin{pmatrix} H^+ \\ H^0 \end{pmatrix}. \tag{1.20}$$

Adding its scalar potential V(H) and kinetic terms, the Lagrangian in Eqn. (1.19) becomes

$$\mathcal{L}_{EW} = \mathcal{L} + \left| \left(i \partial_{\mu} - \frac{g}{2} \tau^{a} \cdot W_{\mu}^{a} - g' Y B_{\mu} \right) H \right|^{2} - V(H), \tag{1.21}$$

where

$$V(H) = \mu_H^2(H^{\dagger}H) + \lambda_H(H^{\dagger}H)^2.$$
 (1.22)

For $\mu_H^2 < 0$ and $\lambda_H > 0$, the potential finds the minima at $H^{\dagger}H = -\mu_H^2/2\lambda_H$ and the vacuum can be denoted as

$$\langle H \rangle = \frac{1}{\sqrt{2}} \begin{pmatrix} 0 \\ v \end{pmatrix}, \tag{1.23}$$

where $v = \sqrt{\frac{-\mu_H^2}{\lambda_H}}$. Fluctuations near the vacuum can be parameterized in terms of four fields h, θ_1 , θ_2 and θ_3 as

$$H(x) = \frac{1}{\sqrt{2}} \begin{pmatrix} \theta_2 + i\theta_1 \\ v + h(x) - i\theta_3 \end{pmatrix}. \tag{1.24}$$

For small perturbations, the above parameterization can be written in the form

$$H(x) \simeq e^{i\alpha_a'(x)\cdot\tau_a/v} \frac{1}{\sqrt{2}} \begin{pmatrix} 0\\ v + h(x) \end{pmatrix}. \tag{1.25}$$

Perturbation of this form avoids the unwanted massless fields $\theta_{1,2,3}$ appearing in the model but they only stay as the additional degrees of freedom in the process of gauge transformation. The vacuum expectation value (v) of the doublet H breaks the symmetry associated with the generator T'_3 i.e., $SU(2)_L$. And also, with the presence of non-zero hypercharge, it breaks $U(1)_Y$ gauge symmetry as well. However, the symmetry corresponding to the charge Q in Eqn. (1.18) remains unbroken i.e., $U(1)_{\rm em}$. In simple words, the symmetry breaking pattern is given by

$$SU(2)_L \times U(1)_Y \to U(1)_{\rm em}.$$
 (1.26)

The above mechanism of ground state violating the Lagrangian symmetry is called spontaneous symmetry breaking, which is not forced by any external source but rather the Lagrangian itself does it.

Now, substituting the perturbed doublet of Eqn. (1.25) in Eqn. (1.22), the field h (called Higgs boson), obtains the mass

$$M_h = \sqrt{2\lambda_H v^2}. (1.27)$$

Expanding the kinetic term of the Higgs doublet implies

$$\left| \left(-i \frac{g}{2} \tau^{a} W_{\mu}^{a} - i \frac{g'}{2} B_{\mu} \right) H \right|^{2} = \frac{v^{2}}{8} \left| \left(\frac{g(W_{\mu}^{1} - iW_{\mu}^{2})}{-gW_{\mu}^{3} + g'B_{\mu}} \right) \right|^{2} \\
= \left(\frac{1}{2} v g \right)^{2} W_{\mu}^{+} W^{-\mu} + \frac{1}{2} \left(\frac{1}{2} v \sqrt{g^{2} + g'^{2}} \right)^{2} Z_{\mu} Z^{\mu}, \tag{1.28}$$

where, $W_{\mu}^{\pm} = \frac{W_{\mu}^1 \mp W_{\mu}^2}{\sqrt{2}}$ and the neutral boson basis $(W_{\mu}^3 B_{\mu})$ is shifted to mass basis of $(A_{\mu} Z_{\mu})$ using the relation

$$\begin{pmatrix} A_{\mu} \\ Z_{\mu} \end{pmatrix} = \begin{pmatrix} \cos \theta_W & \sin \theta_W \\ -\sin \theta_W & \cos \theta_W \end{pmatrix} \begin{pmatrix} B_{\mu} \\ W_{\mu}^3 \end{pmatrix}, \text{ where } \theta_W = \tan^{-1} \left(g'/g \right). \tag{1.29}$$

Thus, from Eqn. (1.28), one can see that the three weak bosons W^{\pm} and Z obtain mass, while the photon A remains massless as expected. Now, rewriting Eqn. (1.24) in the convenient form

$$H(x) = \begin{pmatrix} w^{+} \\ \frac{1}{\sqrt{2}}(v + h(x) + iz) \end{pmatrix}, \tag{1.30}$$

the charged (w^{\pm}) and neutral components (z) called 'Goldstone modes' go as longitudinal polarizations of the massive W^{\pm} and Z bosons respectively [5–8]. This whole mechanism is named after the theoretical physicist 'Peter Higgs', called Higgs mechanism [9–14].

Coming to the fermion masses, the Higgs doublet can be employed to generate mass to the fermions through the gauge invariant Yukawa mass term

$$\mathcal{L}_{\text{ferm}} = -\left(Y^{e}\overline{\ell_{L}}He_{R} + Y^{d}\overline{Q_{L}}Hd_{R} + Y^{u}\overline{Q_{L}}\tilde{H}u_{R} + \text{h.c.}\right), \tag{1.31}$$

where $\tilde{H} = -i\tau_2 H^*$. Thus the charged leptons attain the mass of the form $M_{\ell} = \frac{Y^{\ell}}{\sqrt{2}}v$ and similarly for quarks, $M_q = \frac{Y^q}{\sqrt{2}}v$.

1.1.3 Shortcomings of Standard Model

As every theory has its own limitations and region of validity, SM cannot explain some compelling evidences such as existence of dark matter (DM), dark energy (DE), baryon asymmetry of the Universe (BAU), neutrino mass and oscillations etc. These beyond SM signals are assumed to have obtained from a higher energy theory obeying the basic principles on which the SM is built upon.

Of all the above mentioned failures, one that is perplexing the high energy physics group since 80 odd years is the existence of second major energy component of the Universe i.e., dark matter, whose nature and identity is a mystery till date.

1.2 Introduction to dark matter

Unlocking the nature of DM of the Universe remains one of the long standing quest, involving cosmology and particle physics. Observation of anisotropies in power spectrum infer all the visible matter constitutes about 4%, dark matter and dark energy take the share of 27% and 69% respectively, reported by well-known WMAP and Planck satellites. The identity of the dominant particle component of the Universe still persists a secret over eight decades since it was first pointed out by Zwicky in 1933. It is supposed to be a massive neutral particle which does not interact with electromagnetic radiation. Its existence is solely established by its gravitational influence. However, there are many open questions still persist: (a) Is the dark matter fundamental? (b) Does the dark sector is similar to visible sector with various kinds of fundamental particles? (c) Whether it is fermionic or bosonic? Unravelling the pile of unknowns require huge theoretical and experimental hardship. In the phenomenological point of view, this thesis centers its attention to investigate DM in different beyond the SM scenarios and its implications in neutrino and flavor sectors.

1.2.1 Brief history

First, we briefly review the observations [15] that drove to the belief of dark matter existence and the necessity of its establishment in the theories that explain its nature.

1.2.1.1 Rotation curves

The hint of the unknown matter particle was first pointed out and named as 'dark matter' by the pioneer astronomer Fitz Zwicky way back in 1930's. In 1933, he used

viral theorem to estimate the velocity dispersion of the visible galaxies in Coma cluster [16]. He observed the average velocity dispersion to be nearly 1000 km/s rather than the expected 80 km/s. Later in 1937, a more refined analysis [17], also gave the high mass-to-light ratio implying the existence of DM in some state. Similar study was performed by Sinclair Smith for Virgo Cluster in 1936. In 1960s, Rubin and Ford published their spectroscopic observations of M31 rotation curve of Andromeda Galaxy [18]. The first convincing claim of discrepancy in mass is made in the seminal paper [19], where Freeman compared the photometric observations to the 21 cm rotation curve for M33 and NGC 300. Later in 1972, Rogstad and Shostak carried out the similar analysis for M31, M101, IC 342, NGC 2403 and NGC 6946, where the mass-to-light ratios are found to be 20 for large radii. In 1978, Ford, Rubin and Thonnard published a widely cited article [20], confirming the flatness of optical rotation curves of ten most luminous spiral galaxies, shown in Fig. 1.1.

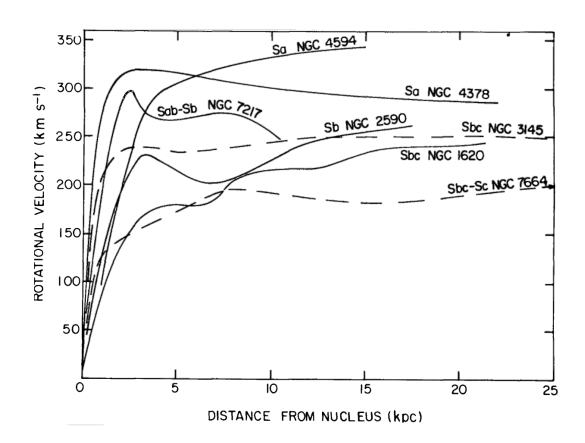


FIGURE 1.1: Rotation curves of high-luminosity galaxies as a function of radial distance [20].

The flatness behavior can be illustrated as follows. Spiral galaxies have most of their mass concentrated in the central bulge and the spiral arms spread out from the disc. For a star at a distance r from the galactic center of spiral galaxy, Virial theorem relates the average potential and kinetic energies as $\langle P.E \rangle + 2 \langle K.E \rangle = 0$. The circular velocity of the star is given by

$$v(r) \propto \sqrt{\frac{M(r)}{r}},$$
 (1.32)

where M(r) denotes the mass enclosed in the disc of radius r. For the region within the central bulge, the velocity goes $v(r) \sim r$ as $M(r) = \frac{4}{3}\pi r^3 \rho$, with ρ denoting the average density of the central hub. Outside the central hub, the velocity obeys the Keplerian decline $v(r) \sim r^{-1/2}$. However, observations claim that the velocity curve seems to

flatten for large radial distance. An invisible matter component is believed to nullify the radial dependence of velocity rotation curve.

1.2.1.2 Primordial nucleosynthesis and CMBR

Primordial nucleosynthesis is one of the earliest probes to test the standard model of Cosmology. It indicates that the total luminous matter density (baryonic) is $\Omega_{\rm LUM} \sim 0.01$. Concordance between the observed and predicted abundances suggest $0.014 \leq \Omega_B \leq 0.16$ [21]. These numbers give an intuition that some fraction of baryonic matter is non-luminous. In other words, there is some baryonic dark matter in the Universe.

After the probe of detecting Cosmic Microwave Background Radiation (CMBR) was discovered, experimentalists were able to look deep into the early Universe for the times after the last scattering surface. The anisotropies in CMB gave a route map to predict the energy budget of the Universe. Baryon acoustic oscillations in the primordial plasma during the early Universe is the source of anisotropy in CMB power-spectrum. Baryons and dark matter behave same when looked in gravitational point of view, however, can be distinguished in terms of their interaction with photons. Their impact on acoustic oscillations can be figured out from the CMB spectrum, shown in Fig. 1.2. In particular, the first acoustic peak is mostly because of baryonic component and the third peak is associated with dark matter in the Universe. According to Planck Collaboration, fitting Λ CDM model parameters to the power-law of CMB anisotropy, the baryonic and dark matter densities are given as $\Omega_{\rm B}h^2=0.02237\pm0.00015$ (68% CL) and $\Omega_{\rm DM}h^2=0.12\pm0.0012$ (68% CL) [22]. This implies that the non-baryonic dark matter constitutes more than 84% of the total matter content in the Universe.

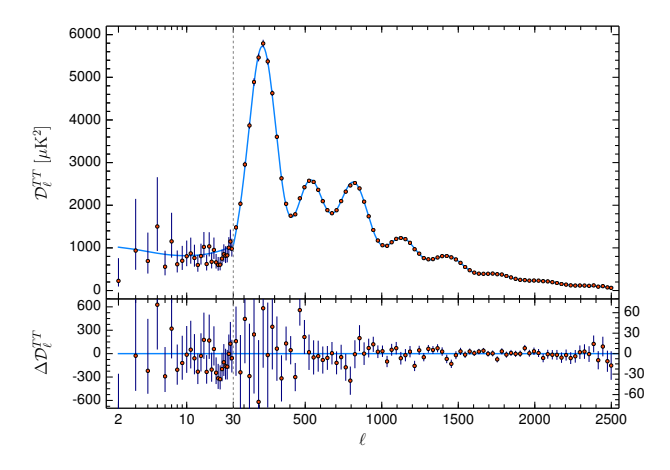


FIGURE 1.2: CMBR power spectrum [22] with the blue curve representing Λ CDM based fit to Planck data. Error bars denote $\pm 1\sigma$ diagonal uncertainties.

1.2.1.3 Numerical simulations

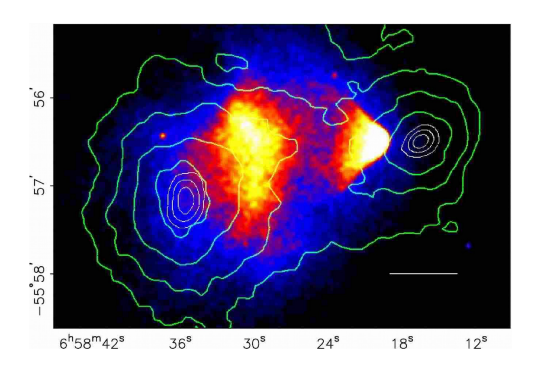
Computer based simulations were used in early 60's to understand the evolution of gravitationally interacting massive bodies of the Universe. Considering dark matter in the energy component, it was found that the resulting pattern of these cosmological simulations is sensitive to the DM initial velocity distribution. This gave the hint to the cosmologists to classify whether dark matter is relativistic (hot) or non-relativistic (cold). At large scales, the impact of dark matter velocity on simulated structure is minimal. However, in case of small scale structures, the density fluctuations get washed out due to hot dark matter (HDM), thereby suppressing its growth. In contrast, cold dark matter (CDM) with shorter free-streaming length can form very low mass halos. These halos at early Universe merge with one another to give large scale structures. The paper of 1984 [23], first appreciated CDM over HDM in the structure formation simulation study. Later in 1996, Navarro, Frenk and White published the analysis of the halos produced in their high-resolution CDM simulations [24].

1.2.1.4 Bullet cluster

Bullet cluster 1E0657-558 [25] is one of the vivid direct evidence for dark matter existence. It was formed due to the collision of two enormous galaxies, where one passes through other. The gas in these galaxies that got heated up due to the collision, emits X-rays. The X-ray spectrum reveals the spread of baryonic matter of the system after collision shown in the left panel of Fig. 1.3. It was found that the images of background galaxies got distorted due to gravity of cluster's mass. Measuring the magnitude of distortion by the method of weak lensing studies, the mass in the cluster can be estimated. The green contours of Fig. 1.3 describe the reconstructed lensing signal for the projected mass in the system. If there is no dark matter, the contours will trace the X-ray spectrum. From Fig. 1.3, it is clear that the contours do not trace the visible region (baryonic). So, only the baryonic matter content in the system alone cannot explain the amount of distortion. The hypothesis of collisionless dark matter was found to be the most convincing argument that causes the lensing effect in the outer part of X-ray region.

1.2.2 Possible nature of dark matter

Considering the above hints, the possible features of the dark matter particle can be deduced as follows:



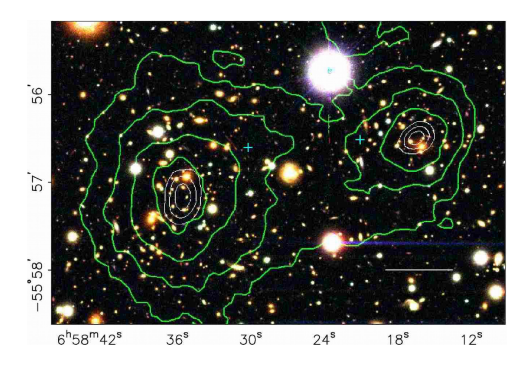


FIGURE 1.3: Images of Bullet cluster [25] with green contours representing the weak lensing reconstruction. Left panel shows the X-ray picture obtained by 500 ks exposure to Chandra. Right panel shows Magellan pictures of merging cluster 1E0657-558.

- As it is indeed invisible, it should not undergo significant interaction with the photons. Conclusively, an electrically neutral particle satisfies the requirement.
- The absence of any decay products in cosmic-ray observations [26], the dark matter is stable over cosmological time scale and its abundance still contributes to energy budget of the Universe.
- It should not be a colored particle. Strongly interacting massive particle (SIMP) fails to produce the observed relic density [27].
- Structure formation simulation studies appreciate non-relativistic nature for dark matter.

Standard model of particle physics, being a successful theoretical framework has no answer to what dark matter is. The stable neutral particle, the neutrino is anticipated to be a dark matter candidate. However, this choice fails because of two reasons. One is due to its relativistic nature, the other is that it can contribute only a small fraction of current relic density i.e., $\Omega_{\nu}h^2 = 0.0062$ (95% CL) [28]. Left out with empty hands, one can expect the unknown dark matter particle emerges from beyond SM frameworks. In the upcoming section, we will show how an electrically neutral non-relativistic particle that self-annihilates weakly i.e., Weakly Interacting Massive Particle (WIMP) can match the predicted relic abundance of dark matter with a cross section of the order $\sigma v \sim 10^{-9}$ GeV⁻².

1.2.3 Early Universe dynamics

Early Universe was very dense and hot, with the interactions between particles are more frequent than today. Production and annihilation went at similar pace maintaining the state of equilibrium. In statistical terms, this state is called as 'Thermal equilibrium', characterized at definite temperature. It turns out that the thermal equilibrium description is a good approximation for most of the early Universe epochs. However, the expansion of the Universe never gives a state of perfect thermal equilibrium. Universe is said to be in nearly equilibrium state until annihilation rate Γ is greater than the expansion rate H (= $\frac{\dot{a}}{a}$) i.e., $\Gamma \leq H$. Departures from thermal equilibrium is essential and the notable ones include neutrino decoupling, inflation, primordial nucleosynthesis, decoupling of dark matter etc.

1.2.3.1 Equilibrium thermodynamics

In equilibrium thermodynamics, the most essential realization in case of scattering is that the distributions of particles involved, obey the Bose-Einstein or Fermi-Dirac distribution (kinetic equilibrium). The description follows with two parameters, temperature (T) and chemical potential (μ) , with μ is conserved during the interaction (chemical equilibrium), given as

$$f(p) = \frac{1}{e^{(E(p)-\mu)} + 1},\tag{1.33}$$

E(p) infers the energy of the particle with momentum p and +(-) is taken for fermions (bosons). The number and energy densities at the early times are given by

$$n = \frac{g}{(2\pi)^3} \int d^3p \ f(p),$$

$$\rho = \frac{g}{(2\pi)^3} \int d^3p \ E(p) \ f(p),$$
(1.34)

where g denotes the internal degree of freedom of the particle. Neglecting the small chemical potentials of the particles in early times, we get

$$n = \frac{g}{2\pi^2} \int_0^\infty dp \frac{p^2}{e^{E(p)/T} \pm 1},$$

$$\rho = \frac{g}{2\pi^2} \int_0^\infty dp \frac{p^2 E(p)}{e^{E(p)/T} \pm 1}, \text{ where } E(p) = \sqrt{p^2 + m^2}.$$
(1.35)

Defining $\xi = p/T$ and using the standard integrals

$$\int_{0}^{\infty} \frac{\xi^{n}}{e^{\xi} - 1} d\xi = \zeta(n+1)\Gamma(n+1), \qquad \int_{0}^{\infty} \xi^{n} e^{-\xi^{2}} d\xi = \frac{1}{2}\Gamma\left(\frac{1}{2}(n+1)\right), \quad (1.36)$$

where $\zeta(z)$ denotes the Riemann zeta-function, the densities can be looked for, in two cases. In relativistic limit i.e., for $m \ll T$, the integrals give

$$n = \frac{\zeta(3)}{\pi^2} g T^3 \begin{cases} 1 & \text{bosons,} \\ \frac{3}{4} & \text{fermions,} \end{cases} \qquad \rho = \frac{\pi^2}{30} g T^4 \begin{cases} 1 & \text{bosons,} \\ \frac{7}{8} & \text{fermions.} \end{cases}$$
 (1.37)

For $m \gg T$ (non-relativistic limit), neglecting ± 1 in denominator, we obtain

$$n = g \left(\frac{mT}{2\pi}\right)^{3/2} e^{-m/T}, \qquad \rho = mn. \tag{1.38}$$

Looking at the number density, one can infer that the number density of massive particles is exponentially suppressed at low temperatures. Therefore, as the Universe has evolved from a hot dense state to the present cooled state, the number density of any massive particle today will be negligible. As the dark matter density still persists in the Universe, we now discuss the non-equilibrium thermodynamics to explain its abundance.

1.2.3.2 Non-equilibrium thermodynamics - Relic density

First, we suppose that the dark matter particle (say ψ) is stable with the lifetime more than the age of the Universe. We also suppose that only annihilations and inverse annihilations change the number of ψ 's or $\overline{\psi}$'s. The evolution of particle species in the out-of equilibrium state can be inferred from Boltzamann equation, given by [21, 29, 30]

$$\frac{dn_{\psi}}{dt} + 3Hn_{\psi} = -\int d\Pi_{\psi} d\Pi_{\overline{\psi}} d\Pi_{\chi} d\Pi_{\overline{\chi}} \times (2\pi)^{4} \delta^{4}(p_{\psi} + p_{\overline{\psi}} - p_{\chi} - p_{\overline{\chi}})
\times \left[|M|_{\psi\overline{\psi}\to\chi\overline{\chi}}^{2} f_{\psi} f_{\overline{\psi}}(1 \pm f_{\chi})(1 \pm f_{\overline{\chi}}) - |M|_{\chi\overline{\chi}\to\psi\overline{\psi}}^{2} f_{\chi} f_{\overline{\chi}}(1 \pm f_{\psi})(1 \pm f_{\overline{\psi}}) \right],$$
(1.39)

where $d\Pi = \frac{g}{(2\pi)^3} \frac{d^3p}{2E}$. In the above equation, 1+f applies for boson and 1-f stands for fermion, denoting the Bose enhancement and Pauli blocking respectively. For systems at temperatures $T < E_i$, Maxwell-Boltzmann statistics can be applied for all species i.e., $f_i = e^{-E_i/T}$ and the factors can be taken as, $1 \pm f \simeq 1$. Assuming CP-invariance i.e., $|M|^2_{\psi\bar{\psi}\to\chi\bar{\chi}} = |M|^2_{\chi\bar{\chi}\to\psi\bar{\psi}}$, the Boltzmann equation simplifies to

$$\frac{dn_{\psi}}{dt} + 3Hn_{\psi} = -\int d\Pi_{\psi} d\Pi_{\overline{\psi}} d\Pi_{\chi} d\Pi_{\overline{\chi}} \times (2\pi)^{4} \delta^{4}(p_{\chi} + p_{\overline{\chi}} - p_{\psi} - p_{\overline{\psi}})
\times |M|^{2} \times \left[f_{\psi} f_{\overline{\psi}} - f_{\chi} f_{\overline{\chi}} \right].$$
(1.40)

Assuming the output particles $\chi, \overline{\chi}$ stay in thermal equilibrium,

$$f_{\chi} = e^{-E_{\chi}/T},$$

$$f_{\overline{\chi}} = e^{-E_{\overline{\chi}}/T}.$$
(1.41)

The δ -function enforces energy conservation, $E_{\psi} + E_{\overline{\psi}} = E_{\chi} + E_{\overline{\chi}}$, therefore,

$$f_{\chi}f_{\overline{\chi}} = e^{-(E_{\chi} + E_{\overline{\chi}})/T} = e^{-(E_{\psi} + E_{\overline{\psi}})/T} = f_{\psi}^{EQ} f_{\overline{\psi}}^{EQ}.$$
 (1.42)

Thus, the Boltzmann equation (1.40), takes the form

$$\frac{dn_{\psi}}{dt} + 3Hn_{\psi} = -\langle \sigma | v | \rangle \left[n_{\psi}^2 - \left(n_{\psi}^{\text{EQ}} \right)^2 \right], \tag{1.43}$$

where we have used

$$\langle \sigma | v | \rangle = \left(n_{\psi}^{\text{EQ}} \right)^{-2} \int d\Pi_{\psi} \ d\Pi_{\overline{\psi}} \ d\Pi_{\overline{\chi}} \ d\Pi_{\overline{\chi}} \times (2\pi)^{4} \delta^{4} (p_{\psi} + p_{\overline{\psi}} - p_{\chi} - p_{\overline{\chi}}) |M|^{2} e^{-(E_{\psi} + E_{\overline{\psi}})/T}.$$

$$(1.44)$$

Considering a dimensionless parameter $Y_{\psi} = n_{\psi}/s$, where $s = \frac{2\pi^2}{45}g_{\star s}T^3$ denotes the entropy density¹. Conservation of entropy density in the comoving volume implies $sa^3 =$ constant. Thus, the above equation can be written as

$$\frac{dY_{\psi}}{dt} = -s\langle \sigma | v | \rangle \left[Y_{\psi}^{2} - \left(Y_{\psi}^{\text{EQ}} \right)^{2} \right]. \tag{1.46}$$

It is useful to define a dimensionless parameter $x = m_{\psi}/T$ as the interaction depends on temperature. Furthermore, during the radiation-dominated epoch t and x satisfy

$$t = 0.301 g_{\star}^{-1/2} M_{\rm Pl} \frac{1}{T^2} = 0.301 g_{\star}^{-1/2} M_{\rm Pl} \frac{x^2}{m_{\rm ph}^2}.$$
 (1.47)

Here m_{ψ} denotes the DM mass, $M_{\rm Pl} = 1.22 \times 10^{19}$ GeV and g_{\star} is a temperature dependent function that counts the effectively relativistic degrees of freedom² given by

$$g_{\star}(T) = \sum_{i=\text{bosons}} g_i \left(\frac{T_i}{T}\right)^4 + \frac{7}{8} \sum_{i=\text{fermions}} g_i \left(\frac{T_i}{T}\right)^4. \tag{1.48}$$

$$g_{\star s}(T) = \sum_{i = \text{bosons}} g_i \left(\frac{T_i}{T}\right)^3 + \frac{7}{8} \sum_{i = \text{fermions}} g_i \left(\frac{T_i}{T}\right)^3. \tag{1.45}$$

¹Here $g_{\star s}$ counts the effectively relativistic degrees of freedom contributing to entropy density

 $^{^2 {\}rm In}$ early Universe, g_{\star} and $g_{\star s}$ are equal as all particles are at same temperature.

Now, the Boltzmann equation (1.46) simplifies to

$$\frac{dY_{\psi}}{dx} = -\frac{xs}{H(m)} \langle \sigma | v | \rangle \left[Y_{\psi}^{2} - \left(Y_{\psi}^{EQ} \right)^{2} \right]
= -\frac{2\pi^{2} g_{\star s} m_{\psi}^{3}}{45x^{2} H(m)} \langle \sigma | v | \rangle \left[Y_{\psi}^{2} - \left(Y_{\psi}^{EQ} \right)^{2} \right],$$
(1.49)

where $H(m_{\psi}) = 1.67 g_{\star}^{1/2} \frac{m_{\psi}^2}{M_{\rm Pl}}$. Eqn. (1.49) is a specific form of 'Riccati' equation, which does not have any analytic solutions. However, the behavior of the solution can be identified by using approximate methods. The annihilation cross-section in general can have velocity dependence i.e., $\langle \sigma v \rangle = \langle \sigma v \rangle_0 x^{-n}$, where n = 0 stands for s-wave annihilation, n = 1 corresponds to p-wave annihilation. Now, the Riccati equation becomes

$$\frac{dY_{\psi}}{dx} = -\lambda x^{-(n+2)} \left[Y_{\psi}^2 - \left(Y_{\psi}^{\text{EQ}} \right)^2 \right]. \tag{1.50}$$

Here,

$$\lambda = \frac{2\pi^2 g_{\star s}}{45} \frac{m_{\psi}^3 \langle \sigma v \rangle_0}{H(m)} = \frac{0.264 g_{\star s} m_{\psi} M_{\text{Pl}} \langle \sigma v \rangle_0}{g_{\star}^{1/2}}.$$
 (1.51)

At equilibrium,

$$Y_{\psi}^{\rm EQ} = \frac{n_{\psi}^{\rm EQ}}{s} = 0.145 \frac{g}{g_{\star s}} x^{\frac{3}{2}} e^{-x}, \quad \text{where} \quad n_{\psi}^{\rm EQ} = g \left(\frac{m_{\psi} T}{2\pi}\right)^{3/2} e^{-m_{\psi}/T}. \tag{1.52}$$

Moving on to the differential equation of Eqn. (1.50), and defining $\Delta_{\psi} = Y_{\psi} - Y_{\psi}^{\text{EQ}}$ yields

$$\Delta_{\psi}' = -\frac{dY_{\psi}^{EQ}}{dx} - \lambda x^{-(n+2)} \Delta_{\psi} \left(2Y_{\psi}^{EQ} + \Delta_{\psi} \right), \tag{1.53}$$

where prime denotes d/dx. For $1 < x \ll x_f$ i.e., at early times $(x_f = m/T_f \text{ stands for freeze-out parameter})$, Y_{ψ} traces Y_{ψ}^{EQ} which implies Δ_{ψ} and $\left|\Delta'_{\psi}\right|$ are small. Setting $\Delta'_{\psi} = 0$, the solution is given by

$$\Delta_{\psi} = \frac{1}{2} \left(1 - \frac{3}{2x} \right) \frac{x^{(n+2)}}{\lambda} \simeq \frac{x^{(n+2)}}{2\lambda} ,$$
(1.54)

where we have used the expression for Y_{ψ}^{EQ} in Eqn. (1.52) and neglected higher order terms in Δ_{ψ} . For late times i.e., $x \gg x_f$, $\Delta_{\psi} \simeq Y_{\psi}$ and the terms of Y_{ψ}^{EQ} and its derivative can be dropped, yielding

$$\frac{d\Delta_{\psi}}{dx} = -\frac{\lambda \Delta_{\psi}^2}{x^{(n+2)}} \,. \tag{1.55}$$

Integrating from $x = x_f$ to $x = \infty$, we get

$$\Delta_{\psi} = Y_{\infty} = \frac{(n+1)x_f^{(n+1)}}{\lambda} \ .$$
 (1.56)

Relic density:

Now, relic density at freeze-out can be computed by the formula

$$\Omega_{\psi} = \frac{\rho_{\psi}}{\rho_{\text{crit}}} = \frac{m_{\psi} Y_{\infty} s_{0}}{\rho_{\text{crit}}}$$

$$= 1.07 \times 10^{9} \frac{(n+1) x_{f}^{(n+1)} g_{\star}^{1/2} \text{ GeV}^{-1}}{h^{2} g_{\star s} M_{\text{Pl}} \langle \sigma v \rangle_{0}}, \qquad (1.57)$$

where, we have used

$$\rho_{\text{crit}} = \left(\frac{3H_0^2}{8\pi G}\right) = 1.88 \times 10^{-29} h^2 \text{ g cm}^{-3}, \text{ with } H_0 = 100h \text{ km sec}^{-1} \text{ Mpc}^{-1}. (1.58)$$

The current values of Hubble constant and entropy density are $H_0 = 67.27 \pm 0.60 \text{ km sec}^{-1} \text{ Mpc}^{-1}$ [22] and $s_0 = 2890 \text{ cm}^{-3}$ respectively. The freeze-out parameter x_f takes the value $x_f \gtrsim 3$. Due to annihilations, the abundance can further gets reduced, the present day abundance can be estimated by [31]

$$\Omega_{\psi}h^2 = \frac{1.07 \times 10^9 \text{ GeV}^{-1}}{g_*^{1/2}M_{\text{pl}}} \frac{1}{J(x_f)},$$
(1.59)

where $J(x_f)$ reads as

$$J(x_f) = \int_{x_f}^{\infty} \frac{\langle \sigma v \rangle(x)}{x^2} dx. \tag{1.60}$$

The thermally averaged annihilation cross section $\langle \sigma v \rangle$ can be computed in more general method [32]

$$\langle \sigma v \rangle(x) = \frac{x}{8m_{\psi}^5 K_2^2(x)} \int_{4m_{\psi}^2}^{\infty} \sigma \times (s - 4m_{\psi}^2) \sqrt{s} K_1\left(\frac{x\sqrt{s}}{m_{\psi}}\right) ds. \tag{1.61}$$

In the above formula, s stands for center of mass energy, K_1 and K_2 denote the modified Bessel functions.

WIMP Miracle

For s-wave, Eqn. (1.57) can be written as

$$\Omega_{\psi}h^{2} \simeq 0.1 \left(\frac{1.6 \times 10^{-9} \text{ GeV}^{-2}}{\langle \sigma v \rangle_{0}}\right) \left(\frac{106.75}{g_{\star}}\right)^{1/2} \left(\frac{x_{f}}{20}\right) \left(\frac{1.22 \times 10^{19} \text{ GeV}}{M_{\text{Pl}}}\right).$$
(1.62)

Hence, WIMP $(\sigma v \sim 10^{-9} \text{ GeV}^{-2})$ is the best motivated candidate for DM.

1.2.3.3 Direct detection

In principle, the dark matter can scatter off the detector, is termed as direct detection. In the process of scattering, it suffers a very low recoil (\sim keV) due to weak interaction strength. Analyzing the experimental data by filtering out the background is a challenging task. So, such detectors are installed in very low background environment to reduce the noise in the signal.

To a good approximation, the total scattering cross-section (σ) can be manifested in terms of cross-section at zero momentum transfer (σ_0) as the momentum transfers taking place are usually small in comparison to the typical nuclear scales. The total scattering cross-section is given by [33]

$$\sigma = \frac{\sigma_0}{4\mu^2 v^2} \int d|\bar{q}|^2 F^2(|\bar{q}|^2), \tag{1.63}$$

where v stands for velocity of DM relative to target, $F(|\bar{q}|^2)$ denotes the form factor satisfying F(0) = 1, μ denotes the reduced mass of WIMP-nucleon system and

$$\sigma_0 = \int_0^{4\mu^2 v^2} d|\bar{q}|^2 \frac{d\sigma(q=0)}{d|\bar{q}|^2}.$$
 (1.64)

WIMP-nucleon cross section has two parts, namely spin-independent (SI) and spin-dependent (SD) contributions. Scalar part of SI contribution arises from the interaction term of the form $\overline{\psi}\psi\overline{q}q$, while the term $\overline{\psi}\gamma^{\mu}\psi\overline{q}\gamma_{\mu}q$ accounts for vectorial part of SI contribution. The axial vector term $\overline{\psi}\gamma^{\mu}\gamma^{5}\psi\overline{q}\gamma_{\mu}\gamma_{5}q$ is responsible for SD contribution. The cross-sections for each case can be illustrated as follows [34].

Scalar interaction:

We start with the scalar Lagrangian,

$$\mathcal{L}_S = a_q \overline{\psi} \psi \overline{q} q. \tag{1.65}$$

The SI contribution at zero-momentum transfer is given by

$$\sigma_0^{SI} = \frac{\mu^2}{\pi} \left[Z f_p + (A - Z) f_n \right]^2. \tag{1.66}$$

With m_p , M_q denoting the proton and quark mass, the hadronic matrix element f_p is given as

$$\frac{f_p}{m_p} = \sum_{q=u,d,s} f_{Tq}^p \frac{a_q}{M_q} + \frac{2}{27} \left(1 - \sum_{q=u,d,s} f_{Tq}^p \right) \sum_{q=c,b,t} \frac{a_q}{M_q} . \tag{1.67}$$

	neutron	proton
Δ_u	-0.48 ± 0.02	0.78 ± 0.02
Δ_d	0.78 ± 0.02	-0.48 ± 0.02
Δ_s	-0.15 ± 0.02	-0.15 ± 0.02

Table 1.2: Spin fractions for quark content in proton and neutron.

Typical values for proton are $f_{Tu}^p = 0.020 \pm 0.004$, $f_{Td}^p = 0.026 \pm 0.005$ and $f_{Ts}^p = 0.118 \pm 0.062$ [35].

Vector interaction:

The interaction Lagrangian is of the form

$$\mathcal{L}_V = b_a \overline{\psi} \gamma^\mu \psi \overline{q} \gamma_\mu q. \tag{1.68}$$

The cross-section turns out to be

$$\sigma_0^{SI} = \frac{\mu^2}{\pi} \left[Z b_p + (A - Z) b_n \right]^2, \tag{1.69}$$

where $b_n = b_u + 2b_d$, $b_p = 2b_u + b_d$, and Z, A denote the atomic and mass number of the target nucleus.

Axial-Vector interaction:

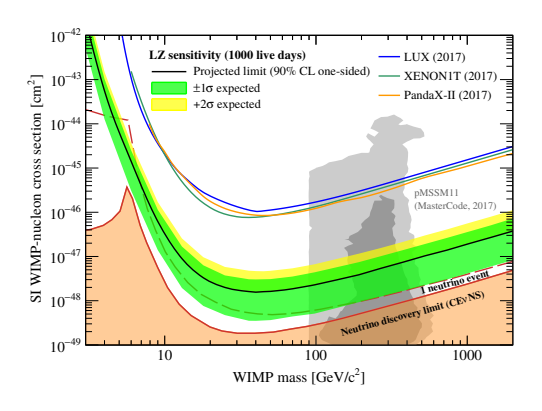
The interaction Lagrangian reads as

$$\mathcal{L}_{A-V} = d_q \overline{\psi} \gamma^\mu \gamma^5 \psi \overline{q} \gamma_\mu \gamma_5 q. \tag{1.70}$$

The corresponding SD contribution becomes

$$\sigma_0^{SD} = \frac{4\mu^2}{\pi} \left[\sum_{q=u,d,s} d_q \Delta_q \right]^2 J_N(J_N + 1). \tag{1.71}$$

Here, in case of free nucleon, Δ_q represents quark spin fractions in the nucleon and the values are provided in Table. 1.2. Currently, the most stringent bounds are provided by the collaborations LUX, XENON1T, PandaX-II on the spin-independent [36–38] contribution, PICO-60, LUX, PandaX-II collaborations on spin-dependent [39–41] cross-sections, displayed in Fig. 1.4.



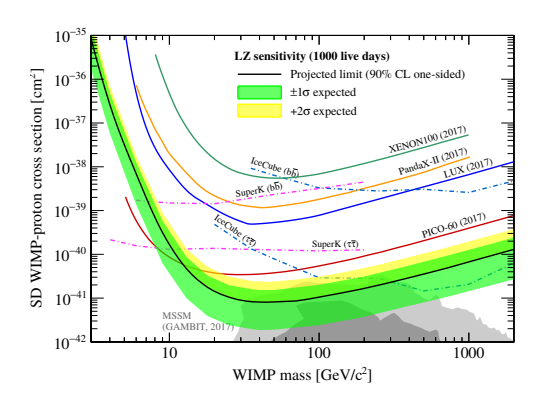


FIGURE 1.4: Current experimental upper limits on WIMP-nucleon cross-section [42]. Left panel shows the bound on SI contribution and right-panel depicts the same in case of SD cross-section.

1.3 Aim and overview of thesis

In the present chapter, we have given a brief overview of SM of elementary particles. Then, we have provided a short description about DM, starting with obliging hints, observables and the experimental limits obtained till the recent past. Concerning to DM, the known is little and the unknown is plenty. The knowns promote WIMP as the best motivated choice and the basic unknowns include mass, spin etc. A phenomenological survey of all possibilities is essential to elevate the chance of detecting this mysterious particle experimentally.

In this regard, we take a step forward to explore DM in few simple extensions of SM. We confine ourselves to fermion and scalar boson type DM. In chapter 2, we propose a $U(1)_{B-L}$ gauge extension of SM with suitable extended fermion and scalar sector to avoid the triangle gauge anomalies and generate masses to all the new particles respectively. We shall make a comprehensive investigation of singlet scalar DM in chapter 2 and Majorana DM in chapter 3. In the process, we invoke collider constraints, an interesting concept of massless Goldstone boson and its impact on DM relic density will be addressed. Chapter 4 discusses fermionic dark matter in connection to recent neutrino oscillation parameters. In chapter 5, we present the $L_{\mu} - L_{\tau}$ model to see how the dark matter and flavor observables affect the anomalies associated with the rare $B_{(s)} \to K^*(\phi) l^+ l^-$ decay modes. Finally, we summarize the thesis in chapter 6.

Chapter 2

Singlet scalar dark matter, massless Goldstone and neutrino mass in a new B-L model

2.1 Introduction to B-L frameworks

Models in which the difference between baryon and lepton number (B-L) is gauged, are economic extensions of the standard model [43–55]. One of the interesting aspects of this kind of models is that in the standard form, the presence of right-handed neutrinos and thus, the type-I seesaw mechanism for neutrino mass generation appears naturally. In addition, attempts have also been made within this economic extensions of SM where dark matter can be incorporated as well [56–66].

It is widely believed that WIMPs fulfill the necessary criteria of DM, not too far from the electroweak scale, which provides the opportunity to test them at the current or near future direct or indirect DM detection experiments. One of the fundamental questions is how to address the stability of the DM. Within the gauged B-L extensions of the SM, the stability of the DM can be taken care of by imposing an extra discrete symmetry on top of the gauge symmetry [51, 59–61, 64, 67]. In these class of models one of the right-handed neutrinos introduced for gauge anomaly cancellation is odd under the additional discrete symmetry and acts as a DM candidate. Attempts are also made to ensure the stability of the DM by choosing the appropriate B-L charge of DM [57, 58, 62, 63, 65]. There are other variants of gauged B-L extension of SM, where the additional fermions carry exotic integer value of B-L charge. The discussion of scalar

dark matter and neutrino phenomenology have been explored in the recent works [68–70], while a beautiful connection between dark matter abundance and matter-antimatter asymmetry has been investigated in Ref. [65] within WIMPy Leptogenesis.

In this chapter, we study the phenomenology of a scalar DM within the context of gauged B-L model without the introduction of any right-handed neutrinos, which are generally present in the conventional B-L theory. The induced gauge anomalies are cancelled by assigning appropriate B-L charges to the additional fermions. The key point to note here is that the stability of the scalar singlet dark matter is ensured by the peculiar choice of B-L charges and not by introducing any ad-hoc discrete symmetry. The proposed model provides another variant of the class of gauged B-Lmodels. Similar work on singlet scalar DM phenomenology has been recently explored in [57] where three right-handed neutrinos are added to make the model anomaly free and the model structure itself takes care of the stability of scalar DM. Dirac DM has also recently been investigated in a B-L model [71], where four exotic fermions are added to overcome the gauge anomalies. The current model describes a new variant of B-Lmodels with a different scalar content and exotic charges assigned to the newly added fermions. Moreover, the B-L charge assigned to the scalar DM and its corresponding annihilation channels, the arising parameter scan are different from the conventional B-L models.

To proceed with the chapter, we start with a brief note on triangle gauge anomalies in B-L scenarios and advertise the possible solutions to avoid them in a model design. We then flash light on the new $U(1)_{B-L}$ gauge extended framework. Then we move on to the technical details in the thorough investigation of singlet scalar dark matter in the vector boson and scalar portal context. We incorporate the collider constraints in the analysis and also mention a discussion related to neutrino mass generation at one-loop level. We finally give an appealing scenario of semi-annihilation in relic density context and conclude the chapter.

2.2 The model framework

It is believed that the B-L gauge extension of SM is the simplest model one can think of from the point of view of a self-consistent gauge theory where the difference between baryon and lepton number is promoted to local gauge symmetry. The gauge group of this simplest B-L model is $SU(2)_L \times U(1)_Y \times U(1)_{B-L}$, omitting the $SU(3)_C$ structure for simplicity. Originally, these models are motivated to cancel the triangle gauge anomalies

$$\mathcal{A}_1\left[U(1)_{B-L}^3\right], \ \mathcal{A}_2\left[\left(\text{gravity}\right)^2 \times U(1)_{B-L}\right],$$
 (2.1)

with the inclusion of right-handed neutrinos ν_{Ri} (i = 1, 2, 3) having the B-L charges -1 (the other gauge anomalies i.e., $\mathcal{A}_3 \left[SU(3)_C^2 \times U(1)_{B-L} \right]$ and $\mathcal{A}_4 \left[SU(2)_L^2 \times U(1)_{B-L} \right]$ trivially cancel). All the triangle gauge anomaly diagrams are shown in Fig. 2.1. These right-handed neutrinos can generate light neutrino masses via the type-I seesaw mechanism [72–75] and account for matter-antimatter asymmetry of the Universe. However, we present below few other possible solutions to overcome these anomalies.

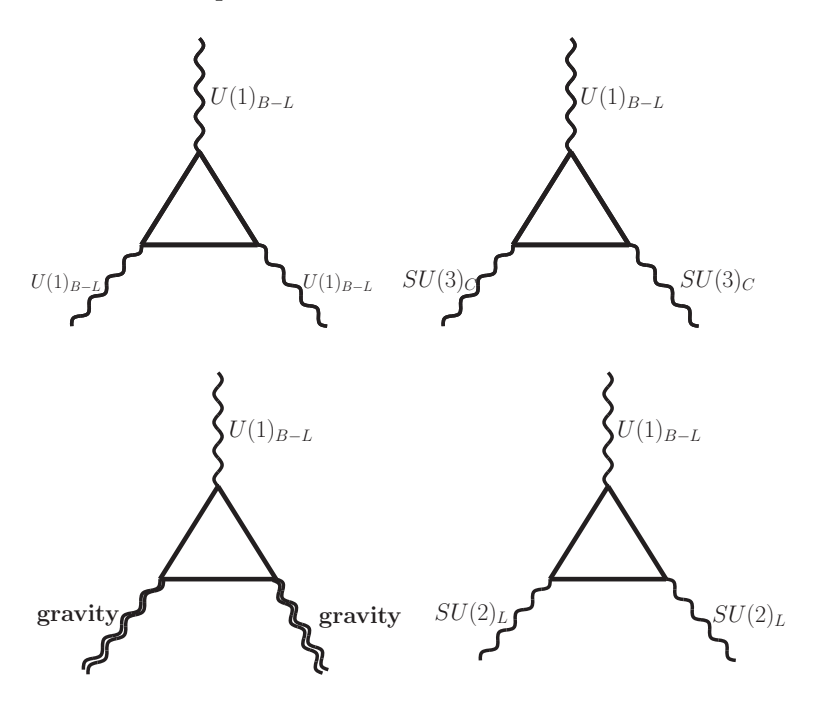


FIGURE 2.1: The one-loop triangle gauge anomalies for the present B-L model.

2.2.1 Anomaly cancellation with additional fermions having exotic B-L charges

In order to build an anomaly free B-L gauge extended framework, the charges of the additional fermion content have to satisfy two simple equations given as [76]

$$\sum_{i=1}^{n_R} x_i^3 = 3 \quad \text{and} \quad \sum_{i=1}^{n_R} x_i = 3, \tag{2.2}$$

where n_R denotes the number of additional fermions and x_i denotes the B-L charge of each fermion. $n_R = 1$ gives no solution and $n_R = 2$ gives a complex solution. $n_R \ge 3$ is always suitable to have real solutions. For instance, choosing the charges as -4, -4 and +5 is one such solution satisfying (2.2), and has been explored in [68, 69]. We show

below the explicit check

$$\mathcal{A}_{1}\left[U(1)_{B-L}^{3}\right] = \mathcal{A}_{1}^{\text{SM}}\left(U(1)_{B-L}^{3}\right) + \mathcal{A}_{1}^{\text{New}}\left(U(1)_{B-L}^{3}\right) = -3 + (4^{3} + 4^{3} + (-5)^{3}) = 0,$$

$$\mathcal{A}_{2}\left[\text{gravity}^{2} \times U(1)_{B-L}\right] \propto \mathcal{A}_{2}^{\text{SM}}\left(U(1)_{B-L}\right) + \mathcal{A}_{2}^{\text{New}}\left(U(1)_{B-L}\right) = -3 + (4 + 4 + (-5)) = 0.$$

$$(2.3)$$

There could also be a different solution to cancel the gauge anomalies, where one requires four additional fermions carrying fractional B-L charges (first proposed in Ref. [71]). We briefly describe below, how the non-trivial gauge anomalies $\mathcal{A}_1\left(U(1)_{B-L}^3\right)$ and $\mathcal{A}_2\left(\text{gravity}^2 \times U(1)_{B-L}\right)$ get cancelled by introducing four exotic fermions with fractional B-L charges, i.e., $\xi_L(4/3)$, $\eta_L(1/3)$, $\chi_{1R}(-2/3)$ and $\chi_{2R}(-2/3)$, where the corresponding B-L charges are shown in the parenthesis,

$$\mathcal{A}_{1} \left[U(1)_{B-L}^{3} \right] = \mathcal{A}_{1}^{\text{SM}} \left(U(1)_{B-L}^{3} \right) + \mathcal{A}_{1}^{\text{New}} \left(U(1)_{B-L}^{3} \right)
= -3 + \left[\left(\frac{4}{3} \right)^{3} + \left(\frac{1}{3} \right)^{3} + \left(\frac{2}{3} \right)^{3} + \left(\frac{2}{3} \right)^{3} \right] = 0,
\mathcal{A}_{2} \left[\text{gravity}^{2} \times U(1)_{B-L} \right] \propto \mathcal{A}_{2}^{\text{SM}} \left(U(1)_{B-L} \right) + \mathcal{A}_{2}^{\text{New}} \left(U(1)_{B-L} \right)
= -3 + \left[\left(\frac{4}{3} \right) + \left(\frac{1}{3} \right) + \left(\frac{2}{3} \right) + \left(\frac{2}{3} \right) \right] = 0.$$
(2.4)

In this work, we consider the first category of anomaly free model built up based on $U(1)_{B-L}$ extension of the standard model which includes three neutral exotic fermions N_{iR} (where i=1,2,3), with the B-L charges -4,-4 and +5. We include two more scalar singlets ϕ_1 and ϕ_8 to provide Majorana masses for all the exotic fermions and also to spontaneously break the B-L gauge symmetry. We also introduce a scalar dark matter $\phi_{\rm DM}$, singlet under the SM gauge group but charged under $U(1)_{B-L}$. It does not get any VEV, it does flow in the loop to generate light neutrino mass. The particle content of the present model is given in Table 2.1.

	Field	$SU(2)_L \times U(1)_Y$	$U(1)_{B-L}$
Fermions	$Q_L \equiv (u, d)_L^T$	(2,1/6)	1/3
	u_R	(1,2/3)	1/3
	d_R	(1, -1/3)	1/3
	$\ell_L \equiv (\nu, e)_L^T$	(2, -1/2)	-1
	e_R	(1,-1)	-1
	N_{1R}	(1,0)	-4
	N_{2R}	(1,0)	-4
	N_{3R}	(1,0)	5
Scalars	H	(2,1/2)	0
	$\phi_{ m DM}$	(1,0)	$n_{ m DM}$
	ϕ_1	(1,0)	-1
	ϕ_8	(1,0)	8

Table 2.1: Particle spectrum and their charges of the proposed $U(1)_{B-L}$ model.

The relevant terms in the Lagrangian for fermions in the present model is given by

$$\mathcal{L}_{Kin.}^{fermion} = \overline{Q}_{L} i \gamma^{\mu} \left(\partial_{\mu} + i g \frac{\vec{\tau}}{2} \cdot \vec{W}_{\mu} + \frac{1}{6} i g' B_{\mu} + \frac{1}{3} i g_{BL} Z'_{\mu} \right) Q_{L}
+ \overline{u}_{R} i \gamma^{\mu} \left(\partial_{\mu} + \frac{2}{3} i g' B_{\mu} + \frac{1}{3} i g_{BL} Z'_{\mu} \right) u_{R}
+ \overline{d}_{R} i \gamma^{\mu} \left(\partial_{\mu} - \frac{1}{3} i g' B_{\mu} + \frac{1}{3} i g_{BL} Z'_{\mu} \right) d_{R}
+ \overline{\ell}_{L} i \gamma^{\mu} \left(\partial_{\mu} + i g \frac{\vec{\tau}}{2} \cdot \vec{W}_{\mu} - \frac{1}{2} i g' B_{\mu} - i g_{BL} Z'_{\mu} \right) \ell_{L}
+ \overline{e}_{R} i \gamma^{\mu} \left(\partial_{\mu} - i g' B_{\mu} - i g_{BL} Z'_{\mu} \right) e_{R}
+ \overline{N}_{1R} i \gamma^{\mu} \left(\partial_{\mu} - 4i g_{BL} Z'_{\mu} \right) N_{1R} + \overline{N}_{2R} i \gamma^{\mu} \left(\partial_{\mu} - 4i g_{BL} Z'_{\mu} \right) N_{2R}
+ \overline{N}_{3R} i \gamma^{\mu} \left(\partial_{\mu} + 5i g_{BL} Z'_{\mu} \right) N_{3R} .$$
(2.5)

The interaction Lagrangian for the scalar sector is as follows

$$\mathcal{L}_{\text{scalar}} = (\mathcal{D}_{\mu}H)^{\dagger} (\mathcal{D}^{\mu}H) + (\mathcal{D}_{\mu}\phi_{\text{DM}})^{\dagger} (\mathcal{D}^{\mu}\phi_{\text{DM}}) + (\mathcal{D}_{\mu}\phi_{1})^{\dagger} (\mathcal{D}^{\mu}\phi_{1}) + (\mathcal{D}_{\mu}\phi_{8})^{\dagger} (\mathcal{D}^{\mu}\phi_{8}) - V(H, \phi_{\text{DM}}, \phi_{1}, \phi_{8}),$$
(2.6)

where the covariant derivatives are

$$\mathcal{D}_{\mu}H = \partial_{\mu}H + i\,g\vec{W}_{\mu L} \cdot \frac{\vec{\tau}}{2}\,H + i\frac{g'}{2}B_{\mu}H\,,$$

$$\mathcal{D}_{\mu}\phi_{\rm DM} = \partial_{\mu}\phi_{\rm DM} + i\,n_{\rm DM}g_{\rm BL}\,Z'_{\mu}\phi_{\rm DM}\,,$$

$$\mathcal{D}_{\mu}\phi_{1} = \partial_{\mu}\phi_{1} - ig_{\rm BL}\,Z'_{\mu}\phi_{1}\,,$$

$$\mathcal{D}_{\mu}\phi_{8} = \partial_{\mu}\phi_{8} + 8ig_{\rm BL}\,Z'_{\mu}\phi_{8},$$
(2.7)

and the scalar potential is given by

$$V(H, \phi_{\rm DM}, \phi_1, \phi_8) = V'(H, \phi_1, \phi_8) + \mu_{\rm DM}^2 \phi_{\rm DM}^{\dagger} \phi_{\rm DM} + \lambda_{\rm DM} (\phi_{\rm DM}^{\dagger} \phi_{\rm DM})^2 + \lambda_{\rm HD} (H^{\dagger} H) (\phi_{\rm DM}^{\dagger} \phi_{\rm DM}) + \lambda_{\rm D1} (\phi_{\rm DM}^{\dagger} \phi_{\rm DM}) (\phi_1^{\dagger} \phi_1) + \lambda_{\rm D8} (\phi_{\rm DM}^{\dagger} \phi_{\rm DM}) (\phi_8^{\dagger} \phi_8).$$

$$(2.8)$$

Here $\phi_{\rm DM} = \frac{S+iA}{\sqrt{2}}$ and

$$V'(H, \phi_1, \phi_8) = \mu_{\rm H}^2 H^{\dagger} H + \lambda_{\rm H} (H^{\dagger} H)^2 + \mu_1^2 \phi_1^{\dagger} \phi_1 + \lambda_1 (\phi_1^{\dagger} \phi_1)^2 + \mu_8^2 \phi_8^{\dagger} \phi_8 + \lambda_8 (\phi_8^{\dagger} \phi_8)^2 + \lambda_{\rm H1} (H^{\dagger} H) (\phi_1^{\dagger} \phi_1) + \lambda_{\rm H8} (H^{\dagger} H) (\phi_8^{\dagger} \phi_8) + \lambda_{18} (\phi_1^{\dagger} \phi_1) (\phi_8^{\dagger} \phi_8).$$
(2.9)

The Yukawa interaction for the present model is given by

$$\mathcal{L}_{\text{Yuk}} = Y^{u} \overline{Q_{L}} \widetilde{H} u_{R} + Y^{d} \overline{Q_{L}} H d_{R} + Y^{e} \overline{\ell_{L}} H e_{R}$$

$$+ \sum_{\alpha=1,2} y_{\alpha 3} \phi_{1} \overline{N_{\alpha R}^{c}} N_{3R} + \sum_{\alpha,\beta=1,2} y_{\alpha \beta} \phi_{8} \overline{N_{\alpha R}^{c}} N_{\beta R} .$$

$$(2.10)$$

From the above Yukawa interaction terms, one can write the exotic fermion mass matrix and diagonalize it to obtain non-zero masses to all the Majorana mass eigenstates.

2.2.2 Vacuum stability criteria and unitarity constraints

The vacuum stability conditions of the scalar potential are given by [77, 78]

$$\lambda_{\rm H} \geq 0, \ \lambda_{\rm HD} \geq 0, \ \lambda_{\rm DM} \geq 0, \ \lambda_{1} \geq 0, \ \lambda_{8} \geq 0,$$

$$\lambda_{\rm D1} + \sqrt{\lambda_{\rm DM}\lambda_{1}} \geq 0, \ \lambda_{\rm D8} + \sqrt{\lambda_{\rm DM}\lambda_{8}} \geq 0, \ \lambda_{18} + \sqrt{\lambda_{1}\lambda_{8}} \geq 0,$$

$$\sqrt{\lambda_{\rm DM}\lambda_{1}\lambda_{8}} + \lambda_{\rm D1}\sqrt{\lambda_{8}} + \lambda_{\rm D8}\sqrt{\lambda_{1}} + \lambda_{18}\sqrt{\lambda_{\rm DM}} \geq 0.$$
 (2.11)

Now we apply the tree-level perturbative unitarity constraints on the scattering processes of the scalar sector. The formula for the zeroth partial wave amplitude [79] is given by

$$a_0 = \frac{1}{32\pi} \sqrt{\frac{4p_f^{\text{CM}} p_i^{\text{CM}}}{s}} \int_{-1}^{+1} d(\cos \theta) \ T_{2\to 2}.$$
 (2.12)

Here $p_{i,(f)}^{\text{CM}}$ is the the centre of mass (CoM) momentum of the initial (final) state, s is the CoM energy, and $T_{2\to 2}$ denotes the full amplitude of each $2\to 2$ scattering processes. At high energies, the partial wave amplitudes i.e., the quartic couplings gets constrained from perturbative unitarity requirement $|\text{Re}(a_0)| \leq \frac{1}{2}$, giving

$$\lambda_{\rm H}, \lambda_1, \lambda_8, \lambda_{\rm DM} \le \frac{4\pi}{3},$$

$$\lambda_{\rm HD}, \lambda_{\rm D1}, \lambda_{\rm D8}, \lambda_{\rm H1}, \lambda_{\rm H8}, \lambda_{18} \le 4\pi.$$
(2.13)

2.3 Spontaneous symmetry breaking, masses and mixing

The spontaneous symmetry breaking of $SU(2)_L \times U(1)_Y \times U(1)_{B-L}$ down to SM gauge group $SU(2)_L \times U(1)_Y$ is implemented with the scalars ϕ_1 and ϕ_8 . Then the spontaneous symmetry breaking of SM gauge group to low energy theory is achieved by assigning a non-zero VEV to SM Higgs doublet. Similar kind of B-L model with additional scalars with ϕ_1 and ϕ_2 has been discussed in Ref [71], which avoids the presence of any accidental global U(1) symmetry because of cross term $\mu\left(\phi_1^{2\dagger}\phi_2+\phi_1^2\phi_2^{\dagger}\right)$. However, in our model gauge invariance forbids the inclusion of such cross terms between ϕ_1 and ϕ_8 , leading to an accidental global symmetry. As a result, after spontaneous symmetry breaking two massless Goldstone modes arise such that one linear combination of them will be eaten up by the neutral gauge boson corresponding to $U(1)_{B-L}$ gauge group and gives mass to Z' and the other orthogonal combination remains as massless Goldstone boson. We shall discuss the implications for this massless Goldstone boson in subsequent discussions.

The neutral components of the fields H, ϕ_1 and ϕ_8 can be parametrised in terms of real scalars and pseudoscalars as

$$H^{0} = \frac{1}{\sqrt{2}}(v+h) + \frac{i}{\sqrt{2}}z,$$

$$\phi_{1} = \frac{1}{\sqrt{2}}(v_{1}+h_{1}) + \frac{i}{\sqrt{2}}A_{1},$$

$$\phi_{8} = \frac{1}{\sqrt{2}}(v_{8}+h_{8}) + \frac{i}{\sqrt{2}}A_{8}.$$

Here the VEVs of the scalars are given as $\langle H \rangle = (0, v/\sqrt{2})^T$, $\langle \phi_1 \rangle = v_1/\sqrt{2}$, $\langle \phi_8 \rangle = v_8/\sqrt{2}$.

2.3.1 Mixing in scalar sector

In the scalar sector, the CP-even scalar mass matrix takes the form

$$M_E^2 = \begin{pmatrix} 2\lambda_{\rm H}v^2 & \lambda_{\rm H1}vv_1 & \lambda_{\rm H8}vv_8 \\ \lambda_{\rm H1}vv_1 & 2\lambda_1v_1^2 & \lambda_{18}v_1v_8 \\ \lambda_{\rm H8}vv_8 & \lambda_{18}v_1v_8 & 2\lambda_8v_8^2 \end{pmatrix}. \tag{2.14}$$

We assume that the Higgs doublet H mixes equally with the two singlets and the mixing is small so that the decay width of Higgs is consistent with LHC limits. We also consider the VEVs of the new singlets $v_1 \simeq v_8 \gg v$ and the couplings $\lambda_{H1,H8} \ll \lambda_H$, $\lambda_1 \simeq \lambda_8$

then the mass matrix takes a simple form

$$M_E^2 \simeq \begin{pmatrix} a & a & a \\ a & y & b \\ a & b & y \end{pmatrix}. \tag{2.15}$$

Under the assumption of minimal Higgs mixing, the unitary matrix that connects the flavor and mass states is

$$U \simeq \begin{pmatrix} 1 & \beta \cos \alpha - \beta \sin \alpha & \beta \cos \alpha + \beta \sin \alpha \\ -\beta & \cos \alpha & \sin \alpha \\ -\beta & -\sin \alpha & \cos \alpha \end{pmatrix}. \tag{2.16}$$

Here $\beta = \frac{a}{b+y-a}$ is the mixing parameter for $H - \phi_{1,8}$ and $\alpha = \frac{5\pi}{4}$ denotes $\phi_1 - \phi_8$ mixing, obtained from the normalized eigenvector matrix of M_E^2 (2.15). Thus, the relation between flavor and mass eigenstates is given by

$$\begin{pmatrix} h \\ h_1 \\ h_8 \end{pmatrix} = U \begin{pmatrix} H_1 \\ H_2 \\ H_3 \end{pmatrix} = \begin{pmatrix} H_1 - H_3 \beta \sqrt{2} \\ -H_1 \beta - \frac{H_2}{\sqrt{2}} - \frac{H_3}{\sqrt{2}} \\ -H_1 \beta + \frac{H_2}{\sqrt{2}} - \frac{H_3}{\sqrt{2}} \end{pmatrix}. \tag{2.17}$$

The scalar couplings can be written as

$$2\lambda_{H}v^{2} = \lambda_{H1}vv_{1} = \frac{M_{H_{1}}^{2}}{(1 - 2\beta + 2\beta^{2})},$$

$$2\lambda_{1}v_{1}^{2} = 2\lambda_{8}v_{8}^{2} = \frac{(\beta + 1)M_{H_{3}}^{2} + (1 + \beta + 4\beta^{2})M_{H_{2}}^{2}}{2(1 + \beta + 4\beta^{2})},$$

$$\lambda_{18}v_{1}v_{8} = \frac{(\beta + 1)M_{H_{3}}^{2} - (1 + \beta + 4\beta^{2})M_{H_{2}}^{2}}{2(1 + \beta + 4\beta^{2})}.$$
(2.18)

Here H_1 denotes the SM Higgs with $M_{H_1} = 125.09$ GeV with v = 246 GeV. The mixing angle β can be written in terms of the physical scalar masses as

$$\beta = \frac{-M_{H_1}^2 + M_{H_3}^2 - \sqrt{-15M_{H_1}^4 - 10M_{H_3}^2 M_{H_1}^2 + M_{H_3}^4}}{4\left(2M_{H_1}^2 + M_{H_3}^2\right)}.$$
 (2.19)

Since the Higgs mass (M_{H_1}) is fixed, the mass parameter M_{H_3} defines the amount of mixing i.e., say $M_{H_3} \geq 1$ TeV implies $\beta \leq 0.016$. As discussed earlier, $A_{\rm G}$ appears as the longitudinal polarization of Z' and the physical massless Nambu Goldstone, $A_{\rm NG}$

are given by

$$A_{\rm G} = -\frac{8v_8}{\sqrt{v_1^2 + 64v_8^2}} A_8 + \frac{v_1}{\sqrt{v_1^2 + 64v_8^2}} A_1,$$

$$A_{\rm NG} = \frac{v_1}{\sqrt{v_1^2 + 64v_8^2}} A_8 + \frac{8v_8}{\sqrt{v_1^2 + 64v_8^2}} A_1.$$
(2.20)

It should be noted that the massless mode (A_{NG}) doesn't couple to any SM particle except Higgs, as we considered non-zero mixing between H and new scalars. It can give rise to an additional decay channel contributing to the invisible width of SM Higgs, given as

$$\Gamma(H_1 \to A_{\rm NG} A_{\rm NG}) \simeq \frac{M_{H_1}^3 \sin^2 \beta}{32\pi} \left(\frac{v_1^3 + 64v_8^3}{v_1 v_8 (v_1^2 + 64v_8^2)} \right)^2 ,$$
 (2.21)

where β denotes the mixing between H and new scalars. The invisible branching ratio of Higgs is given as

$$Br_{inv} = \frac{\Gamma(H_1 \to A_{NG} A_{NG})}{\Gamma(H_1 \to A_{NG} A_{NG}) + \cos^2 \beta \Gamma_{SM}^{Higgs}}.$$
 (2.22)

Using the constraint, $Br_{inv} \simeq 20\%$ [80, 81], $\Gamma_{SM}^{Higgs} \simeq 4$ MeV, we obtain the upper limit on the mixing angle as

$$|\tan \beta| \lesssim 2.2 \times 10^{-4} \times \left(\frac{v_1}{\text{GeV}}\right).$$
 (2.23)

Moreover, if the NG stays in thermal equilibrium with ordinary matter until muon annihilation, then it mimics as fractional cosmic neutrinos contributing nearly 0.39 to the effective number of neutrino species [82, 83] to give $N_{\rm eff} = 3.36^{+0.68}_{-0.64}$ at 95% C.L, a remarkable agreement with Planck data [84]. This illustration was done by working in the low mass regime of the physical scalar ($\simeq 500$ MeV) [82]. However, in [83] it was found that for masses $\gtrsim 4$ GeV the Goldstone bosons do not contribute to $N_{\rm eff}$. And since in the present work, we consider higher mass regime for the physical scalar spectrum to discuss the effect of NG on relic density, the contribution of NG to $N_{\rm eff}$ is not applicable.

2.3.2 Stability of singlet scalar dark matter

Dark matter particle has to be electrically neutral and should be stable over cosmological time scales. With this motivation numerous frameworks were proposed based on an unbroken discrete symmetry [85, 86] forbidding the decay of DM. Furthermore, this discrete symmetry is expected to break at Planck scale and thus, induce the decay of DM making it unstable. In the present model, we do not assume any ad-hoc discrete symmetry as such which can stabilize the DM. Rather we choose the B-L charge (say

 $n_{\rm DM}$) in such a way that there shall not be any decay channel as displayed in Fig. 2.2, for the DM $\phi_{\rm DM}$ [87]. For example, to avoid the cubic term in the scalar potential of the form $\phi_{\rm DM}H_iH_j$ where H_i, H_j denote the physical masses for any of the scalars H, ϕ_1 or ϕ_8 , the possible values of $n_{\rm DM}=0,\pm 2,\pm 7,\pm 9,\pm 16$ are not allowed. Similarly if we do not want terms like $\phi_{\rm DM}H_iH_jH_k$, the value of $n_{\rm DM}$ is restricted to $n_{\rm DM}\neq\pm 1,\pm 3,\pm 6,\pm 8,\pm 10$. Thus, the allowed values of $n_{\rm DM}$ are $\pm 4,\pm 5$ and fractional charges. The approach of ensuring stability of scalar DM particle with the model structure has been recently implemented in a B-L model with right-handed neutrinos [57], while our model is one such variant with a modified scalar content and variety of exotic charges assigned to the additional fermion content of the B-L model.

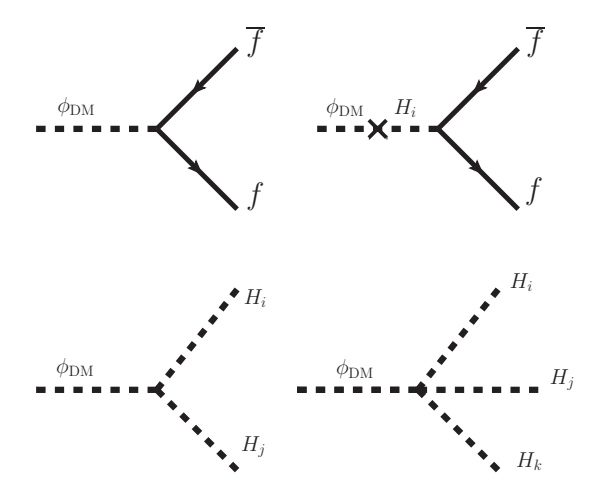


FIGURE 2.2: Feynman diagrams leading to decay of scalar singlet dark matter $\phi_{\rm DM}$. The choice of B-L charge to forbid these decay and stability of scalar singlet dark matter $\phi_{\rm DM}$ is discussed in the text.

We choose $n_{\rm DM}=4$ to ensure the stability of the scalar singlet $\phi_{\rm DM}$ and study its phenomenology in the prospects of dark matter observables such as relic abundance and direct detection cross section. Based on the structure of the model built, the DM can have scalar and gauge portal interactions. We proceed to study in detail the behaviour of DM observables separately in dual portal scenario.

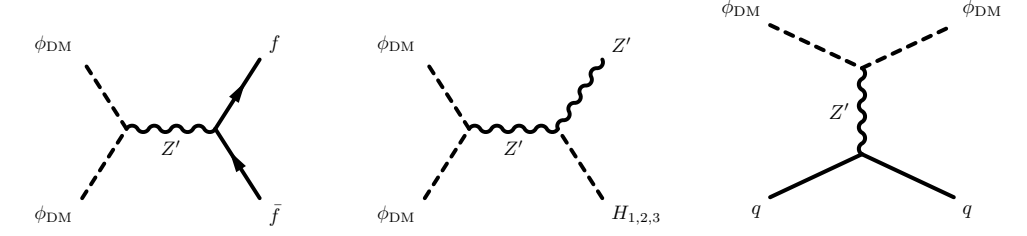


FIGURE 2.3: Feynman diagrams for dark matter annihilation (left and middle) and scattering of DM from nucleon/quark (right panel) through Z' exchange. First two diagrams contribute to the relic density observable and the third one is appropriate in direct detection studies.

2.4 Z' portal phenomenology

2.4.1 Relic abundance

The channels that contribute to relic density are shown in the left and middle panels of Fig. 2.3 and the expression for the corresponding annihilation cross sections are

$$\hat{\sigma}_{ff} = \sum_{f} \frac{n_{\rm DM}^{2} (n_{\rm BL}^{f})^{2} g_{\rm BL}^{4} c_{f}}{12\pi s} \frac{(s - 4M_{\rm DM}^{2})(s + 2M_{f}^{2})}{\left[(s - M_{Z'}^{2})^{2} + M_{Z'}^{2} \Gamma_{Z'}^{2}\right]} \frac{(s - 4M_{f}^{2})^{\frac{1}{2}}}{(s - 4M_{\rm DM}^{2})^{\frac{1}{2}}},$$

$$\hat{\sigma}_{Z'H_{i}} = \frac{n_{\rm DM}^{2} g_{\rm BL}^{6} (C_{H_{i}})^{2}}{16\pi s} \frac{(s - 4M_{\rm DM}^{2})}{\left[(s - M_{Z'}^{2})^{2} + M_{Z'}^{2} \Gamma_{Z'}^{2}\right]} \left[1 + \frac{(s - (M_{Z'} + M_{H_{i}})^{2})(s - (M_{Z'} - M_{H_{i}})^{2})}{12sM_{Z'}^{2}}\right] \frac{\left[(s - (M_{Z'} + M_{H_{i}})^{2})(s - (M_{Z'} - M_{H_{i}})^{2})\right]^{\frac{1}{2}}}{\left[s(s - 4M_{\rm DM}^{2})\right]^{\frac{1}{2}}},$$

$$\frac{\left[(s - (M_{Z'} + M_{H_{i}})^{2})(s - (M_{Z'} - M_{H_{i}})^{2})\right]^{\frac{1}{2}}}{\left[s(s - 4M_{\rm DM}^{2})\right]^{\frac{1}{2}}},$$
(2.24)

where i = 1, 2, 3 and

$$C_{H_1} = 2\beta(64v_8 + v_1),$$

 $C_{H_2} = \sqrt{2}(64v_8 - v_1),$
 $C_{H_2} = \sqrt{2}(64v_8 + v_1).$

The parameters c_f and $n_{\rm BL}^f$ denote the color charge and the B-L charge of the fermion f with mass M_f . $M_{Z'}$ is the mass of the heavy gauge boson Z' associated with the U(1) gauge extension, given by $M_{Z'} = g_{\rm BL} \sqrt{v_1^2 + 64 v_8^2}$ with the decay width $\Gamma_{Z'}$. With the annihilation cross section, relic abundance can be computed from Eqn. (1.59). We have implemented the model in LanHEP [89] to produce the model files required for micrOMEGAs [90–92] package to compute the relic abundance of scalar DM. The parameters that are fixed during the analysis are shown in Table. 2.2. The flexibility of gauge portal study is that, just two parameters are relevant i.e., $g_{\rm BL}$ and $M_{Z'}$. The value of $n_{\rm DM}$ not only stabilizes the DM paricle but also scales the annihilation cross section

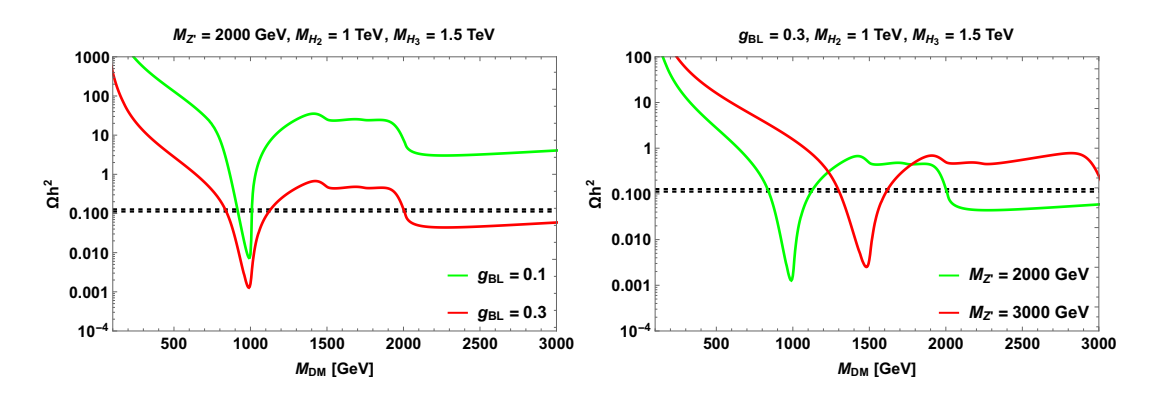


FIGURE 2.4: Variation of relic abundance Ωh^2 with the mass of DM shown with two representative values of $g_{\rm BL}$ (left panel) and $M_{Z'}$ (right panel) for $n_{\rm DM}=4$. Here the horizontal dashed lines denote the 3σ range in current relic density [88].

Parameters	$n_{ m DM}$	M_{H_2} [GeV]	M_{H_3} [GeV]	$v_{1,8} [{ m GeV}]$	β
Values	4	1000	1500	2000	0.007

Table 2.2: Fixed parameters for Z'-mediated DM observables.

thereby showing up in relic density. Fig. 2.4 displays the variation of DM abundance Ωh^2 with the singlet DM mass $M_{\rm DM}$ and the behavior with various parameters. All the curves in Fig. 2.4 reach the current relic density of Planck [88] near the resonance $(M_{\rm DM} \simeq \frac{M_{Z'}}{2})$. The gauge coupling $g_{\rm BL}$ scales the annihilation cross section i.e., lower couplings give lower annihilation cross section. The channels $SS \to f\bar{f}$ drive the relic density until the channels $SS \to Z'H_1$, $SS \to Z'H_2$ and $SS \to Z'H_3$ get kinematically allowed.

2.4.2 Direct searches

Now we look for the constraints on the model parameters due to direct detection limits. The effective Lagrangian for Z'-mediated t-channel processes shown in the extreme right panel of Fig. 2.3 is given as

$$\mathcal{L}_{\text{eff}}^{V} \supset -\frac{n_{\text{DM}}g_{\text{BL}}^{2}}{3M_{Z'}^{2}} \left(S\partial^{\mu}A - A\partial^{\mu}S\right) \bar{u}\gamma_{\mu}u - \frac{n_{\text{DM}}g_{\text{BL}}^{2}}{3M_{Z'}^{2}} \left(S\partial^{\mu}A - A\partial^{\mu}S\right) \bar{d}\gamma_{\mu}d. \tag{2.25}$$

Comparing with Eqn. (1.68), one can find the value of $b_{p,n}$ as

$$b_p = b_n = \frac{n_{\rm DM} g_{\rm BL}^2}{M_{Z'}^2}.$$

From Eqn. (1.69), the SI WIMP-nucleon contribution is given by

$$\sigma_{Z'} = \frac{\mu^2}{\pi} \frac{n_{\rm DM}^2 g_{\rm BL}^4}{M_{Z'}^4}.$$
 (2.26)

We see that the B-L charge $n_{\rm DM}$ remains as a scaling parameter in $\sigma_{Z'}$ alike relic density in Eqn. (2.24). We show in the left panel Fig. 2.5, the parameter space that satisfies the 3σ range in the current relic density limit [88] and the most stringent direct detection bound form XENON1T [37]. The right panel shows the WIMP-nucleon spin-independent cross section with the DM mass for the parameter space shown in the left panel.

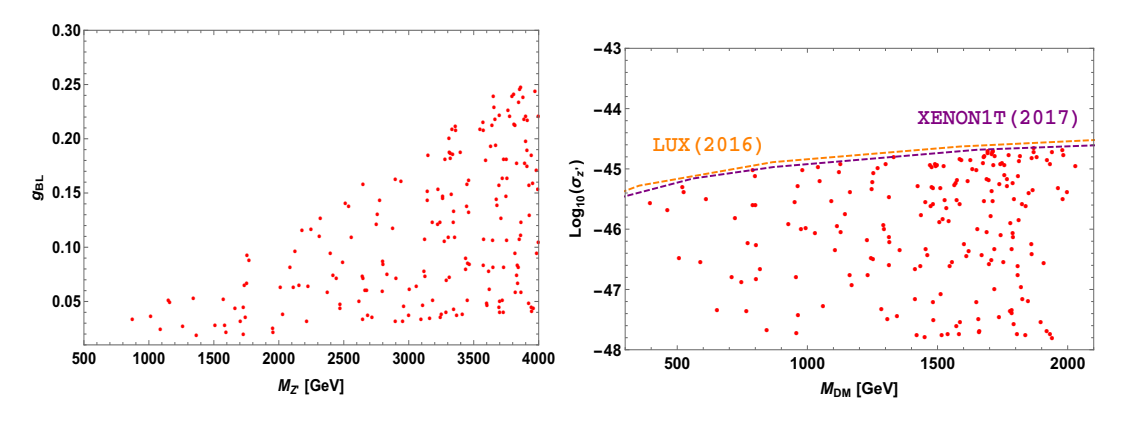


FIGURE 2.5: Left panel denotes the parameters space in the plane of $(M_{Z'}, g_{\rm BL})$ that satisfy the current relic density [88] in 3σ range and XENON1T [37]. The right panel depicts the WIMP-nucleon SI cross section with the mass of the scalar DM for the parameter space shown in the left panel. Here, the horizontal dashed lines denote the current bounds on spin-independent WIMP-nucleon cross section from the direct detection experiments LUX [36] and XENON1T [37].

2.4.3 Collider bounds

In recent past, both ATLAS and CMS experiments have provided extensive studies to search for new heavy resonances in both dilepton and dijet signals. It is found that these two experiments provide lower limit on Z'-boson with dileptons, resulting in stronger bounds than dijets due to relatively fewer background events. ATLAS results [93] from the study of dilepton signals for the Z' boson provide the most stringent limits on the heavy gauge boson mass $M_{Z'}$ and the gauge coupling $g_{\rm BL}$.

We use CalcHEP [94, 95] to compute the production cross section of Z'. In the left panel of Fig. 2.6, we show the Z' production cross section times the branching ratio of dilepton $(ee, \mu\mu)$ signal as a function of $M_{Z'}$. The black dashed line denotes the dilepton bound from ATLAS [96]. It is clear that the region below $M_{Z'} \simeq 3.7$ TeV is excluded

for $g_{\rm BL}=0.4$. For $g_{\rm BL}=0.1$, $M_{Z'}<2.3$ TeV is ruled out. We have $M_{Z'}\gtrsim 1.2$ TeV for $g_{\rm BL}=0.03$ and the mass region of $M_{Z'}\gtrsim 0.5$ TeV is allowed for $g_{\rm BL}=0.01$. The plot in the right panel of Fig. 2.6 shows the parameter space that satisfies 3σ range in the Planck relic density limit and the XENON1T constraint. The region to the right of both the dashed curves is consistent with LEP-II [97] i.e., $M_{Z'}/g_{\rm BL}>6.9$ TeV and ATLAS [96] dilepton limit. We see that the ATLAS gives more stringent limit in the mass region $M_{Z'}\lesssim 2.7$ TeV.

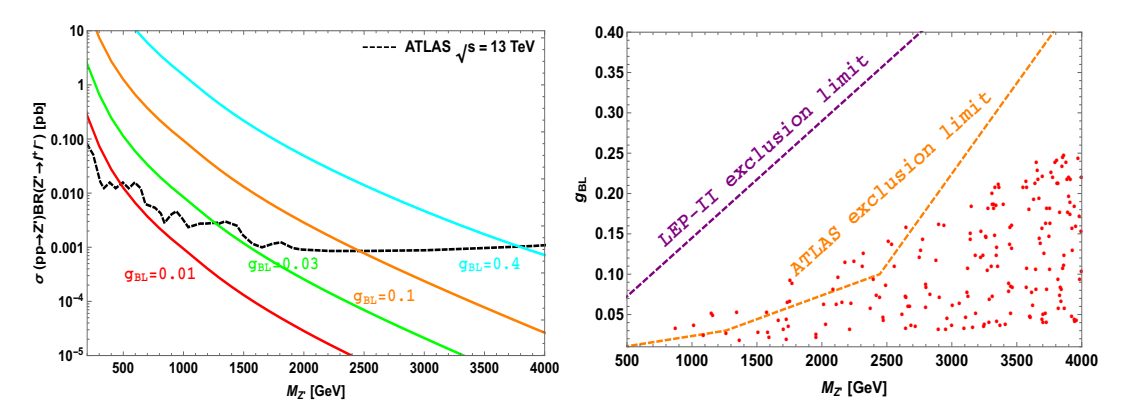


FIGURE 2.6: Dilepton constraints from ATLAS on the current model are shown here. The black dashed line in the left panel represents the exclusion limit from ATLAS [96], with the colored lines being the dilepton signal cross sections for various values of $g_{\rm BL}$ as a function of $M_{Z'}$. The right panel shows exclusion limits from LEP-II and ATLAS exclusion limits in the plane of $M_{Z'} - g_{\rm BL}$. The red points are consistent with the 3σ range of the relic density limit of Planck and the direct detection limits from XENON1T.

2.5 Scalar portal phenomenology

2.5.1 Relic density

With $n_{\rm DM}=4$, one can write a non-trivial term to the scalar potential as

$$V'' = V(H, \phi_{\rm DM}, \phi_1, \phi_8) + \frac{\mu_{\rm D8}}{2} \left[(\phi_{\rm DM})^2 \phi_8^{\dagger} + (\phi_{\rm DM}^{\dagger})^2 \phi_8 \right]. \tag{2.27}$$

The masses of real and imaginary components of $\phi_{\rm DM}$ are given by

$$M_S^2 = \mu_{\rm DM}^2 + \frac{\lambda_{\rm HD}}{2} v^2 + \frac{\lambda_{\rm D1}}{2} v_1^2 + \frac{\lambda_{\rm D8}}{2} v_8^2 + \frac{\mu_{\rm D8} v_8}{\sqrt{2}},$$

$$M_A^2 = \mu_{\rm DM}^2 + \frac{\lambda_{\rm HD}}{2} v^2 + \frac{\lambda_{\rm D1}}{2} v_1^2 + \frac{\lambda_{\rm D8}}{2} v_8^2 - \frac{\mu_{\rm D8} v_8}{\sqrt{2}}.$$
(2.28)

For simplicity, we consider $\lambda_{HD} = \lambda_{H1} = \lambda_{H8} = \lambda_{D}$. The expressions for annihilation

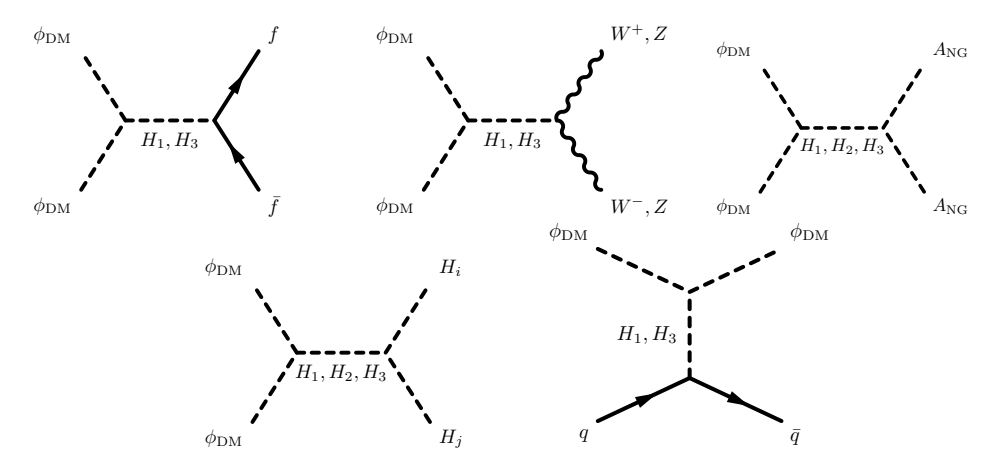


FIGURE 2.7: Feynman diagrams contributing to relic density in the scalar portal case except the figure of t-channel process is relevant in direct detection studies.

cross section of various channels that contribute to relic density shown in Fig. 2.7 are

$$\hat{\sigma}_{ff}^{S} = \frac{1}{8\pi v^{2} s} |F_{1}|^{2} \sum_{f} M_{f}^{2} c_{f} \frac{(s - 4M_{f}^{2})^{\frac{3}{2}}}{(s - 4M_{DM}^{2})^{\frac{1}{2}}}, \qquad (2.29)$$

$$\hat{\sigma}_{WW}^{S} = \frac{s}{16\pi v^2} |F_1|^2 \left(1 - \frac{4M_W^2}{s} + \frac{12M_W^4}{s^2} \right) \frac{(s - 4M_W^2)^{\frac{1}{2}}}{(s - 4M_{DM}^2)^{\frac{1}{2}}} , \qquad (2.30)$$

$$\hat{\sigma}_{ZZ}^{S} = \frac{s}{32\pi v^2} |F_1|^2 \left(1 - \frac{4M_Z^2}{s} + \frac{12M_Z^4}{s^2} \right) \frac{(s - 4M_Z^2)^{\frac{1}{2}}}{(s - 4M_{DM}^2)^{\frac{1}{2}}} , \qquad (2.31)$$

$$\hat{\sigma}_{NG}^{S} = \frac{1}{8\pi} \left(\frac{1}{v_1 v_8 (v_1^2 + 64v_8^2)} \right)^2 |F_2|^2 \frac{s^{\frac{3}{2}}}{(s - 4M_{DM}^2)^{\frac{1}{2}}} , \qquad (2.32)$$

where

$$\begin{split} F_1 = & \frac{\lambda_{\text{DH}1}}{\left[\left(s - M_{H_1}^2 \right) + i M_{H_1} \Gamma_{H_1} \right]} - \frac{\sqrt{2}\beta \lambda_{\text{DH}3}}{\left[\left(s - M_{H_3}^2 \right) + i M_{H_3} \Gamma_{H_3} \right]} \,, \\ F_2 = & - \frac{\lambda_{\text{DH}1} \beta(v_1^3 + 64 v_8^3)}{\left[\left(s - M_{H_1}^2 \right) + i M_{H_1} \Gamma_{H_1} \right]} + \frac{\lambda_{\text{DH}2}(v_1^3 - 64 v_8^3)}{\sqrt{2} \left[\left(s - M_{H_2}^2 \right) + i M_{H_2} \Gamma_{H_2} \right]} - \frac{\lambda_{\text{DH}3}(v_1^3 + 64 v_8^3)}{\sqrt{2} \left[\left(s - M_{H_3}^2 \right) + i M_{H_3} \Gamma_{H_3} \right]} \,. \end{split}$$

Finally, for the Higgs sector annihilation channels we have

$$\hat{\sigma}_{H_i H_j}^S = \frac{1}{16\pi s n_p!} |F_{ij}|^2 \frac{\left[(s - (M_{H_i} + M_{H_j})^2)(s - (M_{H_i} - M_{H_j})^2)\right]^{\frac{1}{2}}}{\left[s(s - 4M_{\rm DM}^2) \right]^{\frac{1}{2}}} , \qquad (2.33)$$

Coupling	Expression [GeV]
$\lambda_{ m DH1}$	$v\lambda_{\rm D} - \frac{1}{4}\beta(8v_1\lambda_{\rm D} - \sqrt{2}\mu_{\rm D8})$
$\lambda_{ m DH2}$	$-rac{\mu_{ m D8}}{4}$
$\lambda_{ m DH3}$	$-\sqrt{2}v_1\lambda_{\rm D} - \sqrt{2}v\beta\lambda_{\rm D} + \frac{\mu_{\rm D8}}{4}$

Table 2.3: Dark matter couplings to scalars.

where $n_p!$ denotes the permutation factor and

$$\begin{split} F_{ij} = & (1+2\beta^2) \lambda_{\mathrm{D}} \delta_{ij} + \frac{\lambda_{\mathrm{DH1}} \lambda_{1ij}}{\left[(s-M_{H_1}^2) + i M_{H_1} \Gamma_{H_1} \right]} + \frac{\lambda_{\mathrm{DH2}} \lambda_{2ij}}{\left[(s-M_{H_2}^2) + i M_{H_2} \Gamma_{H_2} \right]} \\ + & \frac{\lambda_{\mathrm{DH3}} \lambda_{3ij}}{\left[(s-M_{H_3}^2) + i M_{H_3} \Gamma_{H_3} \right]} \; . \end{split}$$

In the above expressions λ_{1ij} , λ_{2ij} , λ_{3ij} having mass dimension denote the trilinear scalar couplings with i, j = 1, 2, 3 and λ_{DHi} denote the coupling of the terms A^2H_i . We show in Fig. 2.8, the scalar portal relic abundance as a function of DM mass. The Planck limit on relic density is met near the resonance of three scalar propagators. The channels with H_1H_1 and $A_{\text{NG}}A_{\text{NG}}$ in final state can only give resonance near $M_{\text{DM}} \simeq \frac{M_{H_2}}{2}$. However, the coupling λ_{211} vanishes. Hence, the channel with NG pair plays a crucial role in giving the resonance in H_2 propagator for non-zero λ_{DH2} (= μ_{D8}) given in Table. 2.3. One can also notice that the coupling μ_{D8} induces mass splitting in the scalar components given in Eqn. (2.28), which is essential to generate light neutrino mass at one loop level to be discussed in the upcoming section.

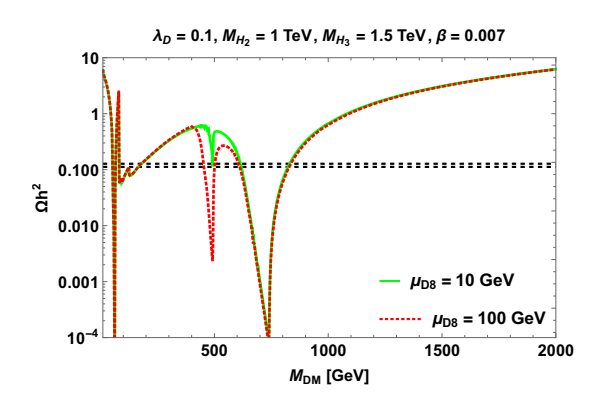


FIGURE 2.8: Variation of relic abundance Ωh^2 with the mass of DM for various values of μ_{D8} parameter.

2.5.2 Direct searches

In the scalar portal scenario, the effective interaction Lagrangian takes the form

$$\mathcal{L}_{\text{eff}}^S = a_q S S \overline{q} q. \tag{2.34}$$

where $a_q = \frac{M_q}{v M_{\rm DM}} \left[\frac{\lambda_{\rm DH1}}{M_{H_1}^2} - \frac{\sqrt{2} \lambda_{\rm DH3} \beta}{M_{H_3}^2} \right]$. Referring to Eqns. (1.66), (1.67), the SI WIMP-nucleon cross section is estimated as

$$\sigma_S = \frac{\mu^2}{\pi} f_p^2. \tag{2.35}$$

Varying the model parameters given in Table. 2.4, Fig. 2.9 left panel denotes the parameter space in $M_{\rm DM}-M_{H_3}$ plane satisfying 3σ range on current relic density limit by Planck and the right panel denotes the allowed parameter space (corresponding to the allowed parameters of the left panel), consistent with XENON1T limit. We see that the data points near the resonance of SM Higgs H_1 does not satisfy the XENON1T limit on WIMP-nucleon cross section.

Parameters	Range
$\mu_{\mathrm{D8}} \; [\mathrm{GeV}]$	10 - 100
$\lambda_{ m D}$	0.001 - 0.1
$v_{1,8} \; [\mathrm{GeV}]$	2000
M_{H_2} [GeV]	1000, 2000
M_{H_3} [GeV]	$M_{H_2} - 4000$
$M_{\rm DM}~{ m [GeV]}$	20 - 2000
β	0.001 - 0.016

Table 2.4: Parameters and their ranges for scalar portal analysis.

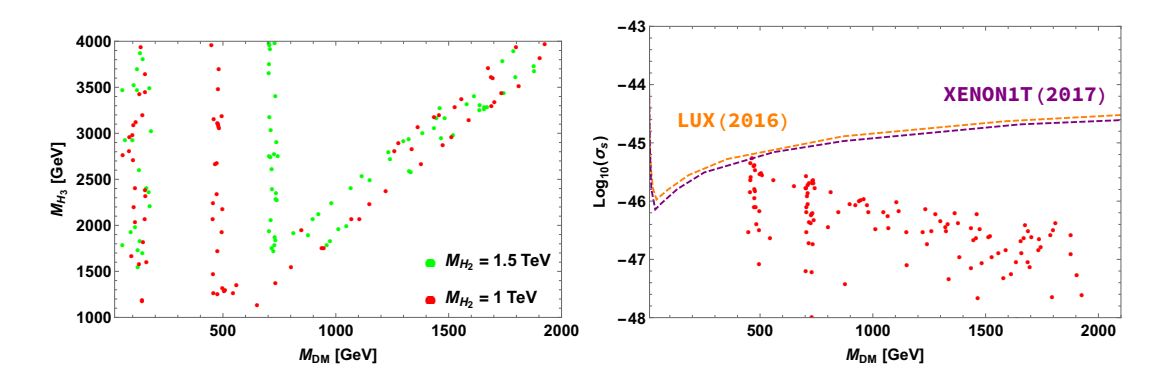


FIGURE 2.9: Region of $M_{\rm DM}-M_{H_3}$ that meets the 3σ range on current relic density limit of Planck in left panel. Right panel denotes the parameter space taken from left panel that satisfies the XENON1T limit as well. Dashed lines denote the upper limit on WIMP-nucleon cross section by LUX [36] and XENON1T [37].

Sl. No.	μ_{D8}	$\sqrt{ Y_{i\alpha_1}Y_{j\alpha_1} }$	$M_{\rm DM}~{ m [GeV]}$	$\Lambda \ [{ m TeV}]$	$m_{\nu} \; [{\rm GeV}]$	Ωh^2	$Log_{10}\sigma_{\rm S} \ [{\rm cm}^2]$
1.	96.8	0.026	448	50	4.01×10^{-11}	0.1154	-46.517
2.	21.3	0.056	483	50	4.09×10^{-11}	0.123	-46.376
3.	21.3	0.22	483	100	3.95×10^{-11}	0.123	-46.376

Table 2.5: Sample benchmark for radiative ν -mass.

2.6 Light neutrino mass

The light neutrino mass in this model can be achieved by radiative mechanism. The model structure permits us to write a dim-6 Yukawa interaction term of the form

$$\frac{1}{\Lambda^2} \sum_{\alpha=1,2} Y_{i\alpha} \overline{(\ell_L)}_i \tilde{H} N_{\alpha R} \phi_{\rm DM} \phi_1. \tag{2.36}$$

Now, it is possible to generate the light neutrino mass at one loop level as shown in Fig. 2.10. We use Eqn. (2.28) and also assume that the masses of real and imaginary parts of $\phi_{\rm DM}$ satisfy the relation $(M_S^2 + M_A^2)/2 \gg M_S^2 - M_A^2 = \sqrt{2}\mu_{\rm D8}v_8$, then the expression for the radiatively generated neutrino mass is given by [85]

$$(\mathcal{M}_{\nu})_{ij} = \frac{\sqrt{2}\mu_{\rm D8}v_8v^2v_1^2}{16\pi^2\Lambda^4} \sum_{\alpha=1}^2 \frac{Y_{i\alpha}Y_{j\alpha}M_{D\alpha}}{m_{\phi_{\rm DM}}^2 - M_{D\alpha}^2} \left[1 - \frac{M_{D\alpha}^2}{m_{\phi_{\rm DM}}^2 - M_{D\alpha}^2} \ln \frac{m_0^2}{M_{D\alpha}^2} \right], \qquad (2.37)$$

where we denote $m_{\phi_{\rm DM}}^2=(M_S^2+M_A^2)/2$ and $M_{D\alpha}$ represent masses of the exotic fermion mass eigenstates. If $M_{D\alpha}^2\gg m_{\phi_{\rm DM}}^2$, then

$$(\mathcal{M}_{\nu})_{ij} = \frac{\sqrt{2}\mu_{\rm D8}v_8v^2v_1^2}{16\pi^2\Lambda^4} \sum_{\alpha=1}^2 \frac{Y_{i\alpha}Y_{j\alpha}}{M_{D\alpha}} \left[\ln \frac{M_{D\alpha}^2}{m_{\phi_{\rm DM}}^2} - 1 \right]. \tag{2.38}$$

Considering $(v_1, v_8, M_{D\alpha}) \sim (2, 2, 3)$ TeV, we show sample benchmark values in Table. 2.5 that satisfy Planck, XENON1T limit and ν -mass simultaneously. We conclude that this model is quite advantageous to explain the light neutrino mass even without the small Yukawa couplings.

2.7 Semi-annihilations of scalar dark matter

Fractional B-L charge to the inert scalar can induce semi-annihilations which can show up in dark matter relic abundance (see Refs.[57, 98]). For instance when $n_{\rm DM}=1/3$, there is a quartic term in the Lagrangian of the form

$$\mathcal{L}_{1/3} = \frac{\lambda'_{\rm DM}}{3} \phi_{\rm DM}^3 \phi_1 + \text{h.c.}$$
 (2.39)

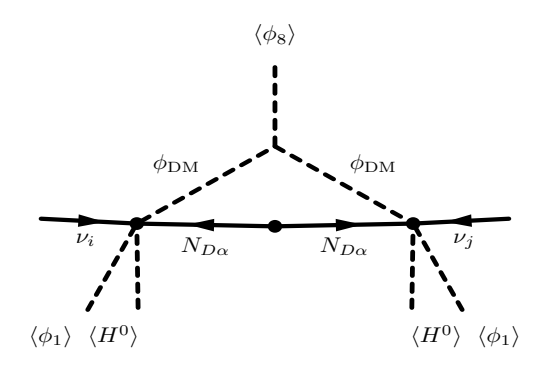


Figure 2.10: Radiative generation of neutrino mass.

With the Feynman diagram shown in Fig. 2.11, the cross section of all possible semiannihilation channels are

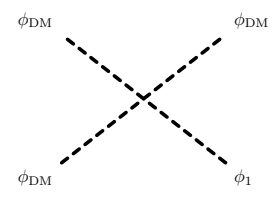


FIGURE 2.11: Feynman diagram for the semi-annihilation vertex.

$$\hat{\sigma}_{H_{1}}^{1/3} = \frac{\lambda'_{\rm DM}^{2}\beta^{2}}{64\pi s} \frac{\left[(s - (M_{\rm DM} + M_{H_{1}})^{2})(s - (M_{\rm DM} - M_{H_{1}})^{2}) \right]^{\frac{1}{2}}}{\left[s(s - 4M_{\rm DM}^{2}) \right]^{\frac{1}{2}}},$$

$$\hat{\sigma}_{H_{2}}^{1/3} = \frac{\lambda'_{\rm DM}^{2}}{128\pi s} \frac{\left[(s - (M_{\rm DM} + M_{H_{2}})^{2})(s - (M_{\rm DM} - M_{H_{2}})^{2}) \right]^{\frac{1}{2}}}{\left[s(s - 4M_{\rm DM}^{2}) \right]^{\frac{1}{2}}},$$

$$\hat{\sigma}_{H_{3}}^{1/3} = \frac{\lambda'_{\rm DM}^{2}}{128\pi s} \frac{\left[(s - (M_{\rm DM} + M_{H_{3}})^{2})(s - (M_{\rm DM} - M_{H_{3}})^{2}) \right]^{\frac{1}{2}}}{\left[s(s - 4M_{\rm DM}^{2}) \right]^{\frac{1}{2}}}.$$
(2.40)

We display in Fig. 2.12 the effect of semi-annihilation channel on the relic abundance

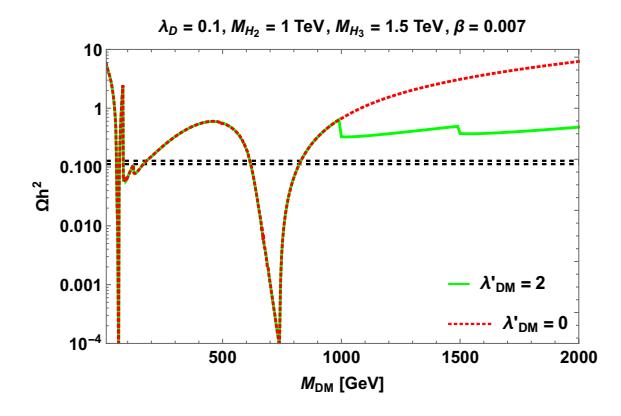


FIGURE 2.12: Relic abundance Ωh^2 with the mass of DM plotted for two values of $\lambda'_{\rm DM}$ with the choice of $n_{\rm DM}=1/3$.

observable. Resonance near $M_{\rm DM} \simeq \frac{M_{H_2}}{2}$ is not achieved for $n_{\rm DM}=1/3$, as $\lambda_{\rm DH2}$ (in Table. 2.3) vanishes. These new channels begin to pop up once mass of DM is above the mass of the physical scalar appearing in the final state. We see that the channel with H_2 and H_3 as one of the final state particles have a significant effect while the Higgs channel attains a β^2 suppression. This scenario is very appealing as the dark matter phenomenology is determined by three free parameters i.e, $\lambda'_{\rm DM}$, $M_{\rm DM}$ and the mass of the physical scalar. Similarly, one can also perform the same analysis for $n_{\rm DM}=8/3$ as well.

2.8 Conclusion

We have presented in detail the scalar dark matter phenomenology in the context of an anomaly free $U(1)_{B-L}$ extension of SM. A possible solution to cancel out the resulting non-trivial triangle anomalies of the gauge extension, three heavy neutral fermions N_{iR} (i=1,2,3) with B-L charges -4, -4 and +5 are added to the existing lepton content of the standard model. Furthermore, the scalar sector is enriched with two scalar singlets ϕ_1 and ϕ_8 to spontaneously break the $U(1)_{B-L}$ gauge symmetry and also to provide the Majorana mass terms for the newly added fermions N_{iR} . A scalar singlet $\phi_{\rm DM}$ is introduced such that the $U(1)_{B-L}$ symmetry takes the burden to forbid its decay making it a stable dark matter candidate. Three physical scalars and a heavy gauge boson Z', resultant of having $U(1)_{B-L}$ as local gauge symmetry act as mediators between the visible and dark sector.

We have studied the scalar spectrum emphasizing the minimization conditions, vacuum stability, perturbative unitarity conditions and their acquired masses after spontaneous symmetry breaking of $SU(2)_L \times U(1)_Y \times U(1)_{B-L}$ gauge symmetry. Choosing a particular B-L charge that can stabilize $\phi_{\rm DM}$, we have investigated thoroughly the relic density and of scalar singlet dark matter in the Z' and scalar-portal scenarios. Applying the limits on relic density by Planck and the most stringent bounds on WIMP-nucleon spin-independent cross section by LUX and XENON1T, we have obtained the consistent parameter space. In collider studies, we have used ATLAS dilepton limits on the gauge coupling $g_{\rm BL}$ and the mass of the new vector boson $M_{Z'}$. We found that there is enough region for the model parameters to meet all the experimental bounds.

This remarkable gauge extension is economical in particle content and rich in phenomenology. A unique feature of this model is that a massless physical Goldstone boson, which plays a key role in scalar-portal relic density. We have discussed the mechanism to obtain the light neutrino mass at the one-loop level, with the dark matter singlet running in the loop, and a suitable benchmark, where the dark matter observables and

light neutrino mass are simultaneously consistent. Finally, we have included discussions regarding semi-annihilations of dark matter and its imprint on relic density for a choice of fractional B-L charge for the scalar dark matter.

Chapter 3

Majorana dark matter in a $U(1)_{B-L}$ extension of the standard model

In this chapter, we revisit the proposed B-L framework of the previous chapter. We do not account the dark matter singlet $\phi_{\rm DM}$ of the model in the present context, rather we carefully observe the exotic fermion mass matrix to explore the Majorana dark matter phenomenology. The procedure of investigation and the discussions will be analogous to the preceding chapter.

3.1 Recap of proposed model and outlook

The new field content of the suggested model includes three exotic fermions with B-L charges -4, -4 and +5 to make the model free of anomalies and two scalar singlets charged -1 and +8 to generate the mass terms for all the new particles after spontaneous breaking the $U(1)_{B-L}$ gauge symmetry.

As mentioned in chapter 2, conventional B-L gauge extensions impose an additional discrete symmetry besides the $U(1)_{B-L}$ local gauge symmetry to qualify right-handed neutrino as dark matter [51, 59–61, 64, 67]. Otherwise, the dark matter fermion can decay through the Yukawa mass term $\overline{\ell_L}\tilde{H}N_R$. However, the exotic B-L charges of the new fermion sector can avoid this decay interaction term, thereby naturally providing a stable dark matter fermion. This approach was followed in a model with four exotic fermions charged 4/3, 1/3, -2/3 and -2/3 under new U(1) and studied in dark matter

context in [99]. However, we perform the analysis in our present choice of only three fermions.

3.2 Revisiting the exotic fermion mass matrix

The heavy Majorana mass matrix can be written for the mass term in Eqn. (2.10) as

$$M_R = \begin{pmatrix} y_{11} \langle \phi_8 \rangle & y_{12} \langle \phi_8 \rangle & y_{13} \langle \phi_1 \rangle \\ y_{12} \langle \phi_8 \rangle & y_{22} \langle \phi_8 \rangle & y_{23} \langle \phi_1 \rangle \\ y_{13} \langle \phi_1 \rangle & y_{23} \langle \phi_1 \rangle & 0 \end{pmatrix} . \tag{3.1}$$

For simplicity, we consider the above mass matrix with real entries of the form¹

$$M_R = \begin{pmatrix} x & a & b \\ a & x & b \\ b & b & 0 \end{pmatrix}, \tag{3.2}$$

which can be obtained by assuming the Yukawa couplings to satisfy the relations $y_{11} \approx y_{22}$ and $y_{13} \approx y_{23}$ along with $v_1 \approx v_8$. The above mass matrix can be diagonalized using the unitary matrix as $(U_1 \cdot K)^T \cdot M_R \cdot (U_1 \cdot K)$, where U_1 is the normalized eigenvector matrix of M_R and K = diag(1, i, 1) is a diagonal phase matrix used to avoid the negative mass eigenvalues. Thus, one obtains the mass matrix in the diagonal basis $M^{\text{diag}} = \text{diag}(M_{D1}, M_{D2}, M_{D3})$ as

$$M^{\text{diag}} = \begin{pmatrix} x - a & 0 & 0 \\ 0 & \frac{1}{2} \left(-(x+a) + \sqrt{8b^2 + (x+a)^2} \right) & 0 \\ 0 & 0 & \frac{1}{2} \left((x+a) + \sqrt{8b^2 + (x+a)^2} \right) \end{pmatrix}.$$
(3.3)

To make the analysis simpler, we consider $M_{D2} = \frac{1}{2}M_{D3}$, which implies b = x + a. Thus, the final diagonal matrix¹ is given by

$$\operatorname{diag}(M_{D1}, M_{D2}, M_{D3}) = \begin{pmatrix} x - a & 0 & 0 \\ 0 & x + a & 0 \\ 0 & 0 & 2(x + a) \end{pmatrix}.$$
(3.4)

¹The lightest mass eigenstate is taken as the dark matter candidate while the heavier ones are taken to be sufficiently massive such that they decouple from the phenomenology and play no role in our final results. To illustrate this scenario, we make the assumption of $M_{D2} = \frac{M_{D3}}{2}$ which makes N_{D1} the dark matter candidate while N_{D2} and N_{D3} are very massive and effectively decouple from the theory.

Considering x > a, we get positive eigenvalues and the mass eigenstates N_{Di} can be written as

$$N_{D1} = \frac{N_2 - N_1}{\sqrt{2}},$$

$$N_{D2} = \frac{i(N_1 + N_2 - 2N_3)}{\sqrt{6}},$$

$$N_{D3} = \frac{N_1 + N_2 + N_3}{\sqrt{3}}.$$
(3.5)

The Yukawa couplings can be expressed in terms of the physical masses as

$$y_{11} = y_{22} = \frac{\sqrt{2} (M_{D1} + M_{D2})}{2v_8},$$

$$y_{12} = \frac{\sqrt{2} (-M_{D1} + M_{D2})}{2v_8},$$

$$y_{13} = y_{23} = \frac{\sqrt{2} M_{D2}}{v_1}.$$
(3.6)

The interaction terms between the new fermions and the Z' gauge boson can be written in the mass eigenstate basis as

$$\mathcal{L}_{N_{Di}}^{V} = g_{BL} \left[-4 \overline{N_{D1}^{c}} \gamma^{\mu} N_{D1} + 2 \overline{N_{D2}^{c}} \gamma^{\mu} N_{D2} - \overline{N_{D3}^{c}} \gamma^{\mu} N_{D3} - 3i \sqrt{2} \overline{N_{D2}^{c}} \gamma^{\mu} N_{D3} + 3i \sqrt{2} \overline{N_{D3}^{c}} \gamma^{\mu} N_{D2} \right] Z_{\mu}^{\prime} .$$
(3.7)

Similarly, the interaction terms with the singlets ϕ_1 and ϕ_8 are

$$\mathcal{L}_{N_{Di}}^{S} = (y_{11} - y_{12}) \overline{N_{D1}^{c}} N_{D1} \phi_{8} + \frac{1}{3} \left(4y_{13} \overline{N_{D2}^{c}} N_{D2} \phi_{1} - (y_{11} + y_{12}) \overline{N_{D2}^{c}} N_{D2} \phi_{8} \right)
+ \frac{2}{3} \left(2y_{13} \overline{N_{D3}^{c}} N_{D3} \phi_{1} + (y_{11} + y_{12}) \overline{N_{D3}^{c}} N_{D3} \phi_{8} \right)
+ \frac{2\sqrt{2}i}{3} \left(y_{13} \overline{N_{D2}^{c}} N_{D3} \phi_{1} - (y_{11} + y_{12}) \overline{N_{D2}^{c}} N_{D3} \phi_{8} \right).$$
(3.8)

A glance at Eqns. (3.4), and (3.5) confirms that N_{D1} is the lightest Majorana mass eigenstate and we intend to perform a detailed study of Majorana dark matter in this work.

3.3 Dark matter phenomenology

The proposed dark matter particle N_{D1} , the lightest of the three Majorana states can interact with the scalar sector and vector gauge boson Z'. Likewise singlet scalar DM,

we proceed to explore the DM observables in this dual portal scenarios separately².

3.3.1 Relic density for Majorana dark matter

3.3.1.1 Scalar mediated

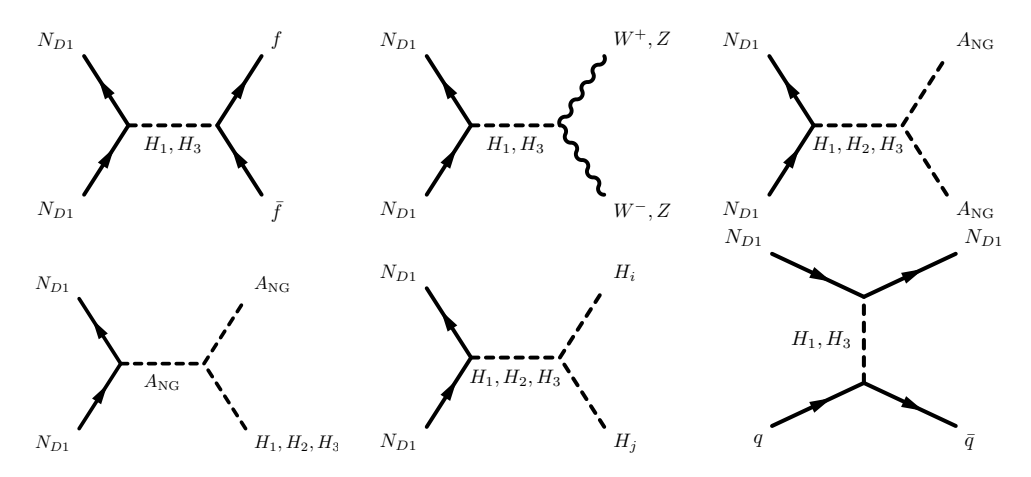


FIGURE 3.1: All the s-channel Feynman diagrams contribute to relic density while the t-channel process is relevant for the direct searches.

The possible annihilation channels that can drive the relic density in the scalar portal scenario are shown in the first five Feynman diagrams of Fig. 3.1. These channels can be either SM fermions, SM gauge bosons (W, Z), Higgs sector scalars and the massless physical Goldstone mode. The cross section for the annihilation channels into SM fermions and gauge bosons are given by

$$\hat{\sigma}_{ff}^{S} = \frac{C}{v^{2}s} |F_{1}|^{2} \sum_{f} M_{f}^{2} c_{f}(s - 4M_{f}^{2})(s - 4M_{D1}^{2}) \frac{(s - 4M_{f}^{2})^{\frac{1}{2}}}{(s - 4M_{D1}^{2})^{\frac{1}{2}}},$$
 (3.9)

$$\hat{\sigma}_{WW}^{S} = \frac{Cs}{2v^2} |F_1|^2 (s - 4M_{D1}^2) \left(1 - \frac{4M_W^2}{s} + \frac{12M_W^4}{s^2} \right) \frac{(s - 4M_W^2)^{\frac{1}{2}}}{(s - 4M_{D1}^2)^{\frac{1}{2}}}, \tag{3.10}$$

$$\hat{\sigma}_{ZZ}^{S} = \frac{Cs}{4v^2} |F_1|^2 (s - 4M_{D1}^2) \left(1 - \frac{4M_Z^2}{s} + \frac{12M_Z^4}{s^2} \right) \frac{(s - 4M_Z^2)^{\frac{1}{2}}}{(s - 4M_{D1}^2)^{\frac{1}{2}}} , \tag{3.11}$$

 $^{^2}$ The phenomenological study is quite different as we shall see that WIMP-nucleon cross-section is insensitive to direct detection experiments in Z'-portal, whereas one can have stringent experimental limits in the scalar-portal. Moreover, the discussion becomes more transparent as the limits from ATLAS and LEP-II are only applicable in Z'-mediated observables and the effect of massless Goldstone is visible only in scalar mediated DM relic density.

while the expressions for channels with NG in final state turn out to be

$$\hat{\sigma}_{NG}^{S} = \frac{Cs}{4v_1^2 v_8^2 (v_1^2 + 64v_8^2)^2} |F_2|^2 (s - 4M_{D1}^2) \frac{s^{\frac{1}{2}}}{(s - 4M_{D1}^2)^{\frac{1}{2}}},$$
(3.12)

$$\hat{\sigma}_{\text{NG H}_1}^S = \frac{C\beta^2}{2v_8^2(v_1^2 + 64v_8^2)^3} \left(v_1^3 + 64v_8^3\right)^2 \frac{(s - 4M_{D1}^2)^{\frac{1}{2}}(s - M_{H_1}^2)^3}{s^{\frac{7}{2}}} , \qquad (3.13)$$

$$\hat{\sigma}_{NG H_2}^S = \frac{C}{4v_8^2(v_1^2 + 64v_8^2)^3} \left(v_1^3 - 64v_8^3\right)^2 \frac{(s - 4M_{D1}^2)^{\frac{1}{2}}(s - M_{H_2}^2)^3}{s^{\frac{7}{2}}} , \qquad (3.14)$$

$$\hat{\sigma}_{\text{NG H}_3}^S = \frac{C}{4v_8^2(v_1^2 + 64v_8^2)^3} \left(v_1^3 + 64v_8^3\right)^2 \frac{(s - 4M_{D1}^2)^{\frac{1}{2}}(s - M_{H_3}^2)^3}{s^{\frac{7}{2}}} , \qquad (3.15)$$

where

$$C = \frac{(y_{11} - y_{12})^2}{8\pi} \,, \tag{3.16}$$

$$F_1 = -\frac{\beta}{\left[(s - M_{H_1}^2) + iM_{H_1}\Gamma_{H_1} \right]} + \frac{\beta}{\left[(s - M_{H_3}^2) + iM_{H_3}\Gamma_{H_3} \right]},$$
(3.17)

$$F_{2} = \frac{\beta^{2} \left(v_{1}^{3} + 64v_{8}^{3}\right)}{\left[\left(s - M_{H_{1}}^{2}\right) + iM_{H_{1}}\Gamma_{H_{1}}\right]} + \frac{1/2\left(v_{1}^{3} - 64v_{8}^{3}\right)}{\left[\left(s - M_{H_{2}}^{2}\right) + iM_{H_{2}}\Gamma_{H_{2}}\right]} + \frac{1/2\left(v_{1}^{3} + 64v_{8}^{3}\right)}{\left[\left(s - M_{H_{3}}^{2}\right) + iM_{H_{3}}\Gamma_{H_{3}}\right]}.$$

$$(3.18)$$

Finally, the Higgs sector annihilation channels we have

$$\hat{\sigma}_{H_i H_j}^S = \frac{C}{2s \ n_p!} |F_{ij}|^2 (s - 4M_{D1}^2) \frac{\left[(s - (M_{H_i} + M_{H_j})^2)(s - (M_{H_i} - M_{H_j})^2)\right]^{\frac{1}{2}}}{\left[s(s - 4M_{D1}^2) \right]^{\frac{1}{2}}} \ , \quad (3.19)$$

where

$$F_{ij} = -\frac{\lambda_{1ij}\beta}{\left[(s-M_{H_1}^2) + iM_{H_1}\Gamma_{H_1}\right]} + \frac{\lambda_{2ij}/\sqrt{2}}{\left[(s-M_{H_2}^2) + iM_{H_2}\Gamma_{H_2}\right]} - \frac{\lambda_{3ij}/\sqrt{2}}{\left[(s-M_{H_3}^2) + iM_{H_3}\Gamma_{H_3}\right]} ,$$

where $n_p!$ denotes the permutation factor for identical final state particles and λ_{1ij} , λ_{2ij} , λ_{3ij} having mass dimension denote the trilinear scalar couplings with i, j = 1, 2, 3. Thus we compute the relic density using the formula in Eqn. (1.59). As mentioned in the previous chapter, the mass parameter M_{H_3} determines the value of scalar mixing parameter β in Eqn. (2.19). Fig. 3.2 displays the behavior of relic density with the dark matter mass where the Planck limit is reached on the either side of resonance of the propagators. For lower DM mass region, the channels $f\bar{f}$ and $A_{NG}A_{NG}$ maximally contribute to relic density. Then, the rest of channels contribute to relic density once they get kinematically allowed. The channels with H_1H_1 and $A_{NG}A_{NG}$ in final state can give the resonance in H_2 propagator. Emphasis is given more to the mass of H_3 as the WIMP-nucleon cross section also involves this mass parameter.

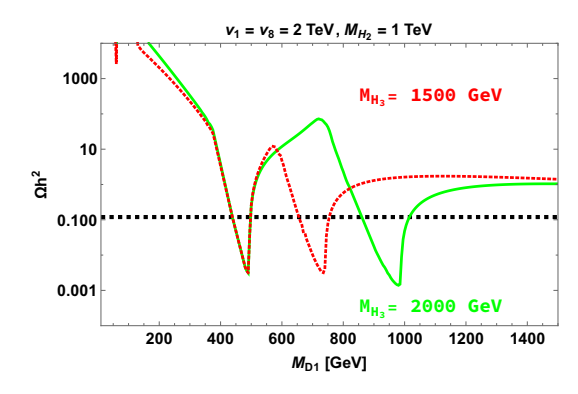


FIGURE 3.2: Scalar-portal relic abundance as a function of DM mass M_{D1} for two specific mass values of the physical scalar H_3 . The horizontal dashed lines represent the 3σ value of the current relic density [88].

3.3.1.2 Vector mediated

Moving to the vector boson portal, the annihilation channels are shown in Fig. 3.3. The cross sections are given by

$$\hat{\sigma}_{ff}^{V} = \sum_{f} \frac{4(n_{\text{BL}}^{f})^{2} g_{\text{BL}}^{4} c_{f} |F_{V}|^{2}}{3\pi s} (s - 4M_{D1}^{2})(s + 2M_{f}^{2}) \frac{(s - 4M_{f}^{2})^{\frac{1}{2}}}{(s - 4M_{D1}^{2})^{\frac{1}{2}}},$$

$$\hat{\sigma}_{Z'H_{3}}^{V} = \frac{4(64v_{8} + v_{1})^{2} g_{\text{BL}}^{6} |F_{V}|^{2}}{\pi s} \frac{((s - (M_{Z'} + M_{H_{3}})^{2})(s - (M_{Z'} - M_{H_{3}})^{2}))^{\frac{1}{2}}}{(s(s - 4M_{D1}^{2}))^{\frac{1}{2}}} C_{H_{3}},$$

$$\hat{\sigma}_{Z'H_{2}}^{V} = \frac{4(64v_{8} - v_{1})^{2} g_{\text{BL}}^{6} |F_{V}|^{2}}{\pi s} \frac{((s - (M_{Z'} + M_{H_{2}})^{2})(s - (M_{Z'} - M_{H_{2}})^{2}))^{\frac{1}{2}}}{(s(s - 4M_{D1}^{2}))^{\frac{1}{2}}} C_{H_{2}},$$

$$\hat{\sigma}_{Z'H_{1}}^{V} = \frac{8(64v_{8} + v_{1})^{2} \beta^{2} g_{\text{BL}}^{6} |F_{V}|^{2}}{\pi s} \frac{((s - (M_{Z'} + M_{H_{1}})^{2})(s - (M_{Z'} - M_{H_{1}})^{2}))^{\frac{1}{2}}}{(s(s - 4M_{D1}^{2}))^{\frac{1}{2}}} C_{H_{1}},$$

$$(3.20)$$

where

$$\begin{split} F_V = & \frac{1}{\left[(s - M_{Z'}^2) + i M_{Z'} \Gamma_{Z'} \right]} \,, \\ C_S = & \left[\frac{(s - 8M_{D1}^2)}{4} + \frac{1}{M_{Z'}^2} \left(2s M_{D1}^2 + \frac{(s + M_{Z'}^2 - M_S^2)^2}{4} \right. \right. \\ & \left. - \frac{1}{48s} (s - 4M_{D1}^2) (s - (M_{Z'} + M_S)^2) (s - (M_{Z'} - M_S)^2) \right) \right] \,, \end{split}$$

with $S = H_1, H_2, H_3$. Fig. 3.4 shows the behaviour of relic abundance with the mass of dark matter particle for various sets of gauge coupling $g_{\rm BL}$ and the mediator mass $M_{Z'}$ consistent with the LEP-II bound. Near the resonance the major contribution comes from the $N_{D1}N_{D1} \to f\bar{f}$ channel. As we go towards high mass regime of M_{D1} , the

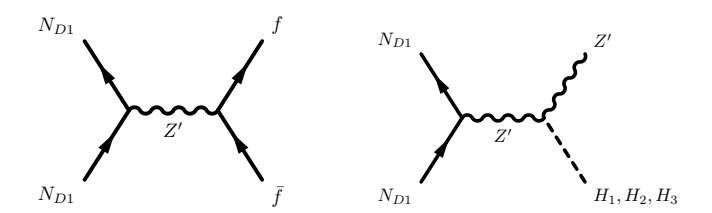


FIGURE 3.3: Feynman diagrams contributing to relic density in the vector-mediated case.

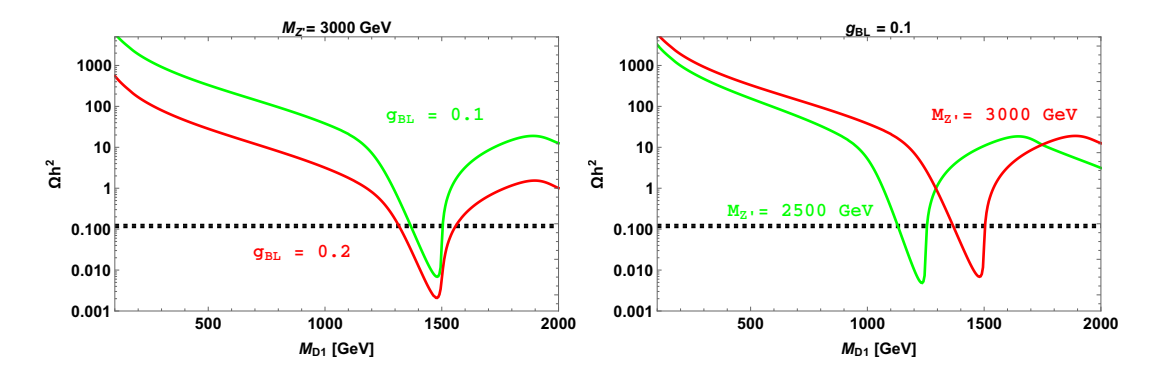


FIGURE 3.4: Variation of relic abundance Ωh^2 with the mass of DM with $(M_{H_2}, M_{H_3}) = (1, 1.5)$ TeV. Left panel depicts the variation for fixed Z' mass and varying B-L gauge coupling $g_{\rm BL}$. The right panel displays the behavior for constant coupling $g_{\rm BL}$ and varying mediator mass.

channels $N_{D1}N_{D1} \rightarrow Z'H_{1,2,3}$ become dominant resulting in a slight decrease in the relic abundance.

3.3.2 Direct searches

In this section, we discuss the direct detection prospects for our model in both scalar and vector mediated DM scenarios. Since the vector boson Z' couples differently to Majorana fermion and quarks i.e., axial vector and vector type, the contribution by WIMP-nucleon interaction is insensitive to direct detection experiments [34, 60]. Hence, we shall only focus on the scalar mediated DM scattering and constraints on it from various experiments. The effective Lagrangian term of scalar mediated channel shown in Fig. 3.1 (t-channel) that contributes to the spin-independent cross section for direct detection is

$$\mathcal{L}_{\text{eff}} = a_q \overline{N}_{D1} N_{D1} \bar{q} q, \qquad (3.21)$$

where

$$a_q = \frac{M_q(y_{11} - y_{12})\beta}{\sqrt{2}v} \left(\frac{1}{M_{H_3}^2} - \frac{1}{M_{H_1}^2}\right). \tag{3.22}$$

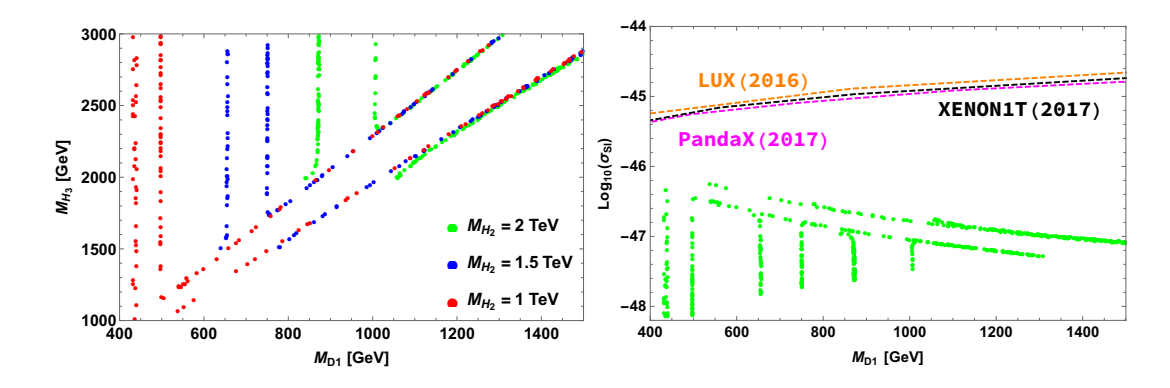


FIGURE 3.5: Left panel shows the parameter space satisfying the 3σ range in current relic density and the most stringent PandaX limit. Right panel depicts WIMP-nucleon cross section for the parameters space depicted in the left panel. The dashed lines denote the upper bound on SI cross section from LUX [36], XENON1T [37] and PandaX [38].

Thus from Eqns. (1.66), (1.67), the WIMP-nucleon SI contribution reads as

$$\sigma_{\rm SI} = -\frac{4}{\pi} \mu^2 f_p^2 \ . \tag{3.23}$$

The additional 4 factor in the numerator comes in the context of Majorana fermion. Varying the parameters in the range shown in Table. 3.1, we show in Fig. 3.5 (left

Parameters	Range
$v_{1,8}$ [GeV]	2000
M_{H_2} [GeV]	1000 - 2000
M_{H_3} [GeV]	$M_{H_2} - 3000$
β	0.016 - 0.0016

Table 3.1: Parameters and their ranges for scalar portal analysis.

panel), the parameter space that satisfies the 3σ range in the current relic density [88] and the PandaX limit [38]. Since the mixing parameter β is small, the direct detection limits on the parameter space is not stringent. It is mainly constrained by relic density where the Planck limit is met near the resonance in two propagators H_2 (vertical data points) and H_3 (diagonal data points). Right panel depicts the WIMP-nucleon cross section with varying mass of the DM of the parameter space shown in the left panel.

3.4 Collider studies

Moving on to the ATLAS dilepton constraints on the gauge parameters, we follow the similar procedure as in previous chapter. Working in the mass range of $M_{Z'} \leq 4$ TeV, we show in the left panel of Fig. 3.6, dilepton $(ee, \mu\mu)$ signal in Z' production as a function

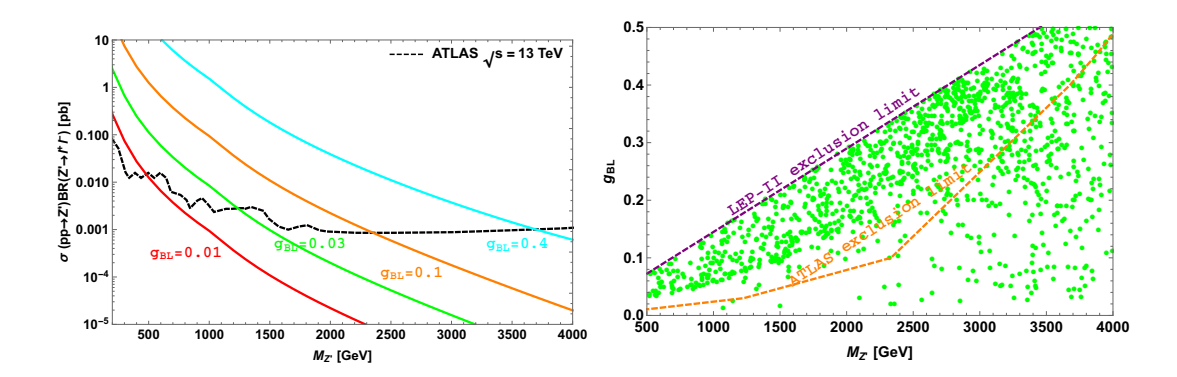


FIGURE 3.6: ATLAS dilepton constraints on the proposed model are shown. In the left panel, the black dashed line represents the exclusion limit from ATLAS [93], while the colored lines represent the dilepton signal cross sections for different values of $g_{\rm BL}$ as a function of $M_{Z'}$. The right panel shows ATLAS and LEP-II exclusion limits from dilepton searches in the plane of $M_{Z'} - g_{\rm BL}$.

Field	$SU(2)_L \times U(1)_Y$	$U(1)_{B-L}$
η'	(2,1/2)	-3

Table 3.2: Inert doublet and its charge assignment.

of $M_{Z'}$. It can be seen that for $g_{\rm BL}=0.4$, the region below $M_{Z'}\simeq 3.7$ TeV is excluded while for $g_{\rm BL}=0.1$, $M_{Z'}<2.3$ TeV is excluded. Thus, for $g_{\rm BL}\gtrsim 0.1$ the parameter space is pushed to heavier $M_{Z'}$ above 2.3 TeV. For $g_{\rm BL}<0.03$ we have $M_{Z'}\gtrsim 1.2$ TeV and for $g_{\rm BL}=0.01$ we have $M_{Z'}\gtrsim 0.5$ TeV. We see that the dilepton signal in Z' decay can impose stringent constraints on these models. The right panel in Fig. 3.6 describes the parameter space in $M_{Z'}-g_{\rm BL}$ plane consistent with the current 3σ limit on relic density from Planck [88]. The region to the right of both the curves is consistent with ATLAS [93] and LEP-II [97] bounds. With ATLAS limit being the most stringent one, from the plot one can see that the model still has a significant portion of the parameter space that can satisfy the relic density. Thus, in general, we conclude that dilepton searches from LHC in Z' models can pose stringent limits on the parameter space.

3.5 Light neutrino mass

Since the current model doesn't contain the right-handed neutrinos, the standard type-I seesaw mechanism to generate light neutrino mass is not feasible with the existing particle content. However, the neutrino masses can be generated at one-loop level through radiative mechanism, which will be briefly described in this section. For this purpose, we introduce an additional inert doublet $\eta' = \begin{pmatrix} \eta_{ch}^+ \\ \frac{\eta_r + i\eta_i}{\sqrt{2}} \end{pmatrix}$ with the charges shown in Table.

3.2. Thus, the trivial scalar potential in Eqn. (2.9) gets modified with the inclusion of additional terms given as

$$V'''(H, \phi_{1}, \phi_{8}, \eta') = V'(H, \phi_{1}, \phi_{8}) + \mu_{\eta'}^{2}(\eta'^{\dagger}\eta') + \lambda_{\eta'}(\eta'^{\dagger}\eta')^{2} + \frac{\lambda_{\eta'18}}{2\Lambda^{3}} \left[(H^{\dagger}\eta')^{2}\phi_{8}\phi_{1}^{2} + \text{h.c.} \right] + \lambda'_{H\eta'}(H^{\dagger}\eta')(\eta'^{\dagger}H) + (\eta'^{\dagger}\eta') \left[\lambda_{H\eta'}(H^{\dagger}H) + \lambda_{\eta'1}(\phi_{1}^{\dagger}\phi_{1}) + \lambda_{\eta'8}(\phi_{8}^{\dagger}\phi_{8}) \right],$$
(3.24)

where Λ is the cut-off parameter. The masses of real and imaginary components of the inert doublet η' are given as

$$M_{\eta_r}^2 = \mu_{\eta'}^2 + \frac{\lambda_{\eta'1}}{2} v_1^2 + \frac{\lambda_{\eta'8}}{2} v_8^2 + \left(\lambda_{H\eta'} + \lambda'_{H\eta'}\right) \frac{v^2}{2} + \lambda_{\eta'18} \frac{v^2 v_1^2 v_8}{4\sqrt{2}\Lambda^3},$$

$$M_{\eta_i}^2 = \mu_{\eta'}^2 + \frac{\lambda_{\eta'1}}{2} v_1^2 + \frac{\lambda_{\eta'8}}{2} v_8^2 + \left(\lambda_{H\eta'} + \lambda'_{H\eta'}\right) \frac{v^2}{2} - \lambda_{\eta'18} \frac{v^2 v_1^2 v_8}{4\sqrt{2}\Lambda^3}.$$
 (3.25)

With these particle content, one can write the interaction term to generate light neutrino

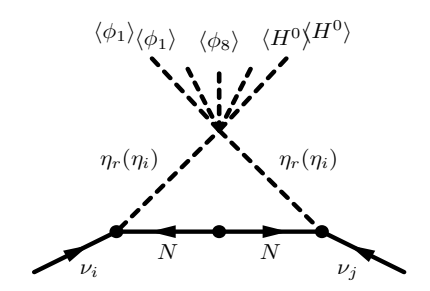


Figure 3.7: Radiative generation of neutrino mass.

mass at one-loop level as shown in Fig. 3.7 as

$$\sum_{\alpha=1,2} Y'_{i\alpha} \overline{(\ell_L)}_i \tilde{\eta'} N_{\alpha R}. \tag{3.26}$$

Thus, from Fig. 3.7, one can write the light neutrino mass matrix [85], as

$$(\mathcal{M}_{\nu})_{ij} = \frac{\lambda_{\eta'18} v^2 v_1^2 v_8}{32\sqrt{2}\pi^2 \Lambda^3} \sum_{\alpha=1}^{2} \frac{Y'_{i\alpha} Y'_{j\alpha} M_{D\alpha}}{m_{\eta'}^2 - M_{D\alpha}^2} \left[1 - \frac{M_{D\alpha}^2}{m_{\eta'}^2 - M_{D\alpha}^2} \ln \frac{m_{\eta'}^2}{M_{D\alpha}^2} \right], \tag{3.27}$$

where $m_{\eta'}^2 = \frac{1}{2} \left(M_{\eta_r}^2 + M_{\eta_i}^2 \right)$. We further assume that inert doublet components are heavier than the DM mass. Note that for the parameter space considered here, the range of cutoff scale Λ , which is allowed by perturbative limits is $\sim [50, 10^4]$ TeV. For example, with $(Y', \lambda_{\eta'18}) \sim (10^{-1}, 10^{-2})$ and $(v_1, v_8, m_{\eta'}, M_{D\alpha}, \Lambda) \sim (2, 2, 2, 0.5, 100)$ TeV, one can have $m_{\nu} \sim 10^{-11}$ GeV. Thus, the light neutrino mass generation can be successfully achieved in the proposed model.

3.6 Conclusion

The lightest mass eigenstate upon the diagonalization of exotic fermion mass matrix, plays the role of dark matter. The scalar portal relic abundance has been studied with all possible annihilation channels and the effect of massless physical Goldstone boson is suitably addressed. The SI cross section has been calculated and investigated with the current limits from LUX (2016), XENON1T (2017) and PandaX (2017). Similar strategy is repeated for Z'-portal channels. But in the Z' case, it is not possible to study for direct searches as the Majorana dark matter couples axial-vectorially with the Z', while SM quarks couple to Z' vectorially. In collider searches, the ATLAS bounds on the Z' mass and $g_{\rm BL}$ impose strong constraints. However, we still have a viable parameter space satisfying the current relic density and the dilepton bounds. We have also addressed the generation of light neutrino mass by adding an additional inert doublet η' with B-L charge assigned as -3. We have made a complete systematic study of Majorana dark matter in a new variant of B-L gauge extended model.

This simple model survives the current collider limits while satisfies dark matter constraints and can be probed in future high luminosity data from LHC.

Chapter 4

Fermionic dark matter and neutrino oscillation in the scotogenic model

We have already been familiar to the concept of the radiative neutrino mass with the dark matter (fermion or inert scalar) running in the loop in the earlier chapters. It would be interesting to do a phenomenological study with the combined application of constrained dark matter observables and the measured neutrino oscillation parameters.

4.1 Brief note on neutrino oscillation

Considerable progress has been made in the determination of neutrino mass squared differences and mixing parameters from the data of various solar and atmospheric neutrino oscillation experiments. Theoretically, the smallness of neutrino mass can be generally explained by the well known seesaw mechanisms namely: type-I [72–75], type-II [100–105], type-III [106] and radiative seesaw [85]. In standard parametrization, the mechanism of mixing can be described by the unitary Pontecorvo-Maki-Nakagawa-Sakata (PMNS) matrix V_{PMNS} [107, 108] written in terms of three rotation angles θ_{12} , θ_{23} , θ_{13} and three CP-violating phases namely δ_{CP} (Dirac type) and ρ , σ (Majorana type) as

$$V_{PMNS} \equiv U_{PMNS} \cdot P_{\nu} = \begin{pmatrix} c_{12}c_{13} & s_{12}c_{13} & s_{13}e^{-i\delta_{CP}} \\ -s_{12}c_{23} - c_{12}s_{13}s_{23}e^{i\delta_{CP}} & c_{12}c_{23} - s_{12}s_{13}s_{23}e^{i\delta_{CP}} & c_{13}s_{23} \\ s_{12}s_{23} - c_{12}s_{13}c_{23}e^{i\delta_{CP}} & -c_{12}s_{23} - s_{12}s_{13}c_{23}e^{i\delta_{CP}} & c_{13}c_{23} \\ & & & & & & & & & & & & & & \\ \end{array} \right) P_{\nu} \; , \label{eq:VPMNS}$$

where $c_{ij} \equiv \cos \theta_{ij}$, $s_{ij} \equiv \sin \theta_{ij}$ and $P_{\nu} \equiv \{e^{i\rho}, e^{i\sigma}, 1\}$ is a diagonal phase matrix. The mixing angles as well as the mass squared differences have been well constrained by various neutrino oscillation experiments. Recently, the Daya Bay [109, 110], RENO [111] and T2K [112] Collaborations have precisely measured the reactor mixing angle θ_{13} with a moderately large value. However, there are several missing pieces such as the neutrino mass hierarchy, the magnitude of the CP violating phase δ_{CP} , the absolute scale of the neutrino mass, and the nature of neutrinos (whether Dirac or Majorana). Various neutrino oscillation parameters derived from a global analysis of recent oscillation data taken from Ref. [113] are presented in Table. 4.1.

Mixing Parameters	Best Fit value	3σ Range
$\sin^2 \theta_{12}$	0.323	$0.278 \to 0.375$
$\sin^2 \theta_{23} \text{ (NO)}$	0.567	$0.392 \to 0.643$
$\sin^2 \theta_{13} \text{ (NO)}$	0.0234	$0.0177 \rightarrow 0.0294$
$\delta_{\rm CP} \ ({ m NO})$	1.34π	$(0 \to 2\pi)$
$\Delta m_{31}^2/10^{-3} \text{ eV}^2 \text{ (NO)}$	2.48	2.3 o 2.65
$\Delta m_{21}^2/10^{-5} \text{ eV}^2$	7.60	$7.11 \rightarrow 8.18$

Table 4.1: Best-fit values with their 3σ ranges of the neutrino oscillation parameters from [113] where NO indicates normal ordering.

The chapter proceeds as follows. We begin with the one-loop radiative neutrino mass matrix in the scotogenic model and derive the conditions on the model parameters to explain recent data of measured neutrino oscillation parameters. The lightest degenerate fermions running in the loop are explored in relic density perspective including co-annihilation effects to further restrict the parameters. Finally, with the allowed parameter region, we make predictions on lepton flavor violating decays.

4.2 Scotogenic model

The scotogenic model is a minimal extension of the SM with an additional inert scalar doublet η and three heavy Majorana right-handed neutrinos N_i (i=1,2,3). The potential is imposed with a discrete symmetry under which all the new particles i.e., N_i and η , are odd, and SM particles are even. The unbroken discrete symmetry guarantees the inert doublet doesn't produce a VEV. This model is rich in phenomenology providing scalar and fermionic dark matter candidates. Scalar dark matter in this model has been studied extensively in the literature [114–116].

The scalar potential of this model is given by [85, 117]

$$V_{\rm sc}(H,\eta) = \mu_{\rm H}^2 H^{\dagger} H + \mu_{\eta}^2 \eta^{\dagger} \eta + \lambda_{\rm H} (H^{\dagger} H)^2 + \lambda_{\eta} (\eta^{\dagger} \eta)^2 + \lambda_3 (H^{\dagger} H) (\eta^{\dagger} \eta) + \lambda_4 (H^{\dagger} \eta) (\eta^{\dagger} H) + \frac{1}{2} \lambda_5 [(H^{\dagger} \eta)^2 + (\eta^{\dagger} H)^2],$$
(4.2)

where $\eta = \begin{pmatrix} \eta^+ \\ \eta^0 \end{pmatrix}$. The Yukawa Lagrangian of this model is

$$\mathcal{L}_{N} = \overline{N_{i}} i \partial \!\!\!/ P_{R} N_{i} + (D_{\mu} \eta)^{\dagger} (D^{\mu} \eta) - \frac{M_{i}}{2} \overline{N_{i}^{c}} P_{R} N_{i} + h_{\alpha i} \overline{\ell_{\alpha}} \eta^{\dagger} P_{R} N_{i} + \text{h.c.}, \qquad (4.3)$$

where $h_{\alpha i}$ are the Yukawa couplings, α denotes the lepton flavor and M_i are the masses of heavy neutrinos N_i . The radiative neutrino mass matrix can be computed for Fig. 4.1, given by

$$(\mathcal{M}_{\nu})_{\alpha\beta} = \sum_{i=1}^{3} h_{\alpha i} h_{\beta i} \Lambda_{i}, \tag{4.4}$$

where Λ_i is defined as

$$\Lambda_i = \frac{\lambda_5 v^2}{8\pi^2 M_i} I(r_i), \qquad I(x) = \frac{x^2}{1 - x^2} \left(1 + \frac{x^2}{1 - x^2} \ln x^2 \right). \tag{4.5}$$

Here the parameters r_i are defined as $r_i = M_i/m_0$ and $m_0^2 = \mu_\eta^2 + (\lambda_3 + \lambda_4)\frac{v^2}{2}$. We take

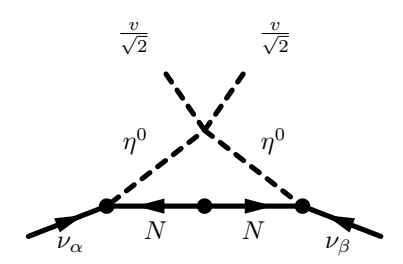


Figure 4.1: Radiative generation of neutrino mass.

 $\lambda_5 \sim 10^{-10}$, a very small value, in order to have correct neutrino masses and also probe for lepton flavor violation [117–120]. We now diagonalize the radiative mass matrix (4.4) using the PMNS matrix to explain neutrino oscillation data.

4.3 Neutrino phenemenology

Various neutrino experiments have confirmed that neutrinos have tiny mass and oscillate from one flavor to another as they propagate. The phenomenon of neutrino oscillation is described by solar (θ_{12}) , atmospheric (θ_{23}) and reactor (θ_{13}) mixing angles. Of these three rotation angles, two are large (θ_{12}) and (θ_{23}) , and one is not so large (θ_{13}) . Originally,

it was believed that the reactor mixing angle would be very small and with this motivation numerous models were proposed which are generally based on some discrete flavor symmetries such as S_3 , S_4 , A_4 , etc [121–125] to explain the neutrino mixing pattern. For instance, the tri-bimaximal (TBM) mixing pattern [126–134], a well motivated model which has $\sin^2 \theta_{12} = \frac{1}{3}$ and $\sin^2 \theta_{23} = \frac{1}{2}$ and which can be expressed in a generalized form as

$$U_{\nu}^{0} = \begin{pmatrix} \cos \theta & \sin \theta & 0 \\ -\frac{\sin \theta}{\sqrt{2}} & \frac{\cos \theta}{\sqrt{2}} & \frac{1}{\sqrt{2}} \\ \frac{\sin \theta}{\sqrt{2}} & -\frac{\cos \theta}{\sqrt{2}} & \frac{1}{\sqrt{2}} \end{pmatrix}, \tag{4.6}$$

with $\theta \simeq 35^{\circ}$. However, in the TBM mixing pattern the value of θ_{13} turns out to be zero. After the experimental evidence of a moderately large θ_{13} , it was found that by adding suitable perturbation terms, the TBM mixing pattern can still describe the neutrino mixing pattern with sizeable θ_{13} . As discussed in [135], here we consider a simple perturbation matrix i.e., a rotation matrix in the 13 plane, which can provide the required corrections to the various mixing angles of the TBM mixing matrix. Assuming the charged lepton mass matrix as diagonal (i.e., the identity matrix), one can write the PMNS mixing matrix, which relates the flavor eigenstates to the corresponding mass eigenstates as

$$U_{PMNS} = U_{\nu}^{0} \begin{pmatrix} \cos \varphi & 0 & e^{-i\zeta} \sin \varphi \\ 0 & 1 & 0 \\ -e^{i\zeta} \sin \varphi & 0 & \cos \varphi \end{pmatrix}. \tag{4.7}$$

In our work, we consider the phase ζ to be zero for convenience. Now we diagonalize the mass matrix (4.4) by the mixing matrix (4.7) using the relation $U_{PMNS}^T \mathcal{M}_{\nu} U_{PMNS} = \text{diag}(m_1, m_2, m_3)$. This in turn provides the following conditions (vanishing off-diagonal elements of the mass matrix) to be satisfied:

$$\sum_{i=1}^{3} \frac{h_{ei}^{2}}{2} \sin 2\theta \cos \varphi + \frac{h_{ei}(h_{\mu i} - h_{\tau i})}{\sqrt{2}} \cos 2\theta \cos \varphi - \frac{(h_{\mu i} - h_{\tau i})^{2}}{4} \sin 2\theta \cos \varphi - \frac{h_{ei}(h_{\mu i} + h_{\tau i})}{\sqrt{2}} \sin \theta \sin \varphi - \frac{(h_{\mu i}^{2} - h_{\tau i}^{2})}{2} \cos \theta \sin \varphi = 0,$$

$$\sum_{i=1}^{3} \frac{h_{ei}^{2}}{2} \sin 2\theta \sin \varphi + \frac{h_{ei}(h_{\mu i} - h_{\tau i})}{\sqrt{2}} \cos 2\theta \sin \varphi - \frac{(h_{\mu i} - h_{\tau i})^{2}}{4} \sin 2\theta \sin \varphi + \frac{h_{ei}(h_{\mu i} + h_{\tau i})}{\sqrt{2}} \sin \theta \cos \varphi + \frac{(h_{\mu i}^{2} - h_{\tau i}^{2})}{2} \cos \theta \cos \varphi = 0,$$

$$\sum_{i=1}^{3} \frac{h_{ei}^{2}}{2} \cos^{2} \theta \sin 2\varphi - \frac{h_{ei}(h_{\mu i} - h_{\tau i})}{2\sqrt{2}} \sin 2\theta \sin 2\varphi + \frac{(h_{\mu i} - h_{\tau i})^{2}}{4} \sin^{2} \theta \sin 2\varphi + \frac{h_{ei}(h_{\mu i} + h_{\tau i})}{\sqrt{2}} \cos \theta \cos 2\varphi - \frac{(h_{\mu i}^{2} - h_{\tau i}^{2})}{2} \sin \theta \cos 2\varphi - \frac{(h_{\mu i} + h_{\tau i})^{2}}{4} \sin 2\varphi = 0.$$

$$(4.8c)$$

The neutrino mass eigenvalues are given by

$$m_{1} = \sum_{i=1}^{3} (h_{ei}^{2} \cos^{2} \theta \cos^{2} \varphi - \frac{1}{\sqrt{2}} h_{ei} (h_{\mu i} - h_{\tau i}) \sin 2\theta \cos^{2} \varphi - \frac{1}{\sqrt{2}} h_{ei} (h_{\mu i} + h_{\tau i}) \cos \theta \sin 2\varphi$$

$$+ \frac{1}{2} (h_{\mu i} + h_{\tau i})^{2} \sin^{2} \varphi + \frac{1}{2} (h_{\mu i}^{2} - h_{\tau i}^{2}) \sin \theta \sin 2\varphi + \frac{1}{2} (h_{\mu i} - h_{\tau i})^{2} \sin^{2} \theta \cos^{2} \varphi) \Lambda_{i} ,$$

$$m_{2} = \sum_{i=1}^{3} (h_{ei}^{2} \sin^{2} \theta + \frac{1}{\sqrt{2}} h_{ei} (h_{\mu i} - h_{\tau i}) \sin 2\theta + \frac{1}{2} (h_{\mu i} - h_{\tau i})^{2} \cos^{2} \theta) \Lambda_{i} ,$$

$$m_{3} = \sum_{i=1}^{3} (h_{ei}^{2} \cos^{2} \theta \sin^{2} \varphi - \frac{1}{\sqrt{2}} h_{ei} (h_{\mu i} - h_{\tau i}) \sin 2\theta \sin^{2} \varphi + \frac{1}{\sqrt{2}} h_{ei} (h_{\mu i} + h_{\tau i}) \cos \theta \sin 2\varphi$$

$$+ \frac{1}{2} (h_{\mu i} + h_{\tau i})^{2} \cos^{2} \varphi - \frac{1}{2} (h_{\mu i}^{2} - h_{\tau i}^{2}) \sin \theta \sin 2\varphi + \frac{1}{2} (h_{\mu i} - h_{\tau i})^{2} \sin^{2} \theta \sin^{2} \varphi) \Lambda_{i} . (4.9)$$

Solving (4.8a), (4.8b) and substituting in (4.8c), we obtain two solutions given by

1.
$$h_{\mu i_1} \neq -h_{\tau i_1}, \quad \tan \theta = \frac{(h_{\tau i_1} - h_{\mu i_1})}{\sqrt{2}h_{ei_1}},$$

$$-\left(\frac{h_{ei_1}(h_{\mu i_1} + h_{\tau i_1})}{\sqrt{2}}\cos \theta - \frac{(h_{\mu i_1}^2 - h_{\tau i_1}^2)}{2}\sin \theta\right)$$

$$\tan 2\varphi = \frac{\left(\frac{h_{ei_1}^2(h_{\mu i_1} + h_{\tau i_1})}{\sqrt{2}}\cos \theta - \frac{(h_{\mu i_1}^2 - h_{\tau i_1})}{2}\sin \theta\right)}{\left(\frac{h_{ei_1}^2}{2}\cos^2 \theta - \frac{h_{ei_1}(h_{\mu i_1} - h_{\tau i_1})}{2\sqrt{2}}\sin 2\theta + \frac{(h_{\mu i_1} - h_{\tau i_1})^2}{4}\sin^2 \theta - \frac{(h_{\mu i_1} + h_{\tau i_1})^2}{4}\right)},$$

2.
$$h_{\mu i_2} = -h_{\tau i_2}, \quad \tan \theta = \frac{h_{ei_2}}{\sqrt{2}h_{\mu i_2}},$$
 (4.10)

where i_1 , i_2 can take any value of i(=1,2,3). As shown in Ref. [135], the above mixing matrix can explain recent neutrino oscillation data with the unperturbed mixing as TBM type (i.e., with $\theta = 35^{\circ}$) and the perturbed angle $\varphi = 12^{\circ}$, which accommodates the experimentally measured mixing angles. Thus, Eqn. (4.10) gets further simplified to three simple solutions and the obtained flavor structure written in terms of $h_{ei}(=h_i)$ in a matrix labelled with the lepton flavor α as row index and i = 1, 2, 3 as column index, is given by

$$h_{\alpha i} = \begin{pmatrix} h_1 & h_2 & h_3 \\ -0.68 & h_1 & h_2 & 3.56 & h_3 \\ 0.31 & h_1 & -h_2 & 4.55 & h_3 \end{pmatrix}. \tag{4.11}$$

Here $i_1 = 1, 3$ and $i_2 = 2$ is assumed so that the mass eigenvalues (4.9) get non-zero contributions given as

$$m_1 = c_1(h_1^2 \Lambda_1),$$

 $m_2 = c_2(h_2^2 \Lambda_2),$
 $m_3 = c_3(h_3^2 \Lambda_3),$ (4.12)

where the coefficients $c_1 = 1.55$, $c_2 = 3.04$, $c_3 = 34.44$. Thus, the flavor structure (4.11) is suitable to explain normal hierarchy i.e., $(m_3 \gg m_2 > m_1)$ provided we assume that N_1 and N_2 are degenerate. Imposing the best fit values given in Table. 4.1, the constraints from neutrino mass squared differences are given by

$$[(c_2 h_2^2)^2 - (c_1 h_1^2)^2] \Lambda_1^2 = 7.6 \times 10^{-5} \text{ eV}^2,$$

$$[(c_3 h_3^2 \Lambda_3)^2 - (c_2 h_2^2 \Lambda_1)^2] = 2.4 \times 10^{-3} \text{ eV}^2.$$
(4.13)

Thus, we have a free parameter space spanned by h_i , $r_{1,3}$ and $M_{1,3}$. We now proceed to constrain the parameter space with the DM relic abundance choosing the lightest of the odd particles as a DM candidate.

4.4 Relic abundance

We choose N_1 as the lightest odd particle and since N_2 is its degenerate partner, the relic abundance gets contributions from annihilation as well as coannihilation channels. To include the coannihilation effects, we adopt the procedure given in [31] in the estimation of relic abundance. We introduce a parameter δ given by $\delta \equiv (M_2 - M_1)/M_1$ which depicts the mass splitting ratio of the degenerate neutrinos. The effective cross section σ_{eff} including contributions from coannihilations is given by

$$\sigma_{\text{eff}} = \frac{g_{N_1}^2}{g_{\text{eff}}^2} \sigma_{N_1 N_1} + 2 \frac{g_{N_1} g_{N_2}}{g_{\text{eff}}^2} \sigma_{N_1 N_2} (1+\delta)^{3/2} e^{-\delta x} + \frac{g_{N_2}^2}{g_{\text{eff}}^2} \sigma_{N_2 N_2} (1+\delta)^3 e^{-2\delta x},$$

$$g_{\text{eff}} = g_{N_1} + g_{N_2} (1+\delta)^{3/2} e^{-\delta x}.$$

$$(4.14)$$

Here g_{eff} denotes the effective degrees of freedom, $g_{N_{1,2}}$ are the number of degrees of freedom for Majorana fermion and $x = M_1/T$, where T is the temperature. (Co)annihilation proceeds via t-channel processes mediated by η^0 and η^{\pm} giving the lepton-antilepton pair in the final state. The corresponding cross section of N_i and N_j is given by [117]

$$\sigma_{N_{i}N_{j}}|v_{\text{rel}}| = \frac{1}{8\pi} \frac{M_{1}^{2}}{(M_{1}^{2} + m_{0}^{2})^{2}} \left[1 + \frac{m_{0}^{4} - 3m_{0}^{2}M_{1}^{2} - M_{1}^{4}}{3(M_{1}^{2} + m_{0}^{2})^{2}} v_{\text{rel}}^{2} \right] \times \sum_{\alpha,\beta} (h_{\alpha i}h_{\beta j} - h_{\alpha j}h_{\beta i})^{2} + \frac{1}{12\pi} \frac{M_{1}^{2}(M_{1}^{4} + m_{0}^{4})}{(M_{1}^{2} + m_{0}^{2})^{4}} v_{\text{rel}}^{2} \sum_{\alpha,\beta} h_{\alpha i}h_{\alpha j}h_{\beta i}h_{\beta j}.$$

$$(4.15)$$

In the above expression i, j can be 1 or 2 and $v_{\rm rel}$ represents the relative velocity of annihilating particles. The effective annihilation cross section is defined as $\sigma_{\rm eff}|v_{\rm rel}| = a_{\rm eff} + b_{\rm eff}v_{\rm rel}^2$. The coefficients $a_{\rm eff}$ and $b_{\rm eff}$ for the obtained flavor structure (4.11) are

given by

$$a_{\text{eff}} = \frac{1}{16\pi} \frac{M_1^2}{(M_1^2 + m_0^2)^2} (s_{12}h_1^2h_2^2), \tag{4.16}$$

$$b_{\text{eff}} = \frac{1}{48\pi} \frac{M_1^2 (M_1^4 + m_0^4)}{(M_1^2 + m_0^2)^4} \left[(s_1 h_1^4 + s_2 h_2^4) \right]$$

$$+ \frac{1}{16\pi} \frac{M_1^2}{(M_1^2 + m_0^2)^2} \left[\frac{m_0^4 - 3m_0^2 M_1^2 - M_1^4}{3(M_1^2 + m_0^2)^2} \right] (s_{12} h_1^2 h_2^2), \tag{4.17}$$

where $s_1 = 2.42$, $s_2 = 9.24$ and $s_{12} = 9.47$. Now the thermally averaged cross section is given as $\langle \sigma_{\text{eff}} | v_{\text{rel}} | \rangle = a_{\text{eff}} + 6b_{\text{eff}}/x$ and the relic abundance can be estimated by using the Eqn. (1.59). Using the first relation in Eqn. (4.13), we eliminate h_2 and since N_1 is the lightest odd particle, we take $r_1 < 1$ [117, 120] and $|h_i| < 1.5$ [118]. Fig. 4.2 depicts the allowed parameter space (h_1, r_1) consistent with current bounds on relic abundance [136]. Fig. 4.3 displays the relic abundance as a function of DM mass for various values of h_1 at two representative values of r_1 i.e., $r_1 = 0.5$ in the left panel and $r_1 = 0.6$ in the right panel. This shows that the mass range of DM mass consistent with current relic abundance is proportional with the parameter r_1 and the Yukawa coupling h_1 .

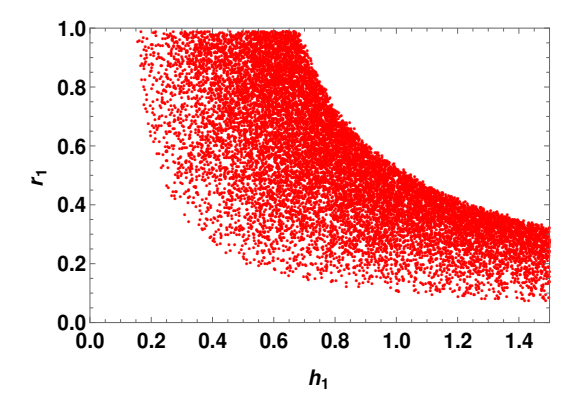


Figure 4.2: Parameter space of h_1 and r_1 consistent with 3σ relic abundance.

As the light neutrinos oscillate in flavor, one-loop diagrams can contribute to lepton flavor violating (LFV) decays. We now further constrain the parameter space of the model using these decays.

4.5 Lepton flavour violating decays

The observation of neutrino oscillations has provided an unambiguous signal for lepton flavor violation in the neutral lepton sector, even though individual lepton number is conserved in electroweak interactions in the SM. The evidence of light neutrino masses

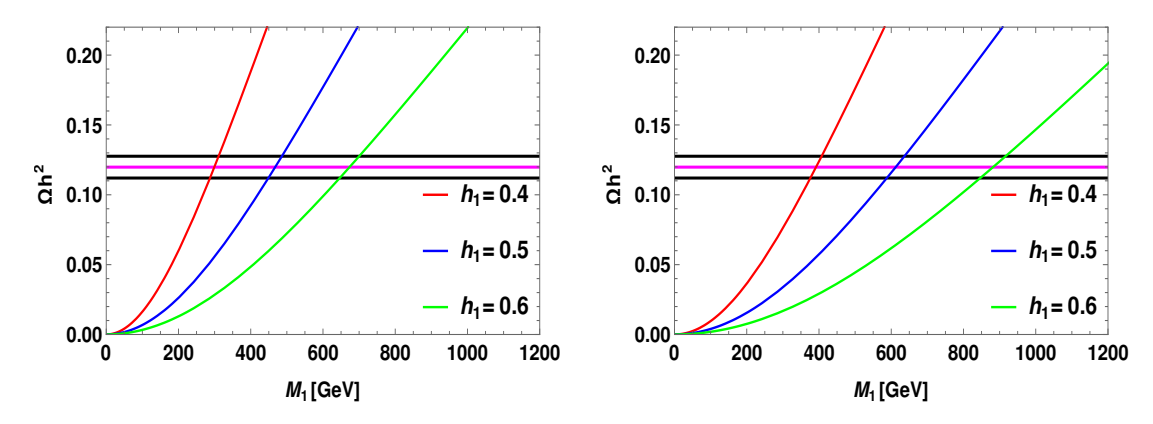


FIGURE 4.3: Variation of relic abundance with DM mass for various values of h_1 at $r_1 = 0.5$ (left panel) and $r_1 = 0.6$ (right panel) where the horizontal line (magenta) represents the central value of the relic density [136] and the black lines denote their corresponding 3σ range.

and mixing and the violation of family lepton number could in principle allow flavor changing neutral current (FCNC) transitions in the charged lepton sector as well, such as $\ell_{\alpha} \to \ell_{\beta} \gamma$ and $\ell_{\alpha} \to \ell_{\beta} \overline{\ell_{\beta}} \ell_{\beta}$.

The expression for the branching ratio of the LFV decay process $\ell_{\alpha} \to \ell_{\beta} \gamma$ written in terms of dipole form factor A_D is given by [119]

$$Br(\ell_{\alpha} \to \ell_{\beta} \gamma) = \frac{3(4\pi)^3 \alpha_{em}}{4G_F^2} |A_D|^2 Br(\ell_{\alpha} \to \ell_{\beta} \nu_{\alpha} \overline{\nu_{\beta}}), \qquad (4.18)$$

where $\alpha_{\rm em} = e^2/4\pi$ is the electromagnetic fine structure constant, G_F is the Fermi constant and α , β represent the lepton flavor. The diagrams contributing to A_D are shown in Fig. 4.4 and the expression is given by

$$A_D = \sum_{i=1}^{3} \frac{h_{i\beta}^* h_{i\alpha}}{2(4\pi)^2} \frac{1}{m_0^2} F_2(r_i).$$
 (4.19)

Here the expression for the loop function $F_2(x)$ is given in Appendix A and for simplicity we consider $\lambda_4 \ll \lambda_3$, thus we get η^+ and η^0 to be degenerate [117]. Applying the flavor structure (4.11), the relation (4.18) becomes

$$Br(\mu \to e\gamma) = \frac{3\alpha_{\rm em}}{64\pi G_F^2 m_0^4} \left| \left(h_2^2 - 0.68h_1^2 \right) F_2(r_1) + (3.56h_3^2) F_2(r_3) \right|^2. \tag{4.20}$$

We consider $r_3 > 1$, $M_1 < 2$ TeV and $M_3, m_0 < 8$ TeV and thus we work in the mass regime $M_1 \simeq M_2 < m_0 < M_3$. Of all the LFV decays, the decay channel $\mu \to e\gamma$ provides the most stringent constraint on the parameter space of this model.

Imposing the constraints from neutrino mass squared differences, relic abundance and current upper bound on $Br(\mu \to e\gamma)$ [137], Fig. 4.5 (left panel) shows the allowed region

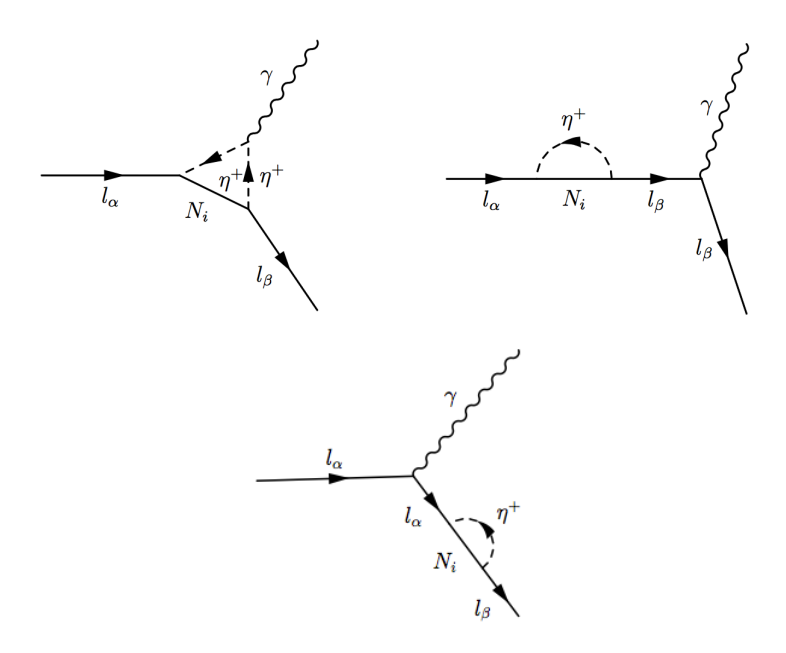


FIGURE 4.4: Diagrams contributing to $l_{\alpha} \to l_{\beta} \gamma$.

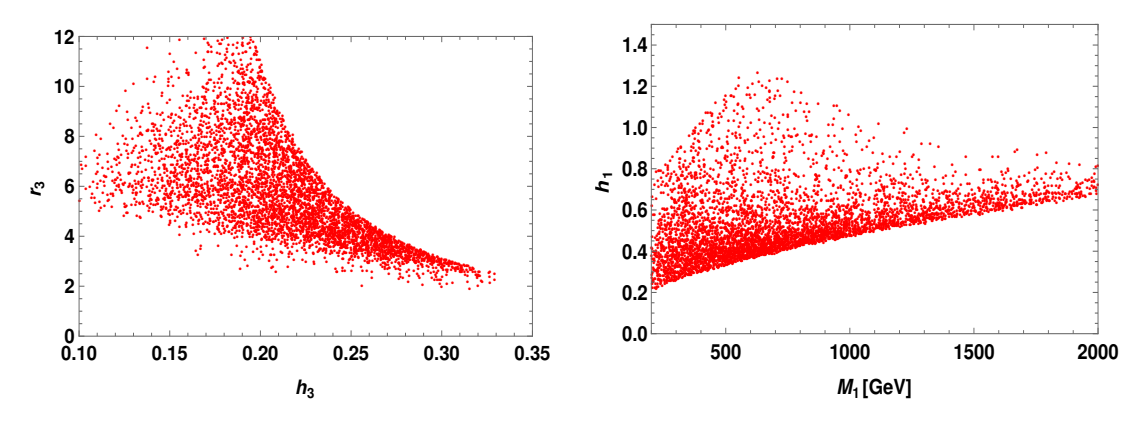


FIGURE 4.5: Parameter space of h_3 and r_3 (left panel) and variation of h_1 with M_1 (right panel) consistent with neutrino oscillation data, relic density and $Br(\mu \to e\gamma)$.

in the (h_3, r_3) parameter space of the model. From the figure, the lower bound on r_3 is 2 (i.e., $r_3 > 2$) and the upper bound on h_3 is 0.33 (i.e., $h_3 < 0.33$). Fig. 4.5 (right panel) depicts the variation of h_1 with the mass of DM. It shows that $\text{Br}(\mu \to e\gamma)$ excludes the values above 1.2 for h_1 . Now taking all the constraints from the flavor and dark sector, one can tabulate the allowed parameter space shown in Table. 4.2.

We follow a similar procedure to compute the branching ratios of $\tau \to e\gamma$ and $\tau \to \mu\gamma$ decays. Using the allowed parameter space given in Table. 4.2, we show in Fig. 4.6 the correlation plot between $\text{Br}(\tau \to e\gamma)$ and $\text{Br}(\tau \to \mu\gamma)$. In our analysis, we have used the measured branching ratios for $\mu \to \nu_{\mu} e \bar{\nu}_{e}$, $\tau^{-} \to \nu_{\tau} \mu^{-} \bar{\nu}_{\mu}$ and $\tau^{-} \to \nu_{\tau} e^{-} \bar{\nu}_{e}$ processes

Parameters	Range
r_1	$0.2 \rightarrow 1$
r_3	$2 \rightarrow 12$
$ h_1 $	$0.2 \rightarrow 1.2$
$ h_2 $	$0.2 \rightarrow 1.0$
$ h_3 $	$0.1 \rightarrow 0.33$

Table 4.2: Scotogenic model parameters with their range.

from [137] as

$$Br(\mu \to \nu_{\mu} e \bar{\nu}_{e}) = 100\% ,$$

$$Br(\tau \to \nu_{\tau} \mu \bar{\nu}_{\mu}) = (17.41 \pm 0.04)\% ,$$

$$Br(\tau \to \nu_{\tau} e \bar{\nu}_{e}) = (17.83 \pm 0.04)\% . \tag{4.21}$$

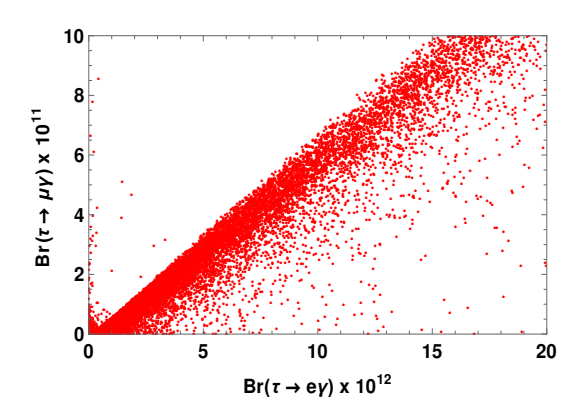


FIGURE 4.6: Correlation plot between $Br(\tau \to e\gamma)$ and $Br(\tau \to \mu\gamma)$.

Now we study lepton flavor violation in 3-body decays. As discussed in Ref.[119], these decays get contributions from three types of loop diagrams namely: γ -penguin, Z-penguin and box diagrams. The branching ratio for $\ell_{\alpha} \to 3 \, \ell_{\beta}$ in the scotogenic model is given by [119]

$$Br \left(\ell_{\alpha} \to \ell_{\beta} \overline{\ell_{\beta}} \ell_{\beta} \right) = \frac{3(4\pi)^{2} \alpha_{\text{em}}^{2}}{8G_{F}^{2}} \left[|A_{ND}|^{2} + |A_{D}|^{2} \left(\frac{16}{3} \log \left(\frac{m_{\alpha}}{m_{\beta}} \right) - \frac{22}{3} \right) + \frac{1}{6} |B|^{2} + \left(-2A_{ND}A_{D}^{*} + \frac{1}{3}A_{ND}B^{*} - \frac{2}{3}A_{D}B^{*} + \text{h.c.} \right) \right] \times Br \left(\ell_{\alpha} \to \ell_{\beta} \nu_{\alpha} \overline{\nu_{\beta}} \right).$$
(4.22)

The coefficient A_{D} denotes the photon dipole contributions given in Eqn. (4.19), while the coefficient A_{ND} represents the form factor with the photonic non-dipole contributions

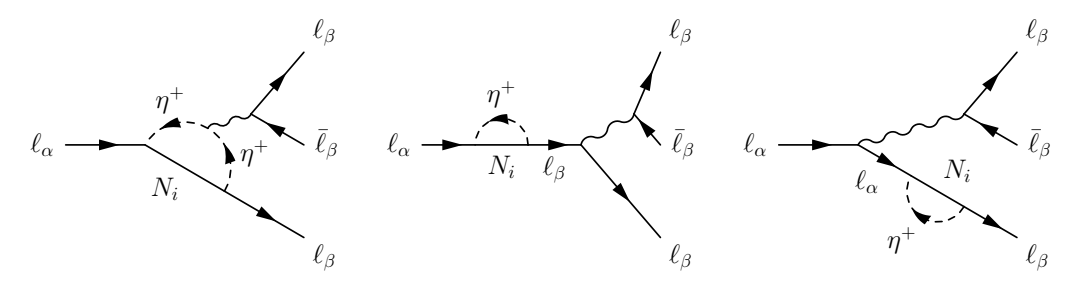


FIGURE 4.7: Penguin diagram contributions to $\ell_{\alpha} \to 3 \ell_{\beta}$. The mediator (wavy line) denotes either a photon or a Z-boson.

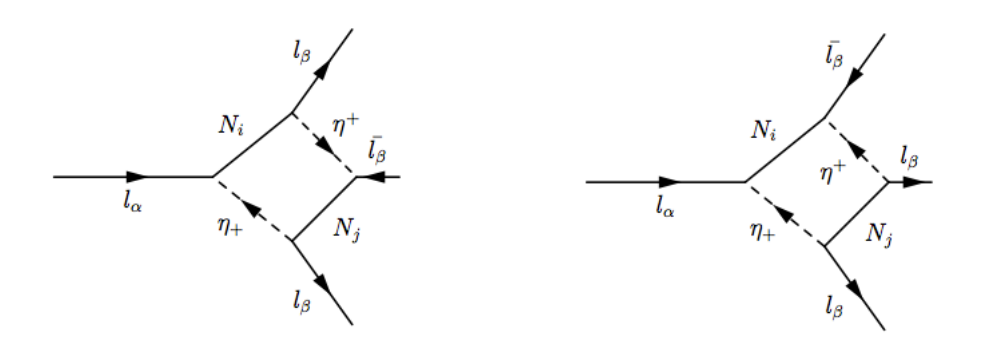


Figure 4.8: Box diagram contributions to $\ell_{\alpha} \to 3 \, \ell_{\beta}$.

given by

$$A_{ND} = \sum_{i=1}^{3} \frac{h_{i\beta}^{*} h_{i\alpha}}{6(4\pi)^{2}} \frac{1}{m_{0}^{2}} G_{2}(r_{i}).$$

$$(4.23)$$

Here $G_2(x)$ is a loop function, which is given in Appendix A. Z-pengiun diagrams shown in Fig. 4.7 give a negligible contribution to the decay width as explained in [119, 120]. Apart from photon dipole and non-dipole penguin contributions, the box diagrams shown in Fig. 4.8 also contribute to the decay width given by

$$B = \frac{1}{(4\pi)^2 e^2 m_0^2} \sum_{i,j=1}^{3} \left[\frac{1}{2} D_1(r_i, r_j) h_{j\beta}^* h_{j\beta} h_{i\beta}^* h_{i\alpha} + r_i r_j D_2(r_i, r_j) h_{j\beta}^* h_{j\beta}^* h_{i\beta} h_{i\alpha} \right]. \tag{4.24}$$

The loop functions $D_1(x,y)$ and $D_2(x,y)$ are provided in Appendix A.

Using the allowed parameter space from Table. 4.2, we show in Fig. 4.9 the correlation plot between $\mu \to e\gamma$ and $\mu \to eee$ (left panel). Similarly the right panel in Fig. 4.9 depicts the correlation plot between branching ratios of $\tau \to eee$ and $\tau \to \mu\mu\mu$. From these figures we conclude that all the obtained branching ratios in the viable parameter space are within the experimental limits.

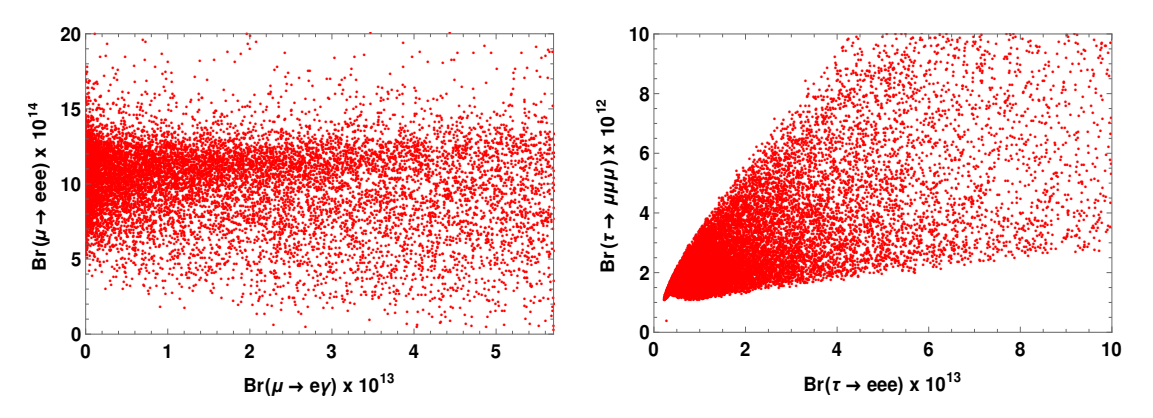


FIGURE 4.9: Correlation plots between $Br(\mu \to eee)$ and $Br(\mu \to e\gamma)$ (left panel) and between $Br(\tau \to \mu\mu\mu)$ and $Br(\tau \to eee)$ (right panel).

4.6 Conclusion

We have considered the scotogenic model, which is an extension of the standard model with an additional inert scalar doublet and three heavy Majorana right-handed neutrinos. We have diagonalized the neutrino radiative mass matrix using the TBM matrix with an additional perturbed matrix as a rotation matrix in the 13 plane. The mixing angles are chosen ($\theta = 35^{\circ}$ and $\varphi = 12^{\circ}$) to accommodate a sizeable θ_{13} . Working in a degenerate heavy neutrino mass spectrum, we have obtained a flavor structure favorable to explain normal neutrino mass ordering. Choosing the lightest of the odd particles as dark matter, we have computed the relic abundance including the co-annihilation effects. Scanning over the entire parameter space and applying the constraints from neutrino oscillation data, dark matter observables and bounds from lepton flavor violating decays such as $\ell_{\alpha} \to \ell_{\beta} \gamma$ and $\ell_{\alpha} \to 3 \ell_{\beta}$, we have shown the suitable range for various parameters in the model.

Chapter 5

Exploring Majorana dark matter in connection to flavor anomalies in $L_{\mu} - L_{\tau}$ Model

So far, we have explored dark matter phenomenology in connection to neutrino sector. In the present chapter, we shift our emphasis to reconcile the quark sector anomalies, which are indirectly linked to new physics beyond the SM, in a simple theoretical framework.

5.1 Brief note on flavor anomalies

Recently, the LHCb experiment has reported discrepancies of $(2-4)\sigma$ [138–143] in several physical observables associated with flavor changing neutral current $b \to s l^+ l^-$ processes. Especially, the observation of 3σ anomaly in the P_5' angular observables [141] and the decay rate [142] of $B \to K^* \mu^+ \mu^-$ processes have attracted a lot of attention in recent times. The decay rate of $B_s \to \phi \mu^+ \mu^-$ has also 3σ deviation compared to its SM prediction [140]. Furthermore, the LHCb Collaboration has observed the violation of lepton universality in $B^+ \to K^+ l^+ l^-$ process in the low $q^2 \in [1,6]$ GeV² region [139]

$$R_K^{\text{Expt}} = \frac{\text{Br}(B^+ \to K^+ \mu^+ \mu^-)}{\text{Br}(B^+ \to K^+ e^+ e^-)} = 0.745^{+0.090}_{-0.074} \pm 0.036, \tag{5.1}$$

which has a 2.6σ deviation from the corresponding SM result [144]

$$R_K^{\rm SM} = 1.0003 \pm 0.0001.$$
 (5.2)

In addition, an analogous lepton non-universality (LNU) parameter (R_{K^*}) has also been observed in $B^0 \to K^{*0}l^+l^-$ processes [138]

$$R_{K^*}^{\text{Expt}} = \frac{\text{Br}(B^0 \to K^{*0} \mu^+ \mu^-)}{\text{Br}(B^0 \to K^{*0} e^+ e^-)} = 0.66_{-0.07}^{+0.11} \pm 0.03, \quad q^2 \in [0.045, 1.1] \text{ GeV}^2,$$

$$= 0.69_{-0.07}^{+0.11} \pm 0.05, \quad q^2 \in [1.1, 6] \text{ GeV}^2, \quad (5.3)$$

which correspond to the deviation of 2.2σ and 2.4σ from their SM predictions [145]

$$R_{K^*}^{\text{SM}}|_{q^2 \in [0.045, 1.1] \text{ GeV}^2} = 0.92 \pm 0.02, \quad R_{K^*}^{\text{SM}}|_{q^2 \in [1.1, 6] \text{ GeV}^2} = 1.00 \pm 0.01.$$
 (5.4)

To resolve the above $b \to sll$ anomalies, we extend the SM gauge group $SU(3)_C \times SU(2)_L \times U(1)_Y$ with a local $U(1)_{L_\mu - L_\tau}$ symmetry. The anomaly free $L_\mu - L_\tau$ gauge extensions [146, 147] are captivating with minimal new particles and parameters, rich in phenomenological perspective. The model is quite simple in structure, suitable to study the phenomenology of DM, neutrino and also the flavor anomalies. It is well explored in dark matter context in literature [148–151], in the gauge and scalar portals. The approach of adding color triplet particles to shed light on the flavor sector thereby connecting with dark sector is interesting. Leptoquarks (LQ) are not only advantageous in addressing the flavor anomalies, but also act as a mediator between the visible and dark sector. Few works were already done with this motivation [152–155].

Leptoquarks are hypothetical color triplet gauge particles, with either spin-0 (scalar) or spin-1 (vector), which connect the quark and lepton sectors and thus, carry both baryon and lepton numbers simultaneously. They can arise from various extended standard model scenarios [156–167], which treat quarks and leptons on equal footing, such as the grand unified theories (GUTs) [156–159], color SU(4) Pati-Salam model [160–164], extended technicolor model [165, 166] and the composite models of quark and lepton [167]. In this chapter, we study a new version of $U(1)_{L_{\mu}-L_{\tau}}$ gauge extension of SM with a $(\bar{3}, 1, 1/3)$ scalar LQ (SLQ) and an inert doublet, to study the phenomenology of dark matter, neutrino mass generation and compute the flavor observables on a single platform. The SLQ mediates the annihilation channels contributing to relic density and also plays a crucial role in direct searches as well, providing a spin-dependent WIMPnucleon cross section which is quite sensitive to the recent and ongoing direct detection experiments such as PICO-60 and LUX. The Z' gauge boson of extended U(1) symmetry and the SLQ also play an important role in settling the known issues of flavor sector. In this regard, we would like to investigate whether the observed anomalies in the rare leptonic/semileptonic decay processes mediated by $b \to s l^+ l^-$ transitions, can be explained in the present framework. We analyze the implications of the model on both the DM and flavor sectors, in particular on $B \to V l^+ l^ (V = K^*, \phi)$ decay modes.

In literature [168–188], there were many attempts being made to explain the observed anomalies of rare B decays in the scalar leptoquark model.

5.2 New $L_{\mu} - L_{\tau}$ model with a scalar leptoquark

We study the well known anomaly free $U(1)_{L_{\mu}-L_{\tau}}$ extension of SM with three neutral fermions N_e, N_{μ}, N_{τ} , with $L_{\mu} - L_{\tau}$ charges 0,1 and -1 respectively. A scalar singlet ϕ_2 , charged +2 under the new U(1) is added to spontaneously break the local $U(1)_{L_{\mu}-L_{\tau}}$ gauge symmetry. We also introduce an inert doublet (η_I) and a scalar leptoquark $S_1(\bar{3},1,1/3)$ with $L_{\mu}-L_{\tau}$ charges 0 and -1 to the scalar content of the model. We impose an additional Z_2 symmetry under which all the new fermions, η_I and the leptoquark are odd and rest are even. The particle content and their corresponding charges are displayed in Table. 5.1.

	Field	$SU(3)_C \times SU(2)_L \times U(1)_Y$	$U(1)_{L_{\mu}-L_{\tau}}$	Z_2
Fermions	$Q_L \equiv (u, d)_L^T$	(3, 2, 1/6)	0	+
	u_R	(3,1, 2/3)	0	+
	d_R	(3,1, -1/3)	0	+
	$e_L \equiv (\nu_e, e)_L^T$	(1,2, -1/2)	0	+
	e_R	(1,1,-1)	0	+
	$\mu_L \equiv (\nu_\mu, \ \mu)_L^T$	(1,2, -1/2)	1	+
	μ_R	(1,1,-1)	1	+
	$\tau_L \equiv (\nu_{\tau}, \ \tau)_L^T$	(1,2, -1/2)	-1	+
	$ au_R$	(1,1,-1)	-1	+
	N_e	(1,1, 0)	0	_
	N_{μ}	(1,1, 0)	1	_
	$N_{ au}$	(1,1, 0)	-1	_
Scalars	Н	(1, 2, 1/2)	0	+
	η_I	(1, 2, 1/2)	0	-
	ϕ_2	(1,1, 0)	2	+
	S_1	$(\bar{\bf 3},{\bf 1},\ 1/3)$	-1	_

Table 5.1: Fields and their charges of the proposed $U(1)_{L_{\mu}-L_{\tau}}$ model.

The Lagrangian of the present model can be written as

$$\mathcal{L} = \mathcal{L}_{SM} - \frac{1}{4} Z'_{\mu\nu} Z'^{\mu\nu} - g_{\mu\tau} \overline{\mu}_L \gamma^{\mu} \mu_L Z'_{\mu} - g_{\mu\tau} \overline{\mu}_R \gamma^{\mu} \mu_R Z'_{\mu} + g_{\mu\tau} \overline{\tau}_L \gamma^{\mu} \tau_L Z'_{\mu} + g_{\mu\tau} \overline{\tau}_R \gamma^{\mu} \tau_R Z'_{\mu}
+ \overline{N}_e i \partial N_e + \overline{N}_{\mu} \left(i \partial - g_{\mu\tau} Z'_{\mu} \gamma^{\mu} \right) N_{\mu} + \overline{N}_{\tau} \left(i \partial + g_{\mu\tau} Z'_{\mu} \gamma^{\mu} \right) N_{\tau} - \frac{f_{\mu}}{2} \left(\overline{N_{\mu}^c} N_{\mu} \phi_2^{\dagger} + \text{h.c.} \right)
- \frac{f_{\tau}}{2} \left(\overline{N_{\tau}^c} N_{\tau} \phi_2 + \text{h.c.} \right) - \frac{1}{2} M_{ee} \overline{N_e^c} N_e - \frac{1}{2} M_{\mu\tau} \left(\overline{N_{\mu}^c} N_{\tau} + \overline{N_{\tau}^c} N_{\mu} \right) - \sum_{q=d,s,b} \left(y_{qR} \overline{d_{qR}^c} S_1 N_{\mu} + \text{h.c.} \right)
- \sum_{i=e,\mu,\tau} Y_{\beta i}^{\nu} (\overline{l_L})_{\beta} \tilde{\eta}_I N_{iR} + \left| \left(i \partial_{\mu} - \frac{g}{2} \tau^a \cdot W_{\mu}^a - \frac{g'}{2} B_{\mu} \right) \eta_I \right|^2 + \left| \left(i \partial_{\mu} - \frac{g'}{3} B_{\mu} + g_{\mu\tau} Z'_{\mu} \right) S_1 \right|^2
+ \left| \left(i \partial_{\mu} - 2 g_{\mu\tau} Z'_{\mu} \right) \phi_2 \right|^2 - V(H, \eta_I, \phi_2, S_1), \tag{5.5}$$

where the scalar potential V is

$$V(H, \eta_{I}, \phi_{2}, S_{1}) = \mu_{H}^{2} H^{\dagger} H + \lambda_{H} (H^{\dagger} H)^{2} + \mu_{\eta_{I}} (\eta_{I}^{\dagger} \eta_{I}) + \lambda_{\eta_{I}} (\eta_{I}^{\dagger} \eta_{I})^{2} + \lambda_{H \eta_{I}} (H^{\dagger} H) (\eta_{I}^{\dagger} \eta_{I})$$

$$+ \lambda'_{H \eta_{I}} (H^{\dagger} \eta_{I}) (\eta_{I}^{\dagger} H) + \frac{\lambda''_{H \eta_{I}}}{2} \left[(H^{\dagger} \eta_{I})^{2} + \text{h.c.} \right] + \mu_{2}^{2} (\phi_{2}^{\dagger} \phi_{2}) + \lambda_{2} (\phi_{2}^{\dagger} \phi_{2})^{2} + \mu_{S}^{2} (S_{1}^{\dagger} S_{1})$$

$$+ \lambda_{S} (S_{1}^{\dagger} S_{1})^{2} + \left[\lambda_{H 2} (\phi_{2}^{\dagger} \phi_{2}) + \lambda_{H S} (S_{1}^{\dagger} S_{1}) \right] (H^{\dagger} H) + \lambda_{S 2} (\phi_{2}^{\dagger} \phi_{2}) (S_{1}^{\dagger} S_{1})$$

$$+ \lambda_{\eta_{I} 2} (\phi_{2}^{\dagger} \phi_{2}) (\eta_{I}^{\dagger} \eta_{I}) + \lambda_{S \eta_{I}} (S_{1}^{\dagger} S_{1}) (\eta_{I}^{\dagger} \eta_{I}). \tag{5.6}$$

The gauge symmetry $SU(2)_L \times U(1)_Y \times U(1)_{L_\mu - L_\tau}$ is spontaneously broken to $SU(2)_L \times U(1)_Y$ by assigning a VEV v_2 to the complex singlet ϕ_2 . Then the SM Higgs doublet breaks the SM gauge group to low energy theory by obtaining a VEV v. The new neutral gauge boson Z' associated with the U(1) extension absorbs the massless pseudoscalar in ϕ_2 to become massive. The neutral components of the fields H and ϕ_2 can be written in terms of real scalars and pseudoscalars as

$$H^{0} = \frac{1}{\sqrt{2}}(v+h) + \frac{i}{\sqrt{2}}z,$$

$$\phi_{2} = \frac{1}{\sqrt{2}}(v_{2} + h_{2}) + \frac{i}{\sqrt{2}}A_{2}.$$
(5.7)

The inert doublet is denoted by $\eta_I = \begin{pmatrix} \eta_c^+ \\ \frac{\eta_c + i\eta_o}{\sqrt{2}} \end{pmatrix}$. The masses of its charged and neural components are given by

$$M_{\eta_c}^2 = \mu_{\eta_I}^2 + \frac{\lambda_{H\eta_I}}{2} v^2 + \frac{\lambda_{\eta_I 2}}{2} v_2^2,$$

$$M_{\eta_e}^2 = \mu_{\eta_I}^2 + \frac{\lambda_{\eta_I 2}}{2} v_2^2 + \left(\lambda_{H\eta_I} + \lambda'_{H\eta_I} + \lambda''_{H\eta_I}\right) \frac{v^2}{2},$$

$$M_{\eta_o}^2 = \mu_{\eta_I}^2 + \frac{\lambda_{\eta_I 2}}{2} v_2^2 + \left(\lambda_{H\eta_I} + \lambda'_{H\eta_I} - \lambda''_{H\eta_I}\right) \frac{v^2}{2}.$$
(5.8)

The masses obtained by the colored scalar and the gauge boson Z' are

$$M_{S_1}^2 = 2\mu_S^2 + \lambda_{HS}v^2 + \lambda_{S2}v_2^2,$$

 $M_{Z'} = 2v_2g_{\mu\tau}.$ (5.9)

In the whole discussion of the results, we consider the benchmark values for the masses of the scalar spectrum as $(M_{S_1}, M_{\eta_c}, M_{\eta_{c,o}}) = (1.2, 2, 1.5)$ TeV.

5.3 Mixing in the fermion and scalar sector

The fermion and scalar mass matrices take the form

$$M_N = \begin{pmatrix} \frac{1}{\sqrt{2}} f_{\mu} v_2 & M_{\mu\tau} \\ M_{\mu\tau} & \frac{1}{\sqrt{2}} f_{\tau} v_2 \end{pmatrix} , \quad M_S = \begin{pmatrix} 2\lambda_H v^2 & \lambda_{H2} v v_2 \\ \lambda_{H2} v v_2 & 2\lambda_2 v_2^2 \end{pmatrix} .$$
 (5.10)

One can diagonalize the above mass matrices by $U_{\alpha(\Theta)}^T M_{N(S)} U_{\alpha(\Theta)} = \text{diag} [M_{N_-(H_1)}, M_{N_+(H_2)}],$ where

$$U_{\theta} = \begin{pmatrix} \cos \theta & \sin \theta \\ -\sin \theta & \cos \theta \end{pmatrix}, \tag{5.11}$$

with
$$\Theta = \frac{1}{2} \tan^{-1} \left(\frac{\lambda_{H2} v v_2}{\lambda_2 v_2^2 - \lambda_H v^2} \right)$$
 and $\alpha = \frac{1}{2} \tan^{-1} \left(\frac{M_{\mu\tau}}{(f_{\tau} - f_{\mu})(v_2/\sqrt{2})} \right)$.

We denote the scalar mass eigenstates as H_1 and H_2 , with H_1 is assumed to be observed Higgs at LHC with $M_{H_1} = 125.09$ GeV and v = 246 GeV. The mixing parameter Θ is taken minimal to stay with LHC limits on Higgs decay width. We indicate N_- and N_+ to be the fermion mass eigenstates, with the lightest one (N_-) as the probable dark matter in the present work.

5.4 Dark matter phenomenology

5.4.1 Relic abundance

The model allows the dark matter (N_{-}) to have gauge and scalar mediated annihilation channels. The possible contributing diagrams are provided in Fig. 5.1 which are mediated by $(H_1, H_2, \eta_c^+, \eta_{e,o}, S_1, Z')$. Majorana DM in $H_{1,2}$ portal (upper row in Fig. 5.1) has already been well explored in literature [99]. Here, we focus on (Z', S_1, η_I) -mediated channels (middle and bottom rows in Fig. 5.1) contributing to DM observables, which

we later make connection with radiative neutrino mass as well as flavor observables.

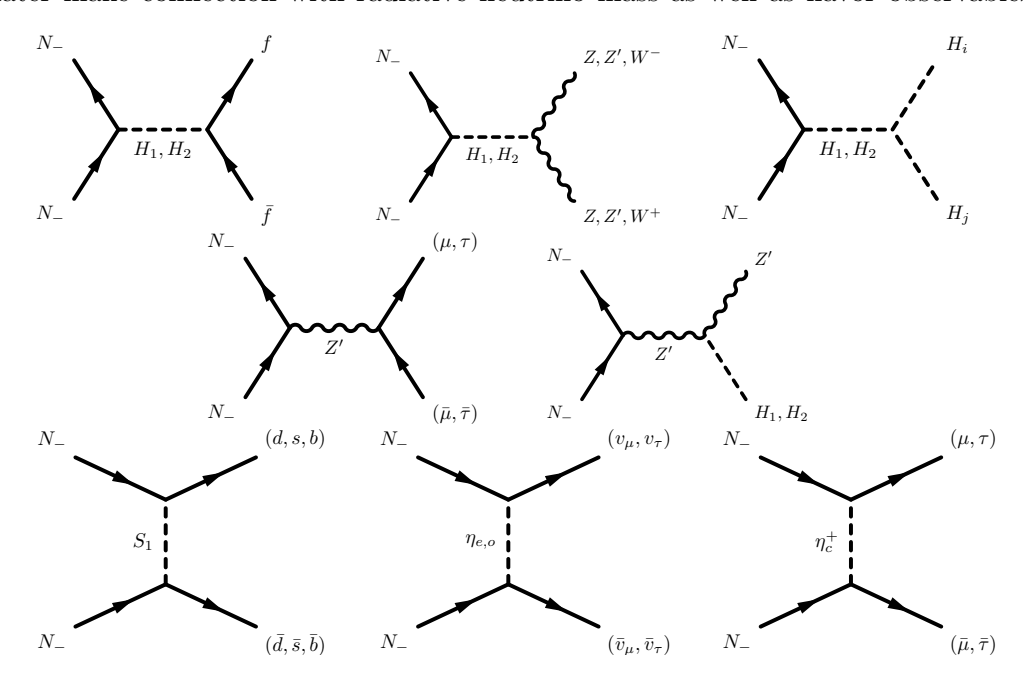


FIGURE 5.1: Feynman diagrams contributing to relic density.

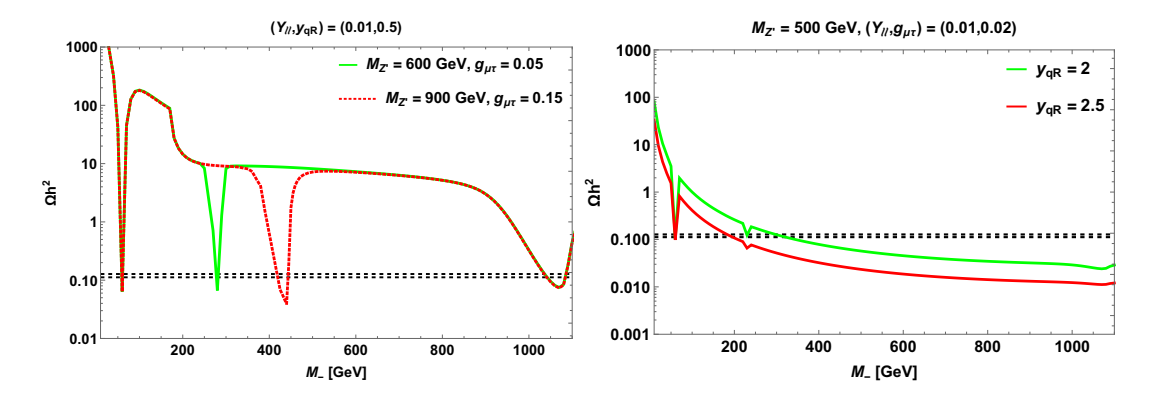


FIGURE 5.2: Behavior of relic density plotted against DM mass with $M_{H_2}=2.2$ TeV, shown with varying $M_{Z'}$ and $g_{\mu\tau}$ (left panel) and y_{qR} (right panel). Black horizontal dotted lines denote the 3σ range of Planck limit [22].

From the annihilation cross section, the relic density can be estimated by the formula given in Eqn. (1.59). As seen from the left panel of Fig. 5.2, the relic density with s-channel contribution is featured to meet the Planck limit [22] near the resonance in propagator (H_1, H_2, Z') , i.e., near $M_- = \frac{M_{\text{prop}}}{2}$. We restrict our discussion to the mass region (in GeV), $100 \le M_{Z'} \le 1000$, $80 \le M_- \le 1000$ and also H_2 is considered to be sufficiently large such that its resonance doesn't meet the Planck limit below 1 TeV region of DM mass. Now, in this mass range of DM, the channels mediated by (Z', η_I, S_1) drive the relic density observable, where the gauge coupling $g_{\mu\tau}$ controls the s-channel

contribution, while Y^{ν} and y_{qR} are relevant in t-channel contributions. The relevant parameters in our investigation are $(M_{-}, g_{\mu\tau}, M_{Z'}, Y^{\nu}, y_{qR})$. The effect of these parameters on the relic abundance is made transparent in Fig. 5.2, where we fixed $Y^{\nu} \sim 10^{-2}$, in order to explain neutrino mass at one loop level. Left panel shows the variation of relic density with varying gauge parameters $g_{\mu\tau}$ and $M_{Z'}$, right panel depicts the behaviour with varying y_{qR} parameter. No significant constraint on $M_{Z'}$, $g_{\mu\tau}$ parameters is observed, however relic density has an appreciable footprint on $M_{-} - (y_{qR})^2$ parameter space, which will be discussed in the next section.

5.4.2 Direct searches

Moving to direct searches, the Z'-portal WIMP-nucleon cross section is insensitive to direct detection experiments as mentioned earlier in section. 3.3.2. The t-channel scalar (H_1, H_2) exchange can give spin-independent contribution, but it doesn't help our purpose of study. In the scalar portal, one can obtain contribution from spin-dependent interaction mediated by SLQ, of the form

$$\mathcal{L}_{\text{eff}} \simeq \frac{y_{qR}^2 \cos^2 \alpha}{4(M_{S_1}^2 - M_-^2)} \overline{N_-} \gamma^{\mu} \gamma^5 N_- \overline{q} \gamma_{\mu} \gamma^5 q. \qquad (5.12)$$

Comparing with Eqn. (1.70), the corresponding cross section can be derived from the formula in Eqn. (1.71),

$$\sigma_{S_1} = \frac{\mu^2}{\pi} \frac{\cos^4 \alpha}{(M_{S_1}^2 - M_-^2)^2} \left[y_{dR}^2 \Delta_d + y_{sR}^2 \Delta_s \right]^2 J_N(J_N + 1), \tag{5.13}$$

The values of quark spin fractions $\Delta_{d,s}$ are provided in Table. 1.2. Now, it is obvious that it can constrain the parameters M_{-} and $(y_{qR})^2$. Fig. 5.3 left panel displays $M_{-} - (y_{qR}^2)$ parameter space (green and red regions) remained after imposing Planck [22] 3σ limit on current relic density. Here, the region shown in green turns out to be excluded by most stringent PICO-60 [39] limit on SD WIMP-proton cross section, as seen from the right panel.

5.5 Radiative neutrino mass

From the Yukawa interaction term involving the inert doublet η_I in Eqn. (5.5), neutrino mass can be calculated for the diagram shown in Fig. 4.1, as

$$(\mathcal{M}_{\nu})_{\beta\gamma} = \frac{\lambda_{H\eta_I}''v^2}{16\pi^2} \sum_{i=e,\mu,\tau} \frac{Y_{\beta i}^{\nu} Y_{\gamma i}^{\nu} M_{Di}}{m_0^2 - M_{Di}^2} \left[1 + \frac{M_{Di}^2}{m_{\eta_I}^2 - M_{Di}^2} \ln \frac{M_{Di}^2}{m_{\eta_I}^2} \right].$$
 (5.14)

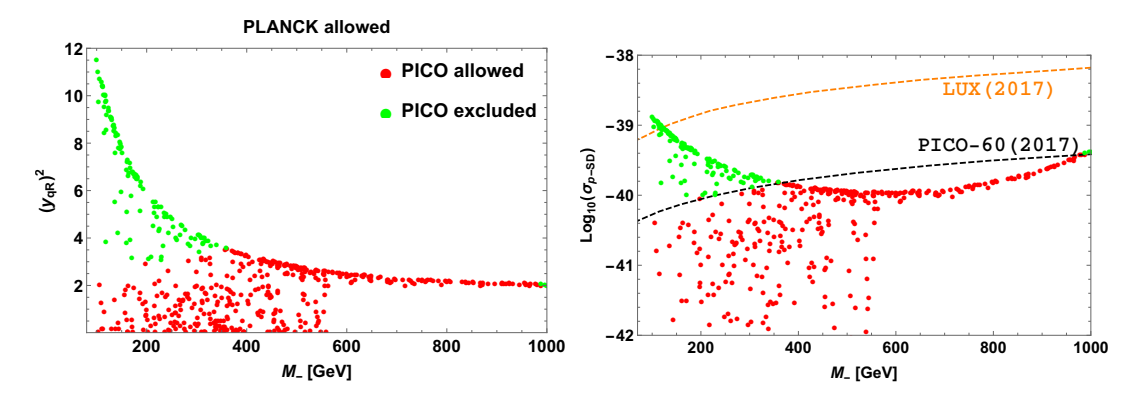


FIGURE 5.3: Left panel depicts the $M_- - (y_{qR})^2$ parameter space consistent upto 3σ level of Planck limit [22] on relic density. Right panel gives the SD WIMP-proton cross section as a function of DM mass. Dashed lines represent the recent bounds obtained from PICO-60 [39] and LUX [40]. Green (red) data points in both the panels represent Planck allowed and PICO excluded (Planck and PICO allowed).

Here $M_{Di} = (U^T M_N U)_i = \text{diag}(M_{ee}, M_-, M_+)$ and the fermion mass eigenstates $N_{Di} = U_{ij}^{\dagger} N_j$. With a sample parameter space, $(Y^{\nu}, \lambda''_{H\eta_I}) \sim (10^{-2}, 10^{-5})$ and $(m_{\eta_I}, M_-, M_{ee}, M_+) \sim (1.5, 0.4, 3, 3)$ TeV, one can explain neutrino mass (m_{ν}) near eV scale. Thus, the light neutrino mass generation can be successfully achieved in the proposed model.

5.6 Flavor phenomenology

The general effective Hamiltonian responsible for the quark level transition $b \to s l^+ l^-$ is given by [189, 190]

$$\mathcal{H}_{\text{eff}} = -\frac{4G_F}{\sqrt{2}} V_{tb} V_{ts}^* \left[\sum_{i=1}^6 C_i(\mu) O_i + \sum_{i=7,9,10} \left(C_i(\mu) O_i + C_i'(\mu) O_i' \right) \right], \quad (5.15)$$

where G_F is the Fermi constant and $V_{qq'}$ denote the Cabibbo-Kobayashi-Maskawa (CKM) matrix elements. The C_i 's stand for the Wilson coefficients evaluated at the renormalized scale $\mu = m_b$ [191], where the sum over i includes the current-current operators (i = 1, 2) and the QCD-penguin operators (i = 3, 4, 5, 6). The quark level operators mediating leptonic/semileptonic processes are given as

$$O_{7}^{(\prime)} = \frac{e}{16\pi^{2}} \Big(\bar{s}\sigma_{\mu\nu} \left(m_{s} P_{L(R)} + m_{b} P_{R(L)} \right) b \Big) F^{\mu\nu},$$

$$O_{9}^{(\prime)} = \frac{\alpha_{\text{em}}}{4\pi} (\bar{s}\gamma^{\mu} P_{L(R)} b) (\bar{l}\gamma_{\mu} l) , \qquad O_{10}^{(\prime)} = \frac{\alpha_{\text{em}}}{4\pi} (\bar{s}\gamma^{\mu} P_{L(R)} b) (\bar{l}\gamma_{\mu}\gamma_{5} l) , \quad (5.16)$$

where $\alpha_{\rm em}$ denotes the fine-structure constant and $P_{L,R} = (1 \mp \gamma_5)/2$ are the chiral operators. The primed operators are absent in the SM, but can exist in the proposed $L_{\mu} - L_{\tau}$ model.

The previous section has discussed the available new parameter space consistent with the DM observables which are within their respective experimental limits. However, these parameters can be further constrained from the quark and lepton sectors, to be presented in the subsequent sections.

5.6.1 $B_s - \bar{B}_s$ mixing

In this subsection, we discuss the constraint on the new parameters from the mass difference between the B_s meson mass eigenstates (ΔM_s) , which characterizes the $B_s - \bar{B}_s$ mixing phenomena. In the SM, $B_s - \bar{B}_s$ mixing proceeds to an excellent approximation through the box diagram with internal top quark and W boson exchange. The effective Hamiltonian describing the $\Delta B = 2$ transition is given by [192]

$$\mathcal{H}_{\text{eff}} = \frac{G_F^2}{16\pi^2} \,\lambda_t^2 \,M_W^2 S_0(x_t) \eta_B(\bar{s}b)_{V-A}(\bar{s}b)_{V-A} \,, \tag{5.17}$$

where $\lambda_t = V_{tb}V_{ts}^*$, η_B is the QCD correction factor and $S_0(x_t)$ is the loop function [192] with $x_t = m_t^2/M_W^2$. Using Eqn. (5.17), the $B_s - \bar{B}_s$ mass difference in the SM is given as

$$\Delta M_s^{\text{SM}} = 2|M_{12}^{\text{SM}}| = \frac{\langle \bar{B}_s | \mathcal{H}_{eff} | B_s \rangle}{M_{B_s}} = \frac{G_F^2}{6\pi^2} M_W^2 \ \lambda_t^2 \ \eta_B \ \hat{B}_s f_{B_s}^2 M_{B_s} S_0(x_t) \ . \tag{5.18}$$

The SM predicted value of ΔM_s by using the input parameters from [193, 194] is

$$\Delta M_s^{\text{SM}} = (17.426 \pm 1.057) \text{ ps}^{-1},$$
 (5.19)

and the corresponding experimental value is [193]

$$\Delta M_s^{\text{Expt}} = 17.761 \pm 0.022 \text{ ps}^{-1}.$$
 (5.20)

Even though the theoretical prediction is in good agreement with the experimental $B_s - \bar{B}_s$ oscillation data, it does not completely rule out the possibility of new physics.

The box diagrams for $B_s - \bar{B}_s$ mixing in the presence of singlet SLQ and N_{\pm} are shown in Fig. 5.4. The effective Hamiltonian in the presence NP is given by

$$\mathcal{H}_{\text{eff}} = \frac{(y_{sR}y_{bR})^2}{128\pi^2 M_{S_1}^2} \cos^2 \alpha \sin^2 \alpha C_{B_s}^{\text{NP}} (\bar{s}b)_{V+A} (\bar{s}b)_{V+A} , \qquad (5.21)$$

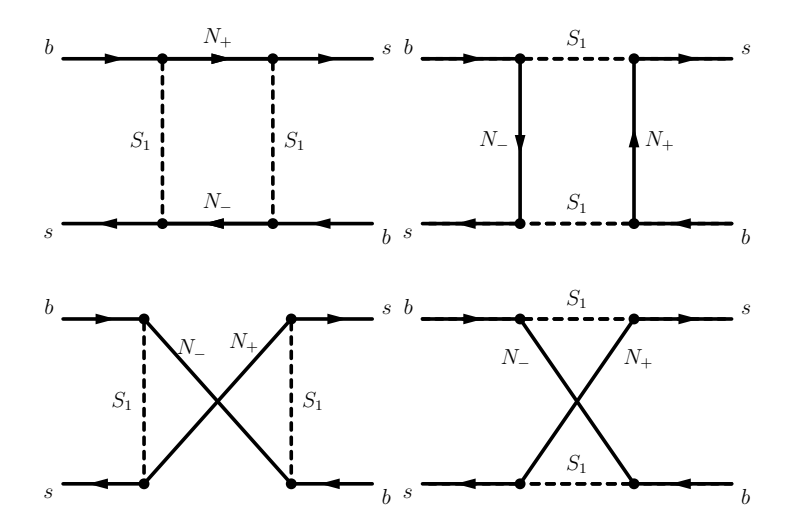


Figure 5.4: Box diagrams of $B_s - \bar{B}_s$ mixing with leptoquark in the loop.

where

$$C_{B_s}^{\text{NP}} = 2k(\chi_{-}, \chi_{-}, 1) + 4k(\chi_{-}, \chi_{+}, 1) + 2k(\chi_{+}, \chi_{+}, 1) + \chi_{-}j(\chi_{-}, \chi_{-}, 1) + 2\sqrt{\chi_{-}\chi_{+}}j(\chi_{-}, \chi_{+}, 1) + \chi_{+}j(\chi_{+}, \chi_{-}, 1),$$
(5.22)

with $\chi_{\mp} = M_{\mp}^2/M_{S_1}^2$ and the loop functions $k(\chi_{\pm}, \chi_{\mp}, 1)$, $j(\chi_{\pm}, \chi_{\mp}, 1)$ are presented in Appendix B [152]. Using Eqn. (5.21), the mass difference of $B_s - \bar{B}_s$ mixing due to the exchange of S_1 and N_{\pm} is found to be

$$\Delta M_s^{\text{NP}} = \frac{(y_{sR}y_{bR})^2}{48\pi^2 M_{S_1}^2} \cos^2 \alpha \sin^2 \alpha C_{B_s}^{\text{NP}} \eta_B \hat{B}_{B_s} f_{B_s}^2 M_{B_s} . \tag{5.23}$$

Including the NP contribution arising due to the SLQ exchange, the total mass difference can be written as

$$\Delta M_s = \Delta M_s^{\text{SM}} \left[1 + \frac{C_{B_s}^{\text{NP}} \cos^2 \alpha \sin^2 \alpha}{8G_F^2 V_{tb}^2 V_{ts}^{*2} M_W^2 S_0(x_t)} \left(\frac{(y_{sR} y_{bR})^2}{M_{S_1}^2} \right) \right] . \tag{5.24}$$

Using Eqns. (5.19) and (5.20) in (5.24), one can put bound on $(y_{qR})^2$ and M_- parameters.

5.6.2 $B \rightarrow Kl^+l^-$ process

The rare semileptonic $B \to K l^+ l^-$ process is mediated via $b \to s l^+ l^-$ quark level transitions. In the current framework, the $b \to s l^+ l^-$ transitions can occur via the Z' exchanging one-loop penguin diagrams shown in Fig. 5.5.

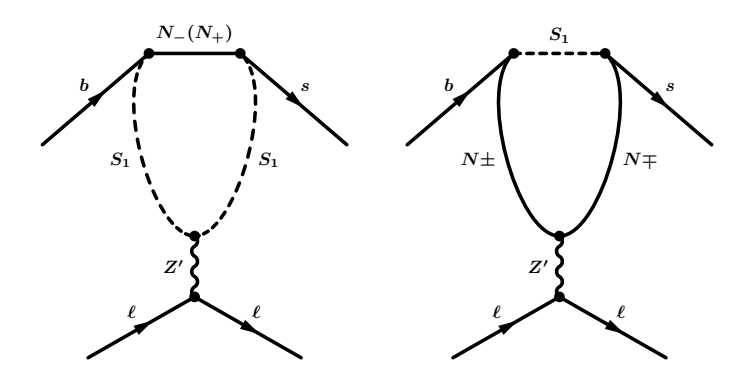


FIGURE 5.5: Penguin diagram of $b \to sll$ processes, where $l = \mu, \tau$ with leptoquark in the loop.

The matrix elements of the various hadronic currents between the initial B meson and K meson in the final state are related to the form factors $f_{+,0}$ as follows [144, 195]

$$\langle K(p_K) | \bar{s} \gamma^{\mu} b | B(p_B) \rangle = f_+(q^2) (p_B + p_K)^{\mu} + \left[f_0(q^2) - f_+(q^2) \right] \frac{M_B^2 - M_K^2}{q^2} q^{\mu}, (5.25)$$

where p_B (p_K) and M_B (M_K) denote the 4-momenta and mass of the B (K) meson and q^2 is the momentum transfer. By using Eqn. (5.25), the transition amplitude of $B \to K \mu^+ \mu^-$ process is given by

$$\mathcal{M} = \frac{1}{2^5 \pi^2} \frac{y_{bR} y_{sR} g_{\mu\tau}^2}{M_{Z'}^2} \mathcal{V}_{sb}(\chi_-, \chi_+) [\bar{u}(p_B) \gamma^{\mu} (1 + \gamma_5) u(p_K))] [\bar{v}(p_2) \gamma_{\mu} u(p_1))], \quad (5.26)$$

where p_1 and p_2 are the four momenta of charged leptons and $\mathcal{V}_{sb}(\chi_-, \chi_+)$ is the loop function [152, 196]. Now comparing this amplitude (5.26) with the amplitude obtained from the effective Hamiltonian (5.15), we obtain a new Wilson coefficient associated with the right-handed semileptonic electroweak penguin operator \mathcal{O}'_9 as

$$C_9^{\text{NP}} = \frac{\sqrt{2}}{2^4 \pi G_F \alpha_{\text{em}} V_{tb} V_{ts}^*} \frac{y_{bR} y_{sR} g_{\mu\tau}^2}{M_{Z'}^2} \mathcal{V}_{sb} \left(\chi_-, \chi_+ \right) . \tag{5.27}$$

The differential branching ratio of $B \to K l l$ process with respect to q^2 is given by

$$\frac{d \text{Br}}{dq^2} = \tau_B \frac{G_F^2 \alpha_{\text{em}}^2 |V_{tb} V_{ts}^*|^2}{2^8 \pi^5 M_B^3} \sqrt{\lambda(M_B^2, M_K^2, q^2)} \beta_l f_+^2 \left(a_l(q^2) + \frac{c_l(q^2)}{3} \right), \tag{5.28}$$

where

$$a_{l}(q^{2}) = q^{2}|F_{P}|^{2} + \frac{\lambda(M_{B}^{2}, M_{K}^{2}, q^{2})}{4}(|F_{A}|^{2} + |F_{V}|^{2}) + 2m_{l}(M_{B}^{2} - M_{K}^{2} + q^{2})\operatorname{Re}(F_{P}F_{A}^{*}) + 4m_{l}^{2}M_{B}^{2}|F_{A}|^{2},$$

$$c_{l}(q^{2}) = -\frac{\lambda(M_{B}^{2}, M_{K}^{2}, q^{2})}{4}\beta_{l}^{2}(|F_{A}|^{2} + |F_{V}|^{2}), \qquad (5.29)$$

with

$$F_{V} = \frac{2m_{b}}{M_{B}} C_{7}^{\text{eff}} + C_{9}^{\text{eff}} + C_{9}^{'\text{NP}}, F_{A} = C_{10},$$

$$F_{P} = m_{l} C_{10} \left[\frac{M_{B}^{2} - M_{K}^{2}}{q^{2}} \left(\frac{f_{0}(q^{2})}{f_{+}(q^{2})} - 1 \right) - 1 \right], (5.30)$$

and

$$\lambda(a,b,c) = a^2 + b^2 + c^2 - 2(ab + bc + ca), \qquad \beta_l = \sqrt{1 - 4m_l^2/q^2} \ . \tag{5.31}$$

For numerical estimation, we have used the lifetime and masses of particles from [193] and the form factors are taken from [197]. The upper limit on the branching ratio of $B^+ \to K^+ \tau^+ \tau^-$ process is [193]

$$Br(B^+ \to K^+ \tau^+ \tau^-)|^{Expt} < 2.5 \times 10^{-3},$$
 (5.32)

while its predicted value in the SM is

$$Br(B^+ \to K^+ \tau^+ \tau^-)|^{SM} = (1.486 \pm 0.12) \times 10^{-7}.$$
 (5.33)

Since Z' doesn't couple to electron, the branching ratio of $B^+ \to K^+ e^+ e^-$ process is considered to be SM like. The anomalies of $b \to sll$ decay modes can put constraint on all the four parameters i.e., $(y_{qR})^2$, $g_{\mu\tau}$, $M_{Z'}$ and M_- .

5.6.3 $B \to X_s \gamma$ process

The $B \to X_s \gamma$ process involves $b \to s \gamma$ quark level transition, the experimental limit on the corresponding branching ratio is given by [198]

$$Br(B \to X_s \gamma)|_{E_{\gamma} > 1.6 \text{ GeV}}^{Expt} = (3.32 \pm 0.16) \times 10^{-4}.$$
 (5.34)

Fig. 5.6 represents the one loop penguin diagram of $b \to s\gamma$ process mediated by SLQ and N_{\pm} .

Including the NP contribution, the total branching ratio of $B \to X_s \gamma$ is given by

$$Br(B \to X_s \gamma) = Br(B \to X_s \gamma) \Big|^{SM} \left(1 + \frac{C_7^{\gamma / NP}}{C_7^{\gamma SM}} \right)^2, \tag{5.35}$$

where the predicted SM branching ratio is [199]

$$\text{Br}(B \to X_s \gamma)|_{E_0 > 1.6 \text{ GeV}}^{\text{SM}} = (3.36 \pm 0.23) \times 10^{-4}.$$
 (5.36)

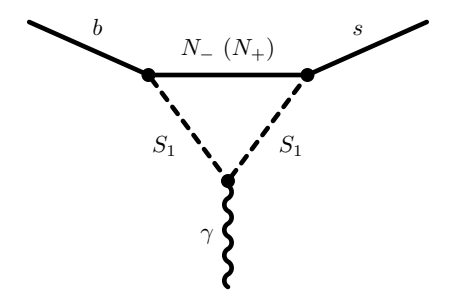


Figure 5.6: Feynman diagram of $b \to s \gamma$ processes in the presence of scalar leptoquark.

The new $C_7^{\gamma\prime\text{NP}}$ Wilson coefficient obtained from Fig. 5.6 is given by

$$C_7^{\gamma'\text{NP}} = -\frac{\sqrt{2}/3}{8G_F V_{tb} V_{ts}^*} \frac{y_{bR} y_{sR}}{M_{S_1}^2} \left(J_1(\chi_-) \cos^2 \alpha + J_1(\chi_+) \sin^2 \alpha \right), \tag{5.37}$$

where the loop functions $J_1(\chi_{\pm})$ are given by [152]

$$J_1(\chi) = \frac{1 - 6\chi + 3\chi^2 + 2\chi^3 - 6\chi^2 \log \chi}{12(1 - \chi)^4}.$$
 (5.38)

Using Eqns. (5.34, 5.36, 5.37) in (5.35), the parameters $(y_{qR})^2$ and M_- can be constrained.

5.6.4 $\tau \to \mu \nu_{\tau} \bar{\nu}_{\mu}$ process

In the presence of Z' boson, the $\tau \to \mu \nu_{\tau} \bar{\nu}_{\mu}$ process can occur via box diagram as shown in Fig. 5.7. There are four possible one-loop box diagrams with the Z' connected to the lepton legs. The total branching ratio of this process is given by [200]

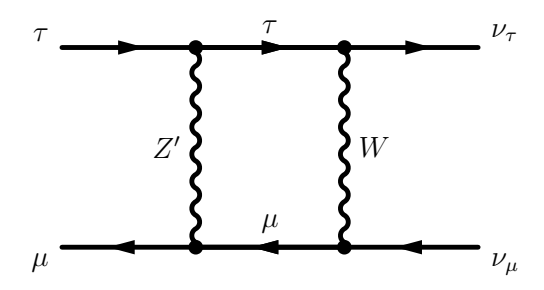


FIGURE 5.7: One loop box diagram of $\tau \to \mu \nu_{\tau} \bar{\nu}_{\mu}$ processes.

$$Br(\tau \to \mu \nu_{\tau} \bar{\nu}_{\mu}) = Br(\tau \to \mu \nu_{\tau} \bar{\nu}_{\mu}) \Big|^{SM} \left(1 + \frac{3g_{\mu\tau}^2}{4\pi^2} \frac{\log(M_W^2/M_{Z'}^2)}{1 - M_{Z'}^2/M_W^2} \right)^2, \tag{5.39}$$

where the branching ratio in the SM is given by [200]

$$\text{Br}(\tau \to \mu \nu_{\tau} \bar{\nu}_{\mu}) \Big|^{\text{SM}} = (17.29 \pm 0.032)\%.$$
 (5.40)

Now comparing the theoretical result with the experimental measured value [193]

$$\text{Br}(\tau \to \mu \nu_{\tau} \bar{\nu}_{\mu})|^{\text{Expt}} = (17.39 \pm 0.04)\%,$$
 (5.41)

one can put bounds on $M_{Z'} - g_{\mu\tau}$ parameter space.

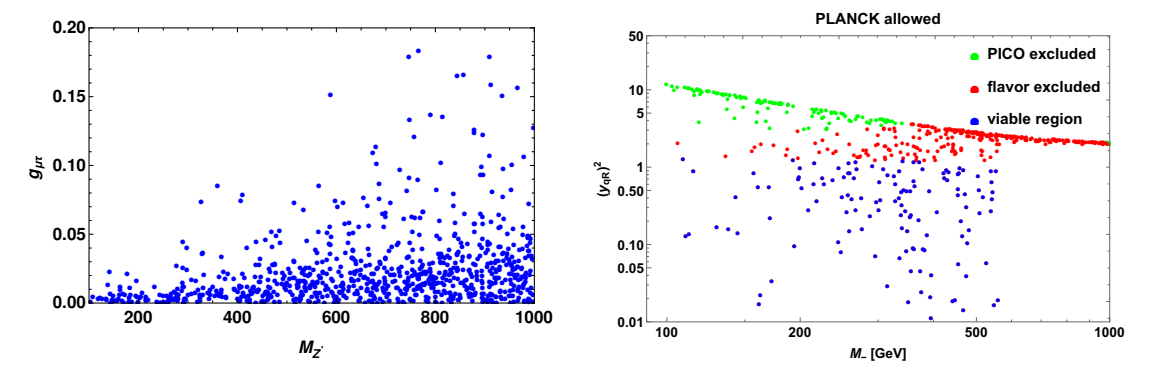


FIGURE 5.8: Left panel projects the constraint on $g_{\mu\tau}$ and $M_{Z'}$ obtained from R_K , ${\rm Br}(B\to K\tau\tau)$ and ${\rm Br}(\tau\to \mu\nu_\tau\bar\nu_\mu)$ observables. In the right panel, blue data points denote the allowed parameter space obtained from R_K , $B_s-\bar B_s$ mixing, ${\rm Br}(B\to K\tau\tau)$, ${\rm Br}(B\to X_s\gamma)$ experimental data, which are also consistent with Planck [22] and PICO-60 limit [39]. Here, green (red) data points denote PICO-60 and flavor excluded (PICO-60 allowed and flavor excluded) region.

Parameters	DM-I	DM-II	DM+Flavor
M_{-} [GeV]	103 - 560	561 - 988	103 - 560
$(y_{qR})^2$	0 - 3.51	1.94 - 2.56	0 - 1.26

TABLE 5.2: Predicted allowed range of parameters M_{-} and $(y_{qR})^2$. Here DM-I and DM-II represent two regions in Fig. 5.3 consistent with only DM observables, DM+Flavor denotes the region favored by both the dark matter and flavor studies.

Now correlating the theoretical predictions of R_K , $\operatorname{Br}(B^+ \to K^+ \tau^+ \tau^-)$ and $\operatorname{Br}(\tau \to \mu \nu_\tau \bar{\nu}_\mu)$ with the corresponding 3σ experimental data, we compute the $M_{Z'} - g_{\mu\tau}$ allowed parameter space. Since Z' does not couple to quarks, these gauge parameters couldn't be constrained from $b \to s\gamma$ decay modes and $B_s - \bar{B}_s$ oscillation data. The constraint on $M_- - (y_{qR})^2$ parameter space is obtained from R_K , $\operatorname{Br}(B^+ \to K^+ \tau^+ \tau^-)$, $\operatorname{Br}(B \to X_s \gamma)$ and $B_s - \bar{B}_s$ mixing results. In addition, the branching ratio of rare semileptonic $B \to K\nu_l\bar{\nu}_l$ process can play a vital role in restricting these parameters. Though the proposed model can allow $b \to s\nu_l\bar{\nu}_l$ decay modes, but the contributions of μ and τ leptons cancel with each other in the leading order of NP due to their equal and opposite $L_\mu - L_\tau$ charges. Since there is no $Z'\mu\tau$ coupling, the neutral and charged lepton flavor violating decay processes like $B \to K^{(*)}\mu^\mp \tau^\pm$, $\tau^- \to \mu^-\gamma$, $\tau \to \mu\mu\mu$ do not play any role. In this

analysis, we consider that the y_{qR} coupling is perturbative i.e., $|y_{qR}| \lesssim \sqrt{4\pi}$. Left (right) panel in Fig. 5.8 denotes the parameter space in the plane of $M_{Z'} - g_{\mu\tau}$ ($M_- - (y_{qR})^2$) consistent with DM and flavor studies. From left panel, one can obtain the lower limit on the ratio $M_{Z'}/g_{\mu\tau}$ around 4615 GeV, which is far more stringent than the lower limit imposed by neutrino trident production [201, 202] i.e., 540 GeV. It is also noted that the allowed region favored by the $(g-2)_{\mu}$ anomaly is completely excluded by the constraint from the neutrino trident production [200]. In the right panel of Fig. 5.8, we redisplay $M_- - (y_{qR})^2$ parameter space of Fig. 5.3 after a combined analysis made by imposing the DM and flavor experimental limits, with the surviving region shown in blue color. In Table 5.2, we report the allowed region of the parameters M_- and $(y_{qR})^2$ which are consistent with only DM studies (DM-I, II), both DM and flavor sectors (DM+Flavor).

5.7 Implication on $B_{(s)} \to K^*(\phi)\mu^+\mu^-$ processes

The constrained parameter space discussed in the previous section can have an impact on the observables of $B \to V l^+ l^-$ process, where $V = K^*, \phi$ are the vector mesons. The $B \to V$ hadronic matrix elements of the local quark bilinear operators can be parametrized as [203, 204]

$$\langle V(k) | \bar{s} \gamma_{\mu} (1 - \gamma_{5}) b | B(p) \rangle = \epsilon_{\mu\nu\alpha\beta} \epsilon^{*\nu} p^{\alpha} q^{\beta} \frac{2V(q^{2})}{M_{B} + M_{V}} + i(\epsilon^{*} \cdot q)(2p - q)_{\mu} \frac{A_{2}(q^{2})}{M_{B} + M_{V}}$$

$$- i\epsilon_{\mu}^{*} (M_{B} + M_{V}) A_{1}(q^{2}) + i \frac{2M_{V}}{q^{2}} (\epsilon^{*} \cdot q) \left[A_{3}(q^{2}) - A_{0}(q^{2}) \right] q_{\mu} ,$$

$$(5.42)$$

where

$$A_3(s) = \frac{(M_B + M_V)}{2M_V} A_1(s) - \frac{(M_B - M_V)}{2M_V} A_2(s), \tag{5.43}$$

 q^2 is the momentum transfer between the B and V mesons, i.e., $q_{\mu}=p_{\mu}-k_{\mu}$ and ϵ_{μ} is the polarization vector of the V meson. The full angular differential decay distribution in terms of q^2 , θ_l , θ_V and ϕ variables is given as [205–207]

$$\frac{d^4\Gamma}{dq^2 d\cos\theta_l d\cos\theta_V d\phi} = \frac{9}{32\pi} J\left(q^2, \theta_l, \theta_V, \phi\right) , \qquad (5.44)$$

where

$$J(q^{2}, \theta_{l}, \theta_{V}, \phi) = J_{1}^{s} \sin^{2}\theta_{V} + J_{1}^{c} \cos^{2}\theta_{V} + \left(J_{2}^{s} \sin^{2}\theta_{V} + J_{2}^{c} \cos^{2}\theta_{V}\right) \cos 2\theta_{l}$$

$$+ J_{3} \sin^{2}\theta_{V} \sin^{2}\theta_{l} \cos 2\phi + J_{4} \sin 2\theta_{V} \sin 2\theta_{l} \cos \phi + J_{5} \sin 2\theta_{V} \sin \theta_{l} \cos \phi$$

$$+ \left(J_{6}^{s} \sin^{2}\theta_{V} + J_{6}^{c} \cos^{2}\theta_{V}\right) \cos \theta_{l} + J_{7} \sin 2\theta_{V} \sin \theta_{l} \sin \phi$$

$$+ J_{8} \sin 2\theta_{V} \sin 2\theta_{l} \sin \phi + J_{9} \sin^{2}\theta_{V} \sin^{2}\theta_{l} \sin 2\phi , \qquad (5.45)$$

 θ_l is the angle between l^- and B in the dilepton frame, θ_V is defined as the angle between K^- and B in the $K^-\pi^+$ (K^-K^+) frame, the angle between the normals of the $K^-\pi^+$ (K^-K^+) and the dilepton planes is given by ϕ . The complete expressions for $J\left(q^2,\theta_l,\theta_V,\phi\right)$ as a function of transversity amplitudes are given in the Appendix B [208]. The transversity amplitudes written in terms of the form factors and Wilson coefficients are as follows [208]

$$A_{\perp L,R} = N\sqrt{2\lambda} \left[\left((C_9^{\text{eff}} + C_9'^{\text{NP}}) \mp C_{10} \right) \frac{V(q^2)}{M_B + M_V} + \frac{2m_b}{q^2} C_7 T_1(q^2) \right],$$

$$A_{\parallel L,R} = -N\sqrt{2} (M_B^2 - M_V^2) \left[\left((C_9^{\text{eff}} + C_9'^{\text{NP}}) \mp C_{10} \right) \frac{A_1(q^2)}{M_B - M_V} + \frac{2m_b}{q^2} C_7 T_2(q^2) \right],$$

$$A_{0L,R} = -\frac{N}{2M_V \sqrt{s}} \left[\left(C_9^{\text{eff}} + C_9'^{\text{NP}} \right) \mp C_{10} \right) \times \left((M_B^2 - M_V^2 - q^2) (M_B + M_V) A_1(q^2) - \lambda \frac{A_2(q^2)}{M_B + M_V} \right) + 2m_B C_7 \left((M_B^2 + 3M_V^2 - q^2) T_2(q^2) - \frac{\lambda}{M_B^2 - M_V^2} \right) \right],$$

$$A_t = 2N\sqrt{\frac{\lambda}{q^2}} C_{10} A_0(q^2), \tag{5.46}$$

where

$$N = V_{tb}V_{ts}^* \left[\frac{G_F^2 \alpha_{\text{em}}^2}{3 \cdot 2^{10} \pi^5 M_B^3} q^2 \beta_l \sqrt{\lambda} \right]^{1/2} , \qquad \lambda = \lambda(M_V^2, M_B^2, q^2).$$
 (5.47)

The dilepton invariant mass spectrum for $B \to V l^+ l^-$ decay after integration over all angles [205] is given by

$$\frac{d\Gamma}{dq^2} = \frac{3}{4} \left(J_1 - \frac{J_2}{3} \right),\tag{5.48}$$

where $J_i = 2J_i^s + J_i^c$. The most interesting observables in these decay modes are the lepton non-universality parameter defined as

$$R_V = \frac{\text{Br}(B \to V \mu^+ \mu^-)}{\text{Br}(B \to V e^+ e^-)},$$
 (5.49)

the form factor independent (FFI) observables [209]

$$P_4' = \frac{J_4}{\sqrt{-J_2^s J_2^c}}, \qquad P_5' = \frac{J_5}{2\sqrt{-J_2^s J_2^c}}.$$
 (5.50)

After getting familiar with the different observables and the allowed values of the new parameters, we now proceed for numerical analysis in the full dilepton mass region i.e.,

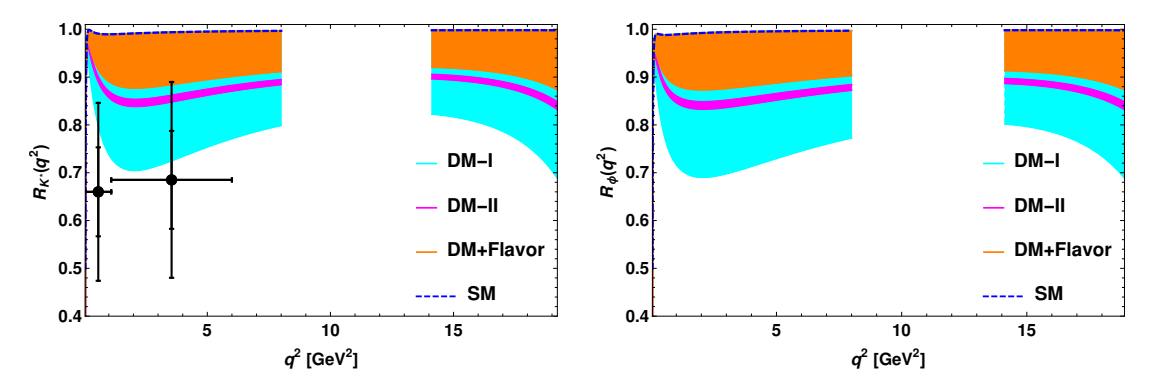


FIGURE 5.9: The q^2 variation of R_{K^*} (left panel) and R_{ϕ} (right panel) LNU parameters in the $L_{\mu}-L_{\tau}$ model. Here the blue dashed lines represent the SM prediction, the cyan (magenta) bands stand for the NP contribution from the dark matter studies i.e., DM-I (DM-II). Orange bands are due to the contribution from both the flavor and DM sectors (DM+Flavor). The experimental data points (with 2σ error bars) [138] are shown in black lines.

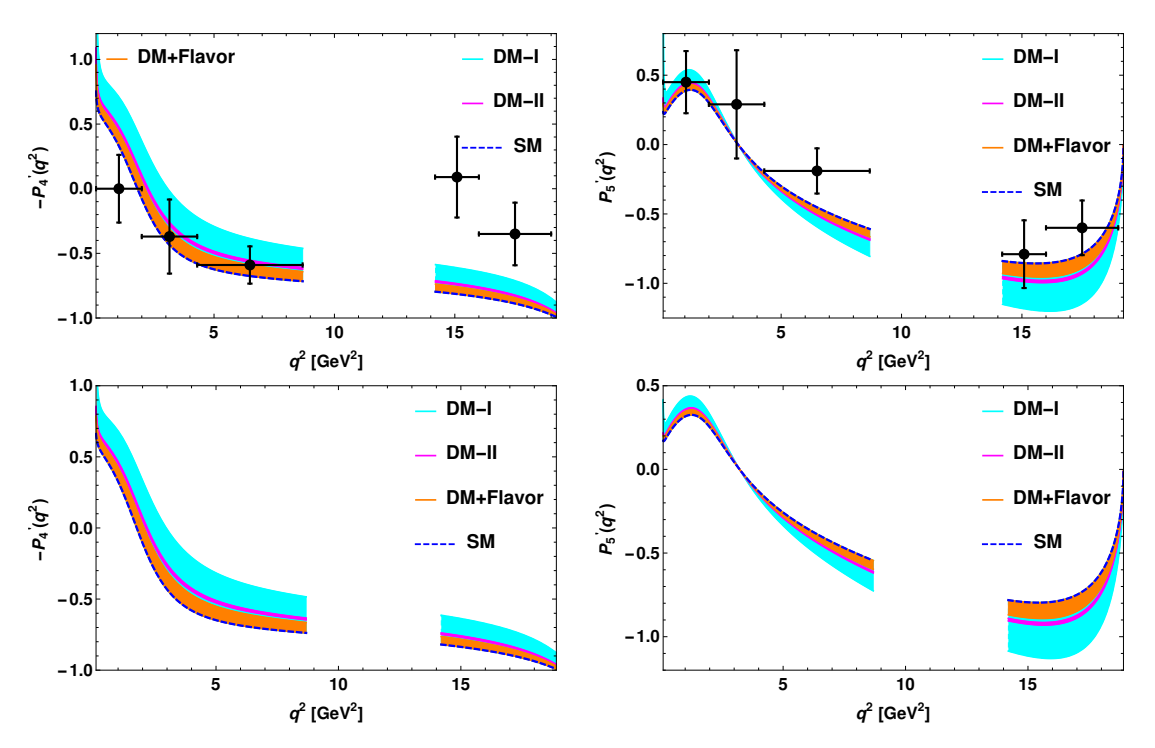


FIGURE 5.10: Top panel represents the variation of P_4' (left panel) and P_5' (right panel) observables of $B \to K^* \mu^+ \mu^-$ process with respect to q^2 . The behaviour of P_4' (left panel) and P_5' (right panel) for $B_s \to \phi \mu^+ \mu^-$ are shown in the bottom panel. The bin-wise experimental data points with error bars are shown in black [141]. Note that P_4' $|^{\text{LHCb}} = -P_4'$.

 $4m_l^2 \leqslant q^2 \leqslant (M_B - M_V)^2$, leaving the regions around $q^2 \sim m_{J/\psi}^2$ and $m_{\psi'}^2$. The cuts are employed to remove the dominant charmonium resonance $(c\bar{c}) = J/\psi, \psi'$ backgrounds from $B \to V(c\bar{c}) \to V l^+ l^-$. In Fig. 5.9, we show the behaviour of R_{K^*} (left panel) and R_{ϕ} (right panel) with respect to q^2 in the full kinematically accessible physical region. In these figures, the blue dashed lines stand for the SM contribution, the orange bands are due to the allowed region of parameters shown in Table 5.2, favored by both DM and

flavor (DM+Flavor) and cyan (magenta) bands for only DM case i.e., DM-I (DM-II). The bin-wise experimental values of R_{K^*} are shown in black. From the left panel of Fig. 5.9, it can be seen that the measured value of R_{K^*} in the $q^2 \in [0.045, 1.1] \text{ GeV}^2$ region can be accommodated within 2σ (DM-I), the $q^2 \in [1.1, 6] \text{ GeV}^2$ bin result can be explained within 1σ (DM-I) and 2σ (DM-II and DM+Flavor). Though there is no experimental evidence for R_{ϕ} parameter, the additional NP contribution arising from the allowed parameter space of all cases (DM-I,II and DM+Flavor) provide significant deviation from the SM prediction, implying the presence of lepton universality violation in the $B_s \to \phi \mu^+ \mu^-$ process. In Table 5.3, we present our predicted values of R_{K^*} and R_{ϕ} for different bins. The q^2 variation of famous optimized observables $-P_4'$ (top-left panel) and P_5' (top-right panel) of $B \to K^* \mu^+ \mu^-$ process are depicted in Fig. 5.10. The bottom panel of this figure describes analogous plots for $B_s \to \phi \mu^+ \mu^-$ process in both the high and low recoil limit. It should be noted that $P_4'|^{\mathrm{LHCb}} = -P_4'$. In the low q^2 region, our predictions on $-P'_4$ observable of $B \to K^*\mu^+\mu^-$ process is in very good agreement with the LHCb data. For $B \to K^* \mu^+ \mu^-$ decay mode, we are able to explain the P_5' observable within 1σ of the experimental limit in the full q^2 region (excluding the intermediate resonance regions). We notice profound deviation between the results of SM and the presented $L_{\mu} - L_{\tau}$ model on the $P'_{4,5}$ observables for $B_s \to \phi \mu^+ \mu^-$ decay modes. The numerical values of all these observables are given in Table 5.3. We found that our results on the angular observables of $B \to Vll$ process, obtained from DM-I parameter space are almost consistent with the corresponding measured experimental data.

Observables	SM Values	DM-I Values	DM-II Values	DM+Flavor Values
$R_{K^*} _{q^2 \in [0.045, 1.1]}$	0.949	0.825 - 0.949	0.884 - 0.89	0.9 - 0.949
$R_{K^*} _{q^2 \in [1.1,6]}$	0.993	0.732 - 0.993	0.852 - 0.865	0.887 - 0.993
$R_{K^*} _{q^2 \ge 14.18}$	0.998	0.793 - 0.998	0.882 - 0.893	0.91 - 0.998
$P_5' _{q^2 \in [1,6]}$	-0.057 ± 0.004	$-0.074 \rightarrow -0.057$	$-0.064 \rightarrow -0.063$	$-0.063 \rightarrow -0.057$
$P_5' _{q^2 \ge 14.18}$	-0.805 ± 0.064	$-1.144 \rightarrow -0.805$	$-0.942 \rightarrow -0.926$	$-0.921 \rightarrow -0.805$
$P_4' _{q^2 \in [1,6]}$	0.398 ± 0.024	0.025 - 0.398	0.242 - 0.26	$0.288 \to 0.398$
$P_4' _{q^2 \ge 14.18}$	0.852 ± 0.068	0.662 - 0.852	0.78 - 0.789	0.8 - 0.852
$R_{\phi} _{q^2 \in [0.045, 1.1]}$	0.9499	0.794 - 0.9499	0.868 - 0.876	0.89 - 0.9499
$R_{\phi} _{q^2 \in [1.1,6]}$	0.994	0.712 - 0.994	0.843 - 0.858	0.881 - 0.994
$R_{\phi} _{q^2 \ge 14.18}$	0.998	0.776 - 0.998	0.874 - 0.886	0.9 - 0.998
$P_5' _{q^2 \in [1,6]}$	-0.049 ± 0.004	$-0.064 \rightarrow -0.049$	$-0.055 \rightarrow -0.054$	$-0.053 \rightarrow -0.049$
$ P_5' _{q^2 \ge 14.18}$	-0.743 ± 0.059	$-1.07 \to -0.743$	$-0.875 \to -0.86$	$-0.837 \rightarrow -0.743$
$P_4' _{q^2 \in [1,6]}$	0.421 ± 0.036	$4.91 \times 10^{-3} - 0.421$	0.266 - 0.284	$0.311 \to 0.421$
$P_4' _{q^2 \ge 14.18}$	0.872 ± 0.07	0.687 - 0.872	0.8 - 0.812	0.825 - 0.872

Table 5.3: Predicted numerical values of LNU parameters (R_V) and $P'_{4,5}$ observables of $B \to Vll$, $V = K^*, \phi$ processes in the high and low recoil limits. The upper part represents the results for $\bar{B} \to \bar{K}^* \mu^+ \mu^-$ and the lower part is for $B_s \to \phi \mu^+ \mu^-$. Here q^2 is in GeV².

5.8 Conclusion

To conclude the chapter, we have studied Majorana dark matter in a new version of $U(1)_{L_{\mu}-L_{\tau}}$ gauge extension of the standard model. The model is free from triangle gauge anomalies with the inclusion of three neutral fermions with $L_{\mu} - L_{\tau}$ charges 0, 1 and -1. A scalar singlet, charged +2 under the new U(1) is added to spontaneously break the $L_{\mu} - L_{\tau}$ gauge symmetry, thereby giving masses to the new fermions and the neutral boson Z' associated with gauge extension. In addition, the scalar sector is enriched with an inert doublet and a $(\bar{3}, 1, 1/3)$ scalar leptoquark to obtain the neutrino mass at one-loop level and address the flavor anomalies respectively. All the new fermions, leptoquark and inert doublet are assigned with charge -1 under \mathbb{Z}_2 symmetry. Choosing the lightest mass eigenstate of the new fermion spectrum as dark matter, we made a thorough study of Majorana dark matter in relic density and direct detection perspective. The channels contributing to relic density are mediated by the scalar leptoquark, Z' and inert doublet components. As Z'-mediated cross section is insensitive to direct detection experiments in Majorana dark matter case, only leptoquark portal channels contribute to spin-dependent WIMP-nucleon cross section. Imposing Planck limit on relic density and well known PICO-60, LUX bounds on spin-dependent cross section, we have constrained the new parameters of the model. We have also shown the mechanism of generating light neutrino mass radiatively using an inert doublet.

We have further restricted the new parameters from quark and lepton sectors i.e., by comparing the theoretical predictions of $Br(\tau \to \mu\nu_{\tau}\bar{\nu}_{\mu})$, $Br(B \to X_s\gamma)$, $Br(B^+ \to X_s\gamma)$ $K^+\tau^+\tau^-$), R_K and $B_s - \bar{B}_s$ mixing with their corresponding 3σ experimental data. The neutral and charged lepton flavor violating decay processes are absent due to zero $Z'\tau\mu$ coupling. And also the vanishing $Z'q\bar{q}$ coupling restricts the involvement of Z'in $B_s - \bar{B}_s$ mixing, $b \to s\gamma$ processes at one-loop level. We have then investigated the implication on $P'_{4,5}$, R_{K^*} and R_{ϕ} observables of $B_{(s)} \to K^*(\phi) l^+ l^-$ decay modes in the full kinematically allowed q^2 region for two cases i.e., dark matter and flavor allowed, only dark matter allowed parameter space. We found that the R_{K^*} observable obtained from the parameter space consistent with only dark matter ($M_{-} \leq 560 \text{ GeV}$) is within its 1σ , only dark matter ($M_{-} > 560 \text{ GeV}$) and both dark matter and flavor is within 2σ experimental limit. In the presence of new physics, the violation of lepton universality is observed in $B_s \to \phi \mu^+ \mu^-$ process, thus, can be probed in LHCb experiment. We noticed that the proposed $L_{\mu} - L_{\tau}$ model is also able to explain the LHCb experimental data of the famous optimized $P'_{4,5}$ observables of $B \to K^*l^+l^-$ process in the high recoil limit. We also perceived that the form factor independent observables for $B_s \to \phi \mu^+ \mu^$ decay modes have sizeable deviation from the standard model. We observed that the

parameter region satisfying only dark matter observables for $M_- \leq 560$ GeV have a good impact on the flavor anomalies.

Chapter 6

Summary and outlook

The stipulation of going physics beyond the standard model is doubtless. The most victorious theory in unravelling the dynamics of visible matter content at elementary level is silent when it comes to dark matter identity. A series of experimental and observational events hint that there is much more in the Universe that is invisible but dynamic. Conclusively, there is a need for a more general framework obeying the basic principles of the well tested theory i.e., the standard model, to unfold the envelope of the second most energy component of the Universe.

In the introductory chapter, we presented a short note on the gauge symmetries that govern the interactions of elementary particles in the framework of standard model. We then outlined some of the important observational evidences that support the existence of dark matter. From the available hints, a possible picture of dark matter from a theoretical view point is advertised. Working through the Boltzmann equation in non-equilibrium state, we have explicitly derived the present abundance of dark matter and also provided a convincing mathematical argument, elevating the chance of a weakly interacting massive particle meeting the requirements levied by the observations and observables. The current experimental bounds on the cross section when dark matter particle meets the detector are also projected.

Chapters 2 and 3 are devoted to the study of dark matter in an uncomplicated $U(1)_{B-L}$ gauge extension of the standard model. We have presented the discussion on triangle gauge anomalies associated with the gauge extension and posted the possible B-L charges required for the new fermion content to overcome. We have put forth a new variant of such extension with three neutral fermions charged -4, -4 and +5 under the new U(1). The scalar sector is enriched accordingly so that every new particle attains mass after the U(1) gauge symmetry is spontaneously broken. The lightest Majorana mass eigenstate is naturally stable as the exotic B-L charge forbids its decay to

Higgs boson and the light neutrino through Yukawa interaction term. In chapter 3, we have explored its dark matter phenomenology. Chapter 2 contains the detailed study of scalar singlet dark matter, for which we have added a scalar singlet to the model that doesn't produce any value in vacuum. We have avoided its decay by allotting a suitable B-L charge. The primary feature of the proposed framework is that the B-Lgauge symmetry plays the role of ad-hoc discrete symmetry in conventional models that stabilize the dark matter particle. The model is fruitful in providing two mediators i.e., the scalar and vector boson, for the dark matter to communicate with the visible matter. Both the portals were analyzed carefully in concern to relic density and direct detection observables. We have included the constraints obtained from ATLAS dilepton jet study, LEP-II data on the gauge coupling and gauge boson mass, associated with the B-L symmetry extension. A leftover massless degree of freedom (Goldstone mode) originating from an accidental global U(1) symmetry is studied in the spotlight of relic density. Additionally, we have also discussed the concept of semi-annihilation in scalar dark matter study. Tiny neutrino mass is demonstrated with the well known one loop diagram involving the dark matter (both scalar and fermion). We have scrutinized the parameter space that survives the constraints from Planck limit on relic density, upper limits on direct detection cross section from various collaborations such as LUX, XENON, PandaX, and collider searches as well.

The interrelated concepts of neutrino mass and oscillations are opaque in the standard model. Theoretical picture for the precisely measured parameters from neutrino oscillation experiments can be drawn in extended frameworks. Tempted to the task of studying neutrino oscillations and dark matter by a common theoretical view point, chapter 4 is included with the investigation of radiative neutrino mass matrix in the scotogenic model. We have projected complete technical details in the process of examining the mass matrix with a tri-bimaximal mixing matrix and a perturbation to trigger for the recently observed non-zero reactor mixing angle (θ_{13}). Working in degenerate heavy neutrino mass spectrum, we have obtained the constraints on the model parameters that provide light neutrino masses obeying normal hierarchy and also gives the correct relic abundance of fermionic dark matter including co-annihilation effects. Using the available parameter space that is consistent with neutrino sector and dark matter sector, we made our estimation on the decay channels that violate lepton flavor such as $\ell_{\alpha} \to \ell_{\beta} \gamma$ and $\ell_{\alpha} \to 3 \, \ell_{\beta}$.

Many devoted experiments like Belle, BaBar as well as LHCb are currently running to verify the utterance of lepton universality violation in the B sector. Chapter 5 is based on the challenging problems of flavor physics in association with the dark matter observables. Revisiting $L_{\mu} - L_{\tau}$ model with an additional inert scalar doublet and a singlet scalar leptoquark, we have scrutinized Majorana dark matter. The channels

mediated by the scalar leptoquark, Z' and inert doublet components contribute to relic density and leptoquark portal s-channel process gives spin-dependent WIMP-nucleon cross section. Using Planck limit on relic density and the most stringent PICO-60, LUX bounds on spin-dependent cross section, we have constrained the new parameters of the model. We have also shown the mechanism of generating light neutrino mass radiatively using the inert doublet. Forbye, the allowed regions of new parameters are procured by implementing the experimental limits on $\text{Br}(\tau \to \mu \nu_{\tau} \bar{\nu}_{\mu})$, $\text{Br}(B \to X_s \gamma)$, R_K and $R_s - \bar{R}_s$ oscillation. We then looked at the impact of compiled parameter space, predicted from only dark matter observables and from both dark matter and flavor observables, on the R_{K^*} , R_{ϕ} and optimized $P'_{4,5}$ parameters of $R_s \to K^*(\phi)\mu^+\mu^-$ decay modes. We have noticed that the dark matter observables describe the flavor anomalies effectively.

Winding up with general remarks, it is fair enough to say that dark matter in particle physics viewpoint encompasses different phenomenological aspects such as neutrino and flavor sector, that have already produced a precisely measured physical observables. In this connection, we have attempted to glitter the probable ingredients and dynamics of invisible component in few simplified frameworks. The approach chosen and the results obtained could be helpful in prospects of upcoming dedicated experiments.

Appendix A

Neutrino oscillations and fermionic dark matter

A.1 Loop functions

The loop functions used in LFV decays are given by

$$F_2(x) = \frac{1 - 6x^2 + 3x^4 + 2x^6 - 6x^4 \log x^2}{6(1 - x^2)^4},$$
(A.1)

$$G_2(x) = \frac{2 - 9x^2 + 18x^4 - 11x^6 + 6x^6 \log x^2}{6(1 - x^2)^4},$$
(A.2)

$$D_1(x,y) = -\frac{1}{(1-x^2)(1-y^2)} - \frac{x^4 \log x^2}{(1-x^2)^2(x^2-y^2)} - \frac{y^4 \log y^2}{(1-y^2)^2(y^2-x^2)}, (A.3)$$

$$D_2(x,y) = -\frac{1}{(1-x^2)(1-y^2)} - \frac{x^2 \log x^2}{(1-x^2)^2(x^2-y^2)} - \frac{y^2 \log y^2}{(1-y^2)^2(y^2-x^2)}.$$
(A.4)

In the limit $y \to x$, the functions D_1 and D_2 become

$$D_1(x,x) = \frac{-1 + x^4 - 2x^2 \log x^2}{(1 - x^2)^3},$$
(A.5)

$$D_2(x,x) = \frac{-2 + 2x^2 - (1+x^2)\log x^2}{(1-x^2)^3}.$$
 (A.6)

Appendix B

Flavor sector in $L_{\mu} - L_{\tau}$ model

B.1 Loop functions required for $B_s - \bar{B}_s$ mixing and B decays

The loop functions used to compute the $B_s - \bar{B}_s$ mixing and rare B decays in $L_{\mu} - L_{\tau}$ model are given by [152]

$$f(\chi_1, \chi_2, \chi_3, \dots) \equiv \frac{f(\chi_1, \chi_3, \dots) - f(\chi_2, \chi_3, \dots)}{\chi_1 - \chi_2},$$
 (B.1)

where $f = j, \kappa$ with

$$j(\chi) = \frac{\chi \log \chi}{\chi - 1}, \qquad \kappa(\chi) = \frac{\chi^2 \log \chi}{\chi - 1}.$$
 (B.2)

B.2 J_i coefficients of $B_{(s)} \to Vll$ processes

The complete expression for the J_i coefficients of $B_{(s)} \to Vll$ processes is given by [206, 208]

$$J_1^s = \frac{\left(2+\beta_l^2\right)}{4} \left[|A_{\perp}^L|^2 + |A_{\parallel}^L|^2 + (L \to R) \right] + \frac{4m_l^2}{q^2} \operatorname{Re}\left(A_{\perp}^L A_{\perp}^{R^*} + A_{\parallel}^L A_{\parallel}^{R^*}\right), (B.3)$$

$$J_1^c = |A_0^L|^2 + |A_0^R|^2 + \frac{4m_l^2}{q^2} \left[|A_t|^2 + 2\operatorname{Re}\left(A_0^L A_0^{R^*}\right) \right] + \beta_l^2 |A_S|^2,$$
 (B.4)

$$J_2^s = \frac{\beta_l^2}{4} \left[|A_\perp^L|^2 + |A_\parallel^L|^2 + (L \to R) \right], \tag{B.5}$$

$$J_2^c = -\beta_l^2 \left[|A_0^L|^2 + (L \to R) \right], \tag{B.6}$$

$$J_3 = \frac{1}{2}\beta_l^2 \left[|A_{\perp}^L|^2 - |A_{\parallel}^L|^2 + (L \to R) \right], \tag{B.7}$$

$$J_4 = \frac{1}{\sqrt{2}} \beta_l^2 \left[\operatorname{Re} \left(A_0^L A_{\parallel}^{L^*} \right) + (L \to R) \right], \tag{B.8}$$

$$J_{5} = \sqrt{2}\beta_{l} \left[\operatorname{Re} \left(A_{0}^{L} A_{\perp}^{L^{*}} \right) - (L \to R) - \frac{m_{l}}{\sqrt{q^{2}}} \operatorname{Re} \left(A_{\parallel}^{L} A_{S}^{*} + A_{\parallel}^{R} A_{S}^{*} \right) \right], \tag{B.9}$$

$$J_6^s = 2\beta_l \left[\operatorname{Re} \left(A_{\parallel}^L A_{\perp}^{L^*} \right) - (L \to R) \right], \tag{B.10}$$

$$J_6^c = 4\beta_l \frac{m_l}{\sqrt{q^2}} \text{Re} \left[A_0^L A_S^* + (L \to R) \right],$$
 (B.11)

$$J_{7} = \sqrt{2}\beta_{l} \left[\operatorname{Im} \left(A_{0}^{L} A_{\parallel}^{L^{*}} \right) - (L \to R) + \frac{m_{l}}{\sqrt{q^{2}}} \operatorname{Im} \left(A_{\perp}^{L} A_{S}^{*} + A_{\perp}^{R} A_{S}^{*} \right) \right], \tag{B.12}$$

$$J_8 = \frac{1}{\sqrt{2}} \beta_l^2 \left[\text{Im} \left(A_0^L A_\perp^{L^*} \right) + (L \to R) \right], \tag{B.13}$$

$$J_9 = \beta_l^2 \left[\operatorname{Im} \left(A_{\parallel}^{L^*} A_{\perp}^L \right) + (L \to R) \right], \tag{B.14}$$

where

$$A_i A_i^* = A_i^L (q^2) A_i^{*L} (q^2) + A_i^R (q^2) A_i^{*R} (q^2) \qquad (i, j = 0, \parallel, \perp),$$
 (B.15)

in shorthand notation.

- [1] E. Noether, "Invariant Variation Problems," Gott. Nachr. 1918 (1918) 235–257, arXiv:physics/0503066. [Transp. Theory Statist. Phys.1,186(1971)].
- [2] S. L. Glashow, "Partial Symmetries of Weak Interactions," Nucl. Phys. 22 (1961) 579–588.
- [3] S. Weinberg, "A Model of Leptons," Phys. Rev. Lett. 19 (1967) 1264–1266.
- [4] A. Salam and J. C. Ward, "Electromagnetic and weak interactions," Phys. Lett. 13 (1964) 168–171.
- [5] Y. Nambu, "Axial vector current conservation in weak interactions," Phys. Rev. Lett. 4 (1960) 380–382.
- [6] Y. Nambu and G. Jona-Lasinio, "Dynamical Model of Elementary Particles Based on an Analogy with Superconductivity. 1.," Phys. Rev. 122 (1961) 345–358.
- [7] J. Goldstone, "Field Theories with Superconductor Solutions," Nuovo Cim. 19 (1961) 154–164.
- [8] J. Goldstone, A. Salam, and S. Weinberg, "Broken Symmetries," Phys. Rev. 127 (1962) 965–970.
- [9] F. Englert and R. Brout, "Broken Symmetry and the Mass of Gauge Vector Mesons," Phys. Rev. Lett. 13 (1964) 321–323.
- [10] P. W. Higgs, "Broken symmetries, massless particles and gauge fields," Phys. Lett. 12 (1964) 132–133.
- [11] P. W. Higgs, "Broken Symmetries and the Masses of Gauge Bosons," Phys. Rev. Lett. 13 (1964) 508–509.
- [12] G. S. Guralnik, C. R. Hagen, and T. W. B. Kibble, "Global Conservation Laws and Massless Particles," Phys. Rev. Lett. 13 (1964) 585–587.
- [13] P. W. Higgs, "Spontaneous Symmetry Breakdown without Massless Bosons," Phys. Rev. **145** (1966) 1156–1163.

[14] T. W. B. Kibble, "Symmetry breaking in nonAbelian gauge theories," Phys. Rev. 155 (1967) 1554–1561.

- [15] G. Bertone and D. Hooper, "History of dark matter," Rev. Mod. Phys. 90 (2018) no. 4, 045002, arXiv:1605.04909.
- [16] F. Zwicky, "How Far Do Cosmic Rays Travel?," Phys. Rev. 43 (Jan, 1933) 147-148. https://link.aps.org/doi/10.1103/PhysRev.43.147.
- [17] F. Zwicky, "On the Masses of Nebulae and of Clusters of Nebulae," Astrophys. J. 86 (1937) 217–246.
- [18] V. C. Rubin and W. K. Ford, Jr., "Rotation of the Andromeda Nebula from a Spectroscopic Survey of Emission Regions," Astrophys. J. 159 (1970) 379–403.
- [19] K. C. Freeman, "On the disks of spiral and SO Galaxies," Astrophys. J. 160 (1970) 811.
- [20] V. C. Rubin, W. K. Ford, Jr., and N. Thonnard, "Extended rotation curves of high-luminosity spiral galaxies. IV. Systematic dynamical properties, Sa through Sc," Astrophys. J. 225 (1978) L107-L111.
- [21] E. W. Kolb and M. S. Turner, "The Early Universe," Front. Phys. 69 (1990) 1–547.
- [22] Planck, N. Aghanim et al., "Planck 2018 results. VI. Cosmological parameters," arXiv:1807.06209.
- [23] G. R. Blumenthal, S. M. Faber, J. R. Primack, and M. J. Rees, "Formation of Galaxies and Large Scale Structure with Cold Dark Matter," Nature 311 (1984) 517–525.
- [24] J. F. Navarro, C. S. Frenk, and S. D. M. White, "The Structure of cold dark matter halos," Astrophys. J. 462 (1996) 563-575, arXiv:astro-ph/9508025.
- [25] D. Clowe, M. Bradac, A. H. Gonzalez, M. Markevitch, S. W. Randall, C. Jones, and D. Zaritsky, "A direct empirical proof of the existence of dark matter," Astrophys. J. 648 (2006) L109–L113, arXiv:astro-ph/0608407.
- [26] A. Ibarra, D. Tran, and C. Weniger, "Indirect Searches for Decaying Dark Matter," Int. J. Mod. Phys. A28 (2013) 1330040, arXiv:1307.6434.
- [27] M. Taoso, G. Bertone, and A. Masiero, "Dark Matter Candidates: A Ten-Point Test," JCAP 0803 (2008) 022, arXiv:0711.4996.

[28] Particle Data Group, M. Tanabashi et al., "Review of Particle Physics," Phys. Rev. D98 (2018) no. 3, 030001.

- [29] R. J. Scherrer and M. S. Turner, "On the Relic, Cosmic Abundance of Stable Weakly Interacting Massive Particles," Phys. Rev. D33 (1986) 1585. [Erratum: Phys. Rev. D34,3263(1986)].
- [30] S. Dodelson, *Modern Cosmology*. Academic Press, Amsterdam, 2003. http://www.slac.stanford.edu/spires/find/books/www?cl=QB981:D62:2003.
- [31] K. Griest and D. Seckel, "Three exceptions in the calculation of relic abundances," Phys. Rev. D43 (1991) 3191–3203.
- [32] P. Gondolo and G. Gelmini, "Cosmic abundances of stable particles: Improved analysis," Nucl. Phys. B360 (1991) 145–179.
- [33] G. Jungman, M. Kamionkowski, and K. Griest, "Supersymmetric dark matter," Phys. Rept. 267 (1996) 195–373, arXiv:hep-ph/9506380.
- [34] P. Agrawal, Z. Chacko, C. Kilic, and R. K. Mishra, "A Classification of Dark Matter Candidates with Primarily Spin-Dependent Interactions with Matter," arXiv:1003.1912.
- [35] J. R. Ellis, A. Ferstl, and K. A. Olive, "Reevaluation of the elastic scattering of supersymmetric dark matter," Phys. Lett. B481 (2000) 304-314, arXiv:hep-ph/0001005.
- [36] LUX, D. S. Akerib et al., "Results from a search for dark matter in the complete LUX exposure," Phys. Rev. Lett. 118 (2017) no. 2, 021303, arXiv:1608.07648.
- [37] **XENON**, E. Aprile et al., "First Dark Matter Search Results from the XENON1T Experiment," arXiv:1705.06655.
- [38] PandaX-II, X. Cui et al., "Dark Matter Results From 54-Ton-Day Exposure of PandaX-II Experiment," Phys. Rev. Lett. 119 (2017) no. 18, 181302, arXiv:1708.06917.
- [39] PICO, C. Amole et al., "Dark Matter Search Results from the PICO-60 C₃F₈ Bubble Chamber," Phys. Rev. Lett. 118 (2017) no. 25, 251301, arXiv:1702.07666.
- [40] LUX, D. S. Akerib et al., "Limits on spin-dependent WIMP-nucleon cross section obtained from the complete LUX exposure," Phys. Rev. Lett. 118 (2017) no. 25, 251302, arXiv:1705.03380.

[41] PandaX-II, C. Fu et al., "Spin-Dependent Weakly-Interacting-Massive-ParticleNucleon Cross Section Limits from First Data of PandaX-II Experiment," Phys. Rev. Lett. 118 (2017) no. 7, 071301, arXiv:1611.06553. [Erratum: Phys. Rev. Lett.120,no.4,049902(2018)].

- [42] **LUX-ZEPLIN**, D. S. Akerib et al., "Projected WIMP Sensitivity of the LUX-ZEPLIN (LZ) Dark Matter Experiment," arXiv:1802.06039.
- [43] E. E. Jenkins, "Searching for a (B-L) Gauge Boson in $p\bar{p}$ Collisions," Phys. Lett. **B192** (1987) 219–222.
- [44] W. Buchmuller, C. Greub, and P. Minkowski, "Neutrino masses, neutral vector bosons and the scale of B-L breaking," Phys. Lett. B267 (1991) 395–399.
- [45] L. Basso, A. Belyaev, S. Moretti, and C. H. Shepherd-Themistocleous, "Phenomenology of the minimal B-L extension of the Standard model: Z' and neutrinos," Phys. Rev. D80 (2009) 055030, arXiv:0812.4313.
- [46] W. Emam and S. Khalil, "Higgs and Z-prime phenomenology in B-L extension of the standard model at LHC," Eur. Phys. J. C52 (2007) 625–633, arXiv:0704.1395.
- [47] S. Khalil, "Low scale B L extension of the Standard Model at the LHC," J. Phys. G35 (2008) 055001, arXiv:hep-ph/0611205.
- [48] S. Iso, N. Okada, and Y. Orikasa, "Classically conformal B L extended Standard Model," Phys. Lett. B676 (2009) 81–87, arXiv:0902.4050.
- [49] S. Kanemura, T. Matsui, and H. Sugiyama, "Neutrino mass and dark matter from gauged $U(1)_{B-L}$ breaking," Phys. Rev. **D90** (2014) 013001, arXiv:1405.1935.
- [50] M. Lindner, D. Schmidt, and T. Schwetz, "Dark Matter and neutrino masses from global U(1)_{BL} symmetry breaking," Phys. Lett. B705 (2011) 324–330, arXiv:1105.4626.
- [51] N. Okada and S. Okada, " Z'_{BL} portal dark matter and LHC Run-2 results," Phys. Rev. **D93** (2016) no. 7, 075003, arXiv:1601.07526.
- [52] N. Okada and S. Okada, "Z'-portal right-handed neutrino dark matter in the minimal U(1)_X extended Standard Model," Phys. Rev. D95 (2017) no. 3, 035025, arXiv:1611.02672.
- [53] S. Bhattacharya, S. Jana, and S. Nandi, "Neutrino Masses and Scalar Singlet Dark Matter," Phys. Rev. D95 (2017) no. 5, 055003, arXiv:1609.03274.

[54] A. Biswas, S. Choubey, and S. Khan, "Galactic gamma ray excess and dark matter phenomenology in a $U(1)_{B-L}$ model," JHEP **08** (2016) 114, arXiv:1604.06566.

- [55] W. Wang and Z.-L. Han, "Radiative linear seesaw model, dark matter, and $U(1)_{B-L}$," Phys. Rev. **D92** (2015) 095001, arXiv:1508.00706.
- [56] M. Klasen, F. Lyonnet, and F. S. Queiroz, "NLO+NLL Collider Bounds, Dirac Fermion and Scalar Dark Matter in the B-L Model," arXiv:1607.06468.
- [57] W. Rodejohann and C. E. Yaguna, "Scalar dark matter in the B-L model," JCAP 1512 (2015) no. 12, 032, arXiv:1509.04036.
- [58] M. Lindner, D. Schmidt, and A. Watanabe, "Dark matter and U(1)' symmetry for the right-handed neutrinos," Phys. Rev. D89 (2014) no. 1, 013007, arXiv:1310.6582.
- [59] N. Okada and O. Seto, "Higgs portal dark matter in the minimal gauged $U(1)_{B-L}$ model," Phys. Rev. **D82** (2010) 023507, arXiv:1002.2525.
- [60] N. Okada and Y. Orikasa, "Dark matter in the classically conformal B-L model," Phys. Rev. D85 (2012) 115006, arXiv:1202.1405.
- [61] T. Basak and T. Mondal, "Constraining Minimal $U(1)_{B-L}$ model from Dark Matter Observations," Phys. Rev. **D89** (2014) 063527, arXiv:1308.0023.
- [62] B. L. Snchez-Vega, J. C. Montero, and E. R. Schmitz, "Complex Scalar DM in a B-L Model," Phys. Rev. D90 (2014) no. 5, 055022, arXiv:1404.5973.
- [63] M. Duerr, P. Fileviez Perez, and J. Smirnov, "Simplified Dirac Dark Matter Models and Gamma-Ray Lines," Phys. Rev. D92 (2015) no. 8, 083521, arXiv:1506.05107.
- [64] J. Guo, Z. Kang, P. Ko, and Y. Orikasa, "Accidental dark matter: Case in the scale invariant local B-L model," Phys. Rev. D91 (2015) no. 11, 115017, arXiv:1502.00508.
- [65] A. Dasgupta, C. Hati, S. Patra, and U. Sarkar, "A minimal model of TeV scale WIMPy leptogenesis," arXiv:1605.01292.
- [66] T. Modak, S. Sadhukhan, and R. Srivastava, "750 GeV diphoton excess from gauged BL symmetry," Phys. Lett. B756 (2016) 405–412, arXiv:1601.00836.
- [67] P. Cox, C. Han, and T. T. Yanagida, "Right-handed Neutrino Dark Matter in a U(1) Extension of the Standard Model," JCAP 1801 (2018) no. 01, 029, arXiv:1710.01585.

[68] E. Ma and R. Srivastava, "Dirac or inverse seesaw neutrino masses with B-L gauge symmetry and S_3 flavor symmetry," Phys. Lett. **B741** (2015) 217–222, arXiv:1411.5042.

- [69] E. Ma and R. Srivastava, "Dirac or inverse seesaw neutrino masses from gauged B - L symmetry," Mod. Phys. Lett. A30 (2015) no. 26, 1530020, arXiv:1504.00111.
- [70] E. Ma, N. Pollard, R. Srivastava, and M. Zakeri, "Gauge B-L Model with Residual Z_3 Symmetry," Phys. Lett. **B750** (2015) 135–138, arXiv:1507.03943.
- [71] S. Patra, W. Rodejohann, and C. E. Yaguna, "A new B-L model without right-handed neutrinos," JHEP **09** (2016) 076, arXiv:1607.04029.
- [72] P. Minkowski, " $\mu \to e \gamma$ at a Rate of One Out of 10^9 Muon Decays?," Phys. Lett. **67B** (1977) 421–428.
- [73] R. N. Mohapatra and G. Senjanovic, "Neutrino Mass and Spontaneous Parity Nonconservation," Phys. Rev. Lett. 44 (1980) 912.
- [74] J. Schechter and J. W. F. Valle, "Neutrino Masses in SU(2) x U(1) Theories," Phys. Rev. D22 (1980) 2227.
- [75] M. Gell-Mann, P. Ramond, and R. Slansky, "Complex Spinors and Unified Theories," Conf. Proc. C790927 (1979) 315–321, arXiv:1306.4669.
- [76] J. C. Montero and V. Pleitez, "Gauging U(1) symmetries and the number of right-handed neutrinos," Phys. Lett. **B675** (2009) 64–68, arXiv:0706.0473.
- [77] K. Kannike, "Vacuum Stability Conditions From Copositivity Criteria," Eur. Phys. J. C72 (2012) 2093, arXiv:1205.3781.
- [78] K. Kannike, "Vacuum Stability of a General Scalar Potential of a Few Fields," Eur. Phys. J. C76 (2016) no. 6, 324, arXiv:1603.02680.
- [79] B. W. Lee, C. Quigg, and H. B. Thacker, "Weak Interactions at Very High-Energies: The Role of the Higgs Boson Mass," Phys. Rev. D16 (1977) 1519.
- [80] G. Belanger, B. Dumont, U. Ellwanger, J. F. Gunion, and S. Kraml, "Status of invisible Higgs decays," Phys. Lett. B723 (2013) 340–347, arXiv:1302.5694.
- [81] P. P. Giardino, K. Kannike, I. Masina, M. Raidal, and A. Strumia, "The universal Higgs fit," JHEP 05 (2014) 046, arXiv:1303.3570.
- [82] S. Weinberg, "Goldstone Bosons as Fractional Cosmic Neutrinos," Phys. Rev. Lett. 110 (2013) no. 24, 241301, arXiv:1305.1971.

[83] C. Garcia-Cely, A. Ibarra, and E. Molinaro, "Dark matter production from Goldstone boson interactions and implications for direct searches and dark radiation," JCAP 1311 (2013) 061, arXiv:1310.6256.

- [84] Planck, P. A. R. Ade et al., "Planck 2013 results. XVI. Cosmological parameters," Astron. Astrophys. 571 (2014) A16, arXiv:1303.5076.
- [85] E. Ma, "Verifiable radiative seesaw mechanism of neutrino mass and dark matter," Phys. Rev. **D73** (2006) 077301, arXiv:hep-ph/0601225.
- [86] G. Blanger, K. Kannike, A. Pukhov, and M. Raidal, "Minimal semi-annihilating \mathbb{Z}_N scalar dark matter," JCAP **1406** (2014) 021, arXiv:1403.4960.
- [87] S. Iso, N. Okada, and Y. Orikasa, "The minimal B-L model naturally realized at TeV scale," Phys. Rev. D80 (2009) 115007, arXiv:0909.0128.
- [88] Planck, P. A. R. Ade et al., "Planck 2015 results. XIII. Cosmological parameters," Astron. Astrophys. **594** (2016) A13, arXiv:1502.01589.
- [89] A. V. Semenov, "LanHEP: A Package for automatic generation of Feynman rules in gauge models," arXiv:hep-ph/9608488.
- [90] A. Pukhov, E. Boos, M. Dubinin, V. Edneral, V. Ilyin, D. Kovalenko, A. Kryukov, V. Savrin, S. Shichanin, and A. Semenov, "CompHEP: A Package for evaluation of Feynman diagrams and integration over multiparticle phase space," arXiv:hep-ph/9908288.
- [91] G. Belanger, F. Boudjema, A. Pukhov, and A. Semenov, "MicrOMEGAs 2.0: A Program to calculate the relic density of dark matter in a generic model," Comput. Phys. Commun. 176 (2007) 367–382, arXiv:hep-ph/0607059.
- [92] G. Belanger, F. Boudjema, A. Pukhov, and A. Semenov, "Dark matter direct detection rate in a generic model with micrOMEGAs 2.2," Comput. Phys. Commun. 180 (2009) 747–767, arXiv:0803.2360.
- [93] "Search for new phenomena in the dilepton final state using proton-proton collisions at s = 13 TeV with the ATLAS detector," Tech. Rep. ATLAS-CONF-2015-070, CERN, Geneva, Dec, 2015. https://cds.cern.ch/record/2114842.
- [94] A. Belyaev, N. D. Christensen, and A. Pukhov, "CalcHEP 3.4 for collider physics within and beyond the Standard Model," Comput. Phys. Commun. 184 (2013) 1729-1769, arXiv:1207.6082.

[95] K. Kong, "TASI 2011: CalcHEP and PYTHIA Tutorials," in The Dark Secrets of the Terascale: Proceedings, TASI 2011, Boulder, Colorado, USA, Jun 6 - Jul 11, 2011, pp. 161-198. 2013. arXiv:1208.0035. https://inspirehep.net/record/1124593/files/arXiv:1208.0035.pdf.

- [96] T. A. collaboration, "Search for new phenomena in the dilepton final state using proton-proton collisions at s = 13 TeV with the ATLAS detector,".
- [97] DELPHI, OPAL, LEP Electroweak, ALEPH, L3, S. Schael et al., "Electroweak Measurements in Electron-Positron Collisions at W-Boson-Pair Energies at LEP," Phys. Rept. 532 (2013) 119–244, arXiv:1302.3415.
- [98] F. D'Eramo and J. Thaler, "Semi-annihilation of Dark Matter," JHEP 06 (2010) 109, arXiv:1003.5912.
- [99] D. Nanda and D. Borah, "Common origin of neutrino mass and dark matter from anomaly cancellation requirements of a $U(1)_{B-L}$ model," Phys. Rev. **D96** (2017) no. 11, 115014, arXiv:1709.08417.
- [100] R. N. Mohapatra and G. Senjanovic, "Neutrino Masses and Mixings in Gauge Models with Spontaneous Parity Violation," Phys. Rev. D23 (1981) 165.
- [101] G. Lazarides, Q. Shafi, and C. Wetterich, "Proton Lifetime and Fermion Masses in an SO(10) Model," Nucl. Phys. B181 (1981) 287–300.
- [102] C. Wetterich, "Neutrino Masses and the Scale of B-L Violation," Nucl. Phys. B187 (1981) 343–375.
- [103] B. Brahmachari and R. N. Mohapatra, "Unified explanation of the solar and atmospheric neutrino puzzles in a minimal supersymmetric SO(10) model," Phys. Rev. D58 (1998) 015001, arXiv:hep-ph/9710371.
- [104] S. Antusch and S. F. King, "Type II Leptogenesis and the neutrino mass scale," Phys. Lett. **B597** (2004) 199–207, arXiv:hep-ph/0405093.
- [105] R. N. Mohapatra, "Neutrino mass: An Overview," Nucl. Phys. Proc. Suppl. 138 (2005) 257–266.
- [106] R. Foot, H. Lew, X. G. He, and G. C. Joshi, "Seesaw Neutrino Masses Induced by a Triplet of Leptons," Z. Phys. C44 (1989) 441.
- [107] B. Pontecorvo, "Inverse beta processes and nonconservation of lepton charge," Sov. Phys. JETP 7 (1958) 172–173. [Zh. Eksp. Teor. Fiz.34,247(1957)].
- [108] Z. Maki, M. Nakagawa, and S. Sakata, "Remarks on the unified model of elementary particles," Prog. Theor. Phys. 28 (1962) 870–880.

[109] **Daya Bay**, F. P. An et al., "Observation of electron-antineutrino disappearance at Daya Bay," Phys. Rev. Lett. **108** (2012) 171803, arXiv:1203.1669.

- [110] **Daya Bay**, F. P. An et al., "Improved Measurement of Electron Antineutrino Disappearance at Daya Bay," Chin. Phys. **C37** (2013) 011001, arXiv:1210.6327.
- [111] RENO, J. K. Ahn et al., "Observation of Reactor Electron Antineutrino Disappearance in the RENO Experiment," Phys. Rev. Lett. 108 (2012) 191802, arXiv:1204.0626.
- [112] **T2K**, K. Abe et al., "Evidence of Electron Neutrino Appearance in a Muon Neutrino Beam," Phys. Rev. **D88** (2013) no. 3, 032002, arXiv:1304.0841.
- [113] D. V. Forero, M. Tortola, and J. W. F. Valle, "Neutrino oscillations refitted," Phys. Rev. D90 (2014) no. 9, 093006, arXiv:1405.7540.
- [114] L. Lopez Honorez, E. Nezri, J. F. Oliver, and M. H. G. Tytgat, "The Inert Doublet Model: An Archetype for Dark Matter," JCAP 0702 (2007) 028, arXiv:hep-ph/0612275.
- [115] R. Barbieri, L. J. Hall, and V. S. Rychkov, "Improved naturalness with a heavy Higgs: An Alternative road to LHC physics," Phys. Rev. **D74** (2006) 015007, arXiv:hep-ph/0603188.
- [116] M. Gustafsson, "The Inert Doublet Model and Its Phenomenology," PoS CHARGED2010 (2010) 030, arXiv:1106.1719.
- [117] D. Suematsu, T. Toma, and T. Yoshida, "Reconciliation of CDM abundance and $mu \dot{g}$ e gamma in a radiative seesaw model," Phys. Rev. **D79** (2009) 093004, arXiv:0903.0287.
- [118] D. Schmidt, T. Schwetz, and T. Toma, "Direct Detection of Leptophilic Dark Matter in a Model with Radiative Neutrino Masses," Phys. Rev. D85 (2012) 073009, arXiv:1201.0906.
- [119] T. Toma and A. Vicente, "Lepton Flavor Violation in the Scotogenic Model," JHEP **01** (2014) 160, arXiv:1312.2840.
- [120] A. Vicente and C. E. Yaguna, "Probing the scotogenic model with lepton flavor violating processes," JHEP 02 (2015) 144, arXiv:1412.2545.
- [121] G. Altarelli and F. Feruglio, "Discrete Flavor Symmetries and Models of Neutrino Mixing," Rev. Mod. Phys. 82 (2010) 2701–2729, arXiv:1002.0211.
- [122] G. Altarelli, F. Feruglio, L. Merlo, and E. Stamou, "Discrete Flavour Groups, theta₁₃ and Lepton Flavour Violation," JHEP **08** (2012) 021, arXiv:1205.4670.

[123] S. F. King and C. Luhn, "Neutrino Mass and Mixing with Discrete Symmetry," Rept. Prog. Phys. **76** (2013) 056201, arXiv:1301.1340.

- [124] S. F. King, A. Merle, S. Morisi, Y. Shimizu, and M. Tanimoto, "Neutrino Mass and Mixing: from Theory to Experiment," New J. Phys. 16 (2014) 045018, arXiv:1402.4271.
- [125] H. Ishimori, T. Kobayashi, H. Ohki, Y. Shimizu, H. Okada, and M. Tanimoto, "Non-Abelian Discrete Symmetries in Particle Physics," Prog. Theor. Phys. Suppl. **183** (2010) 1–163, arXiv:1003.3552.
- [126] P. F. Harrison, D. H. Perkins, and W. G. Scott, "A Redetermination of the neutrino mass squared difference in tri - maximal mixing with terrestrial matter effects," Phys. Lett. B458 (1999) 79–92, arXiv:hep-ph/9904297.
- [127] P. F. Harrison, D. H. Perkins, and W. G. Scott, "Tri-bimaximal mixing and the neutrino oscillation data," Phys. Lett. B530 (2002) 167, arXiv:hep-ph/0202074.
- [128] Z.-z. Xing, "Nearly tri bimaximal neutrino mixing and CP violation," Phys. Lett. **B533** (2002) 85–93, arXiv:hep-ph/0204049.
- [129] P. F. Harrison and W. G. Scott, "Symmetries and generalizations of tribinaximal neutrino mixing," Phys. Lett. **B535** (2002) 163–169, arXiv:hep-ph/0203209.
- [130] P. F. Harrison and W. G. Scott, "Permutation symmetry, tri bimaximal neutrino mixing and the S3 group characters," Phys. Lett. **B557** (2003) 76, arXiv:hep-ph/0302025.
- [131] X. G. He and A. Zee, "Some simple mixing and mass matrices for neutrinos," Phys. Lett. **B560** (2003) 87–90, arXiv:hep-ph/0301092.
- [132] L. Wolfenstein, "Oscillations Among Three Neutrino Types and CP Violation," Phys. Rev. D18 (1978) 958–960.
- [133] Y. Yamanaka, H. Sugawara, and S. Pakvasa, "Permutation Symmetries and the Fermion Mass Matrix," Phys. Rev. D25 (1982) 1895. [Erratum: Phys. Rev.D29,2135(1984)].
- [134] N. Li and B.-Q. Ma, "Parametrization of neutrino mixing matrix in tri-bimaximal mixing pattern," Phys. Rev. **D71** (2005) 017302, arXiv:hep-ph/0412126.

[135] M. Sruthilaya, S. C, K. N. Deepthi, and R. Mohanta, "Predicting Leptonic CP phase by considering deviations in charged lepton and neutrino sectors," New J. Phys. 17 (2015) no. 8, 083028, arXiv:1408.4392.

- [136] Planck, P. A. R. Ade et al., "Planck 2013 results. I. Overview of products and scientific results," Astron. Astrophys. 571 (2014) A1, arXiv:1303.5062.
- [137] Particle Data Group, K. A. Olive et al., "Review of Particle Physics," Chin. Phys. C38 (2014) 090001.
- [138] **LHCb**, R. Aaij et al., "Test of lepton universality with $B^0 \to K^{*0}\ell^+\ell^-$ decays," JHEP **08** (2017) 055, arXiv:1705.05802.
- [139] **LHCb**, R. Aaij et al., "Test of lepton universality using $B^+ \to K^+ \ell^+ \ell^-$ decays," Phys. Rev. Lett. **113** (2014) 151601, arXiv:1406.6482.
- [140] **LHCb**, R. Aaij et al., "Differential branching fraction and angular analysis of the decay $B_s^0 \to \phi \mu^+ \mu^-$," JHEP **07** (2013) 084, arXiv:1305.2168.
- [141] **LHCb**, R. Aaij et al., "Measurement of Form-Factor-Independent Observables in the Decay $B^0 \to K^{*0} \mu^+ \mu^-$," Phys. Rev. Lett. **111** (2013) 191801, arXiv:1308.1707.
- [142] **LHCb**, R. Aaij et al., "Differential branching fractions and isospin asymmetries of $B \to K^{(*)} \mu^+ \mu^-$ decays," JHEP **06** (2014) 133, arXiv:1403.8044.
- [143] LHCb, C. Langenbruch, "Latest results on rare decays from LHCb," in Proceedings, 50th Rencontres de Moriond Electroweak Interactions and Unified Theories: La Thuile, Italy, March 14-21, 2015, pp. 317-324. 2015. arXiv:1505.04160. http://inspirehep.net/record/1370442/files/arXiv:1505.04160.pdf.
- [144] C. Bobeth, G. Hiller, and G. Piranishvili, "Angular distributions of $\bar{B} \to \bar{K} \ell^+ \ell^-$ decays," JHEP 12 (2007) 040, arXiv:0709.4174.
- [145] B. Capdevila, A. Crivellin, S. Descotes-Genon, J. Matias, and J. Virto, "Patterns of New Physics in $b \to s\ell^+\ell^-$ transitions in the light of recent data," JHEP **01** (2018) 093, arXiv:1704.05340.
- [146] X. G. He, G. C. Joshi, H. Lew, and R. R. Volkas, "NEW Z-prime PHENOMENOLOGY," Phys. Rev. D43 (1991) 22–24.
- [147] X.-G. He, G. C. Joshi, H. Lew, and R. R. Volkas, "Simplest Z-prime model," Phys. Rev. **D44** (1991) 2118–2132.

[148] S. Patra, S. Rao, N. Sahoo, and N. Sahu, "Gauged $U(1)_{L_{\mu}-L_{\tau}}$ model in light of muon g-2 anomaly, neutrino mass and dark matter phenomenology," Nucl. Phys. **B917** (2017) 317–336, arXiv:1607.04046.

- [149] A. Biswas, S. Choubey, and S. Khan, "Neutrino Mass, Dark Matter and Anomalous Magnetic Moment of Muon in a $U(1)_{L_{\mu}-L_{\tau}}$ Model," JHEP **09** (2016) 147, arXiv:1608.04194.
- [150] A. Kamada, K. Kaneta, K. Yanagi, and H.-B. Yu, "Self-interacting dark matter and muon g-2 in a gauged $U(1)_{L_{\mu}-L_{\tau}}$ model," JHEP **06** (2018) 117, arXiv:1805.00651.
- [151] M. Bauer, S. Diefenbacher, T. Plehn, M. Russell, and D. A. Camargo, "Dark Matter in Anomaly-Free Gauge Extensions," arXiv:1805.01904.
- [152] S. Baek, "Dark matter contribution to $b \to s\mu^+\mu^-$ anomaly in local $U(1)_{L_\mu-L_\tau}$ model," Phys. Lett. **B781** (2018) 376–382, arXiv:1707.04573.
- [153] R. Mandal, "Fermionic dark matter in leptoquark portal," arXiv:1808.07844.
- [154] G. Arcadi, M. Dutra, P. Ghosh, M. Lindner, Y. Mambrini, M. Pierre, S. Profumo, and F. S. Queiroz, "The Waning of the WIMP? A Review of Models, Searches, and Constraints," arXiv:1703.07364.
- [155] R. Allahverdi, P. S. B. Dev, and B. Dutta, "A simple testable model of baryon number violation: Baryogenesis, dark matter, neutronantineutron oscillation and collider signals," Phys. Lett. B779 (2018) 262–268, arXiv:1712.02713.
- [156] H. Georgi and S. L. Glashow, "Unity of All Elementary Particle Forces," Phys. Rev. Lett. 32 (1974) 438–441.
- [157] H. Georgi, "The State of the ArtGauge Theories," AIP Conf. Proc. 23 (1975) 575–582.
- [158] P. Langacker, "Grand Unified Theories and Proton Decay," Phys. Rept. 72 (1981) 185.
- [159] H. Fritzsch and P. Minkowski, "Unified Interactions of Leptons and Hadrons," Annals Phys. 93 (1975) 193–266.
- [160] J. C. Pati and A. Salam, "Lepton Number as the Fourth Color," Phys. Rev. D10 (1974) 275–289. [Erratum: Phys. Rev.D11,703(1975)].
- [161] J. C. Pati and A. Salam, "Unified Lepton-Hadron Symmetry and a Gauge Theory of the Basic Interactions," Phys. Rev. D8 (1973) 1240–1251.

[162] J. C. Pati and A. Salam, "Is Baryon Number Conserved?," Phys. Rev. Lett. 31 (1973) 661–664.

- [163] O. U. Shanker, "Flavor Violation, Scalar Particles and Leptoquarks," Nucl. Phys. B206 (1982) 253–272.
- [164] O. U. Shanker, " $\pi\ell$ 2, $K\ell$ 3 and $K^0 \bar{K}0$ Constraints on Leptoquarks and Supersymmetric Particles," Nucl. Phys. **B204** (1982) 375–386.
- [165] B. Schrempp and F. Schrempp, "LIGHT LEPTOQUARKS," Phys. Lett. 153B (1985) 101–107.
- [166] B. Gripaios, "Composite Leptoquarks at the LHC," JHEP 02 (2010) 045, arXiv:0910.1789.
- [167] D. B. Kaplan, "Flavor at SSC energies: A New mechanism for dynamically generated fermion masses," Nucl. Phys. **B365** (1991) 259–278.
- [168] A. K. Alok, B. Bhattacharya, A. Datta, D. Kumar, J. Kumar, and D. London, "New Physics in $b \to s\mu^+\mu^-$ after the Measurement of R_{K^*} ," Phys. Rev. **D96** (2017) no. 9, 095009, arXiv:1704.07397.
- [169] D. Beirevi and O. Sumensari, "A leptoquark model to accommodate $R_K^{\rm exp} < R_K^{\rm SM}$ and $R_{K^*}^{\rm exp} < R_{K^*}^{\rm SM}$," JHEP **08** (2017) 104, arXiv:1704.05835.
- [170] G. Hiller and I. Nisandzic, " R_K and R_{K^*} beyond the standard model," Phys. Rev. **D96** (2017) no. 3, 035003, arXiv:1704.05444.
- [171] G. D'Amico, M. Nardecchia, P. Panci, F. Sannino, A. Strumia, R. Torre, and A. Urbano, "Flavour anomalies after the R_{K^*} measurement," JHEP **09** (2017) 010, arXiv:1704.05438.
- [172] D. Beirevi, S. Fajfer, N. Konik, and O. Sumensari, "Leptoquark model to explain the B-physics anomalies, R_K and R_D ," Phys. Rev. **D94** (2016) no. 11, 115021, arXiv:1608.08501.
- [173] M. Bauer and M. Neubert, "Minimal Leptoquark Explanation for the $R_{D^{(*)}}$, R_K , and $(g-2)_g$ Anomalies," Phys. Rev. Lett. **116** (2016) no. 14, 141802, arXiv:1511.01900.
- [174] X.-Q. Li, Y.-D. Yang, and X. Zhang, "Revisiting the one leptoquark solution to the $R(D^{()})$ anomalies and its phenomenological implications," JHEP **08** (2016) 054, arXiv:1605.09308.

[175] L. Calibbi, A. Crivellin, and T. Ota, "Effective Field Theory Approach to bs(), BK(*) and BD(*) with Third Generation Couplings," Phys. Rev. Lett. 115 (2015) 181801, arXiv:1506.02661.

- [176] M. Freytsis, Z. Ligeti, and J. T. Ruderman, "Flavor models for $\bar{B} \to D^{(*)} \tau \bar{\nu}$," Phys. Rev. **D92** (2015) no. 5, 054018, arXiv:1506.08896.
- [177] B. Dumont, K. Nishiwaki, and R. Watanabe, "LHC constraints and prospects for S_1 scalar leptoquark explaining the $\bar{B} \to D^{(*)} \tau \bar{\nu}$ anomaly," Phys. Rev. **D94** (2016) no. 3, 034001, arXiv:1603.05248.
- [178] I. Dorner, S. Fajfer, A. Greljo, J. F. Kamenik, and N. Konik, "Physics of leptoquarks in precision experiments and at particle colliders," Phys. Rept. 641 (2016) 1–68, arXiv:1603.04993.
- [179] I. de Medeiros Varzielas and G. Hiller, "Clues for flavor from rare lepton and quark decays," JHEP **06** (2015) 072, arXiv:1503.01084.
- [180] I. Dorsner, J. Drobnak, S. Fajfer, J. F. Kamenik, and N. Kosnik, "Limits on scalar leptoquark interactions and consequences for GUTs," JHEP 11 (2011) 002, arXiv:1107.5393.
- [181] S. Davidson, D. C. Bailey, and B. A. Campbell, "Model independent constraints on leptoquarks from rare processes," Z. Phys. C61 (1994) 613-644, arXiv:hep-ph/9309310.
- [182] J. P. Saha, B. Misra, and A. Kundu, "Constraining Scalar Leptoquarks from the K and B Sectors," Phys. Rev. **D81** (2010) 095011, arXiv:1003.1384.
- [183] R. Mohanta, "Effect of scalar leptoquarks on the rare decays of B_s meson," Phys. Rev. **D89** (2014) no. 1, 014020, arXiv:1310.0713.
- [184] S. Sahoo and R. Mohanta, "Leptoquark effects on $b \to s\nu\bar{\nu}$ and $B \to Kl^+l^-$ decay processes," New J. Phys. 18 (2016) no. 1, 013032, arXiv:1509.06248.
- [185] S. Sahoo and R. Mohanta, "Lepton flavor violating B meson decays via a scalar leptoquark," Phys. Rev. **D93** (2016) no. 11, 114001, arXiv:1512.04657.
- [186] S. Sahoo and R. Mohanta, "Study of the rare semileptonic decays $B_d^0 \to K^* l^+ l^-$ in scalar leptoquark model," Phys. Rev. **D93** (2016) no. 3, 034018, arXiv:1507.02070.
- [187] S. Sahoo and R. Mohanta, "Scalar leptoquarks and the rare B meson decays," Phys. Rev. **D91** (2015) no. 9, 094019, arXiv:1501.05193.

[188] N. Kosnik, "Model independent constraints on leptoquarks from $b \to s\ell^+\ell^-$ processes," Phys. Rev. **D86** (2012) 055004, arXiv:1206.2970.

- [189] C. Bobeth, M. Misiak, and J. Urban, "Photonic penguins at two loops and m_t dependence of $BR[B \to X_s l^+ l^-]$," Nucl. Phys. **B574** (2000) 291–330, arXiv:hep-ph/9910220.
- [190] C. Bobeth, A. J. Buras, F. Kruger, and J. Urban, "QCD corrections to $\bar{B} \to X_{d,s} \nu \bar{\nu}$, $\bar{B}_{d,s} \to \ell^+ \ell^-$, $K \to \pi \nu \bar{\nu}$ and $K_L \to \mu^+ \mu^-$ in the MSSM," Nucl. Phys. **B630** (2002) 87–131, arXiv:hep-ph/0112305.
- [191] W.-S. Hou, M. Kohda, and F. Xu, "Rates and asymmetries of B^{+-} decays," Phys. Rev. **D90** (2014) no. 1, 013002, arXiv:1403.7410.
- [192] T. Inami and C. S. Lim, "Effects of Superheavy Quarks and Leptons in Low-Energy Weak Processes k(L)— $\dot{\varepsilon}$ mu anti-mu, K+— $\dot{\varepsilon}$ pi+ Neutrino anti-neutrino and K0 j— $\dot{\varepsilon}$ anti-K0," Prog. Theor. Phys. **65** (1981) 297. [Erratum: Prog. Theor. Phys. 65,1772(1981)].
- [193] Particle Data Group, C. Patrignani et al., "Review of Particle Physics," Chin. Phys. C40 (2016) no. 10, 100001.
- [194] J. Charles et al., "Current status of the Standard Model CKM fit and constraints on $\Delta F = 2$ New Physics," Phys. Rev. **D91** (2015) no. 7, 073007, arXiv:1501.05013.
- [195] P. Ball and R. Zwicky, "New results on $B \to \pi, K, \eta$ decay formfactors from light-cone sum rules," Phys. Rev. **D71** (2005) 014015, arXiv:hep-ph/0406232.
- [196] J. Hisano, T. Moroi, K. Tobe, and M. Yamaguchi, "Lepton flavor violation via right-handed neutrino Yukawa couplings in supersymmetric standard model," Phys. Rev. D53 (1996) 2442–2459, arXiv:hep-ph/9510309.
- [197] P. Colangelo, F. De Fazio, P. Santorelli, and E. Scrimieri, "Rare $B \to K^{(*)}$ neutrino anti-neutrino decays at B factories," Phys. Lett. **B395** (1997) 339–344, arXiv:hep-ph/9610297.
- [198] **HFLAV**, Y. Amhis et al., "Averages of b-hadron, c-hadron, and τ -lepton properties as of summer 2016," Eur. Phys. J. **C77** (2017) no. 12, 895, arXiv:1612.07233.
- [199] M. Misiak et al., "Updated NNLO QCD predictions for the weak radiative B-meson decays," Phys. Rev. Lett. 114 (2015) no. 22, 221801, arXiv:1503.01789.

[200] W. Altmannshofer, S. Gori, M. Pospelov, and I. Yavin, "Quark flavor transitions in $L_{\mu} - L_{\tau}$ models," Phys. Rev. **D89** (2014) 095033, arXiv:1403.1269.

- [201] CCFR, S. R. Mishra et al., "Neutrino tridents and W Z interference," Phys. Rev. Lett. 66 (1991) 3117–3120.
- [202] W. Altmannshofer, S. Gori, M. Pospelov, and I. Yavin, "Neutrino Trident Production: A Powerful Probe of New Physics with Neutrino Beams," Phys. Rev. Lett. 113 (2014) 091801, arXiv:1406.2332.
- [203] A. Ali, P. Ball, L. T. Handoko, and G. Hiller, "A Comparative study of the decays $B \to (K, K^*)\ell^+\ell^-$ in standard model and supersymmetric theories," Phys. Rev. **D61** (2000) 074024, arXiv:hep-ph/9910221.
- [204] M. Wirbel, B. Stech, and M. Bauer, "Exclusive Semileptonic Decays of Heavy Mesons," Z. Phys. C29 (1985) 637.
- [205] C. Bobeth, G. Hiller, and G. Piranishvili, "CP Asymmetries in bar $B \to \bar{K}^*(\to \bar{K}\pi)\bar{\ell}\ell$ and Untagged \bar{B}_s , $B_s \to \phi(\to K^+K^-)\bar{\ell}\ell$ Decays at NLO," JHEP **07** (2008) 106, arXiv:0805.2525.
- [206] U. Egede, T. Hurth, J. Matias, M. Ramon, and W. Reece, "New physics reach of the decay mode $\bar{B} \to \bar{K}^{*0} \ell^+ \ell^-$," JHEP 10 (2010) 056, arXiv:1005.0571.
- [207] U. Egede, T. Hurth, J. Matias, M. Ramon, and W. Reece, "New observables in the decay mode $\bar{B}_d \to \bar{K}^{*0} l^+ l^-$," JHEP 11 (2008) 032, arXiv:0807.2589.
- [208] W. Altmannshofer, P. Ball, A. Bharucha, A. J. Buras, D. M. Straub, and M. Wick, "Symmetries and Asymmetries of $B \to K^* \mu^+ \mu^-$ Decays in the Standard Model and Beyond," JHEP **01** (2009) 019, arXiv:0811.1214.
- [209] S. Descotes-Genon, J. Matias, M. Ramon, and J. Virto, "Implications from clean observables for the binned analysis of $B->K*\mu^+\mu^-$ at large recoil," JHEP **01** (2013) 048, arXiv:1207.2753.

List of Publications

Thesis Publications

- 1. "Singlet scalar Dark matter in $U(1)_{B-L}$ models without right-handed neutrinos", S. Singirala, R. Mohanta and S. Patra, Eur. Phys. J. Plus 133, 477 (2018), [arXiv:1704.01107].
- "Majorana Dark Matter in a new B-L model", S. Singirala, R. Mohanta,
 S. Patra and S. Rao, JCAP 1811, 026 (2018), [arXiv:1710.05775].
- 3. "Implications of Fermionic Dark Matter on recent neutrino oscillation data", S. Singirala, Chin. Phys. C 41, 043102 (2017), [arXiv:1607.03309].
- 4. "Exploring dark matter, neutrino mass and $R_{K^{(*)},\phi}$ anomalies in $L_{\mu} L_{\tau}$ model", S. Singirala, S. Sahoo and R. Mohanta, [arXiv:1809.03213].

Conference Proceedings

- 1. "Dark Matter in SM_4 and its Implications in LFV Decays", S. Singirala and R. Mohanta, Springer Proc. Phys. 174, 467-472 (2016).
- "Implications of Fermionic Dark Matter on recent neutrino oscillation data", S. Singirala, Springer Proc. Phys. 203, 733-735 (2018).
- 3. "Majorana dark matter, massless Goldstone and neutrino mass in a new B L model", S. Singirala, R. Mohanta, S. Patra and S. Rao, Proceedings of 16th Conference on Flavor Physics and CP Violation FPCP 2018 (To appear in Springer proceedings).

PROSPECTS OF DARK MATTER IN STANDARD MODEL EXTENSIONS

by Singirala Shiva Rama Krishna

Submission date: 28-Dec-2018 10:19AM (UTC+0530)

Submission ID: 1060728880

File name: Thesis_Shivaramakrishna_plagarism.pdf (5.1M)

Word count: 26650 Character count: 145509

PROSPECTS OF DARK MATTER IN STANDARD MODEL EXTENSIONS

	LINOIOINO				
ORIGINA	ALITY REPORT				
3. SIMILA	5% RITY INDEX	26% INTERNET SOURCES	34% PUBLICATIONS	2% STUDENT PA	PERS
PRIMAR	Y SOURCES				
1	export.a	•		,	17%
2	fermioni	makrishna Singira c dark matter on on data", Chinese	recent neutrin	าด	7%
3	Mohanta matter in	makrishna Singira a, Sudhanwa Pata a U(1)B-L models s", The Europea 18	ra. "Singlet sca s without right	-handed	4%
4	Mohanta Majorana	makrishna Singira a, Sudhanwa Patr a Dark Matter in of Cosmology an 2018	ra, Soumya Ra a new – mode	el ",	1%
F	eprints.w	vhiterose.ac.uk			

eprints.whiterose.ac.uk

Suchismita Sahoo, Rukmani Mohanta. "Study 6 of the rare semileptonic decays in scalar leptoquark model ", Physical Review D, 2016 Publication Suchismita Sahoo, R Mohanta. "Impact of <1% vector leptoquark on B → K *I *I anomalies", Journal of Physics G: Nuclear and Particle Physics, 2018 Publication <1% Sahoo, Suchismita, and Rukmani Mohanta. "Leptoquark effects on \$b\;\to \;s{\boldsymbol{\nu }}\bar{{\boldsymbol{\nu }}}\$ and \$B\;\to \;{{KI}}^{+}{I}^{-}\$ decay processes", New Journal of Physics, 2016. Publication tel.archives-ouvertes.fr <1% Internet Source core.ac.uk 10 Internet Source Submitted to Indian Institute of Technology 11 Guwahati Student Paper Murugeswaran Duraisamy, Suchismita Sahoo, <1% 12 Rukmani Mohanta. "Rare semileptonic decay

This is to certify that the thesis entitled "Prospects of Dark Matter in Standard Model Extensions" has been screened by the Turnitin software at the library of University of Hyderabad. The software shows 35% similarity index out of which, 12% came from the candidate's research articles related to this thesis and 17% (export.arxiv.org) came from his research articles in arXiv (1704.0117, 1710.05775, 1809.03213), which are also related to this thesis. The major part of remaining 6% might have come from his other articles and the use of some scientific terms and equations, which have not been detected by the software. Therefore, this thesis is free from plagiarism.

Prof. Rukmani Mohanta (Thesis Supervisor)